MODIFICATIONS OF RECOMBINANT SPIDER SILK PROTEIN FOR VARIOUS BIOMEDICAL APPLICATIONS

A Dissertation
Submitted to the Graduate Faculty
of the
North Dakota State University
of Agriculture and Applied Science

By

Pranothi Mulinti

In Partial Fulfillment of the Requirements
for the Degree of
DOCTOR OF PHILOSOPHY

Major Department:
Pharmaceutical Sciences

August 2019

Fargo, North Dakota

North Dakota State University
Graduate School

Title

MODIFICATIONS OF RECOMBINANT SPIDER SILK PROTEIN FOR VARIOUS BIOMEDICAL APPLICATIONS

By

Pranothi Mulinti

The Supervisory Committee certifies that this ***disquisition*** complies with North Dakota State University's regulations and meets the accepted standards for the degree of

DOCTOR OF PHILOSOPHY

SUPERVISORY COMMITTEE:

Dr. Amanda Brooks
Chair

Dr. Sanku Mallik

Dr. Kristine Steffen

Dr. Mohiuddin Quadir

Approved:

April 9, 2020
Date

Dr. Jagdish Singh
Department Chair

ABSTRACT

Silk is a natural protein produced by members of the class Arachnida (over 30,000 species of spiders) and by several worms. Silk-based materials have been investigated for medical and biotechnological applications for many years. Although silkworm silk has been studied extensively because of ready availability of the protein, lately the advancements in recombinant technology has made production of spider silk proteins increasingly available. Due to the characteristics like biocompatibility, biodegradability and mechanical strength, silk is highly desirable as a biomaterial for medical purpose. Along with this, techniques for functionalization, has further aided in the development of silk into highly sophisticated material for advanced applications.

The main objective of this thesis has been to investigate novel strategies for functionalization of the recombinant spider silk protein Masp2. Two distinct approaches were used, chemical modification and genetic fusion. In the first modification, we created an infection responsive silk nanospheres by chemically grafting a thrombin sensitive peptide to the silk protein encapsulating antibiotic. These particles were then evaluated for *in vitro* infection responsive drug release and antimicrobial activity. From these assessments, we found that these particles can release the drug effectively in the presence of infection providing the evidence that these particles are enzyme responsive and can be used to formulate targeted drug release. In the second modification, spider silk was genetically modified with a heparin binding peptide to create a fusion protein which can prevent both thrombosis and infection simultaneously. This fusion protein was evaluated for its heparin binding ability and anticoagulant properties in its solution form. Furthermore, due to the similarity in structure of HBP with antimicrobial peptides, it is predicted that the fusion protein will also show antimicrobial property. After establishing these properties, next this fusion protein was utilized as a coating for hemodialysis catheter. Deposition of coating

was evaluated after which anticoagulant and anti-infective properties of the protein as a coating material was investigated.

This thesis provides evidence of successful production of a recombinant silk-based biopolymer that can be chemically and genetically embedded with a various functional motif to create a hybrid product for different applications.

Key words: spider silk, infection, thrombosis, fusion protein, antibiotic

ACKNOWLEDGEMENTS

I would like to express my sincere gratitude to my advisor Dr. Amanda Brooks for her guidance and constant support during the course of this research. Without her guidance and persistent help this dissertation would not have been possible. I am grateful to my committee members Dr. Sanku Mallik, Dr. Kristine Steffen, Dr. Mohiuddin Quadir for their time and guidance during my graduate tenure at North Dakota State University.

I would like to thank my lab members Raquib Hasan, Jacob Shreffler and undergrads Julius, Grace, Mackenzie for their help and sharing their expertise during my research. I would like to thank all the members from Department of Pharmaceutical Sciences specially Divya Sharma, Sanjay Arora, Sushanth, for giving me accommodation and helping me out whenever I struggled with my research. Since science cannot be done without instrumentation, I would like to thank Core facility, research park, electron microscopy facilities for providing me with the necessary equipment.

I cannot be more grateful to my family members especially to my parents, my sister Swathi Mulinti, my brother Rahul Mulinti for their constant support and encouragements throughout my graduate study. Their blessings have helped me to achieve my goals.

My immense gratitude to all the faculty members of Department of Pharmaceutical Sciences who had shared their knowledge and experiences in the field.

Finally, I would like to thank funding agency NIH and EPSCoR Program for providing financial support for my research.

DEDICATION

To my family and to all who came in to my life and supported me to reach here.

TABLE OF CONTENTS

LIST OF TABLES

LIST OF FIGURES

CHAPTER 1. INTRODUCTION

Various biodegradable polymeric materials, including synthetic polymers like poly (lactic-co-glycolic acid) and polycaprolactone and natural polymers like collagen and chitosan, have been explored as drug carriers. However, these polymers have their own drawbacks, which include poor biocompatibility and rapid degradation. Furthermore, natural biopolymers are often rigid with little opportunity for tunability. Interests in protein-based biopolymers for drug delivery have increased in recent years as they have advantages of being water-soluble, biocompatible, biodegradable and non-toxic. They are easily derived from their natural sources and simple to process under mild conditions. A modified spider silk protein may prove to be such an alternative as a biopolymer. Spider silk has been the focus of research in recent years due to its superior mechanical properties, biocompatibility and slow degradation.

1.1. Silk as a biomaterial

Silk is naturally produced by members of the class Arachnida (over 30,000 species of spiders) and by several worms including mites, butterflies and moths. Silk from silkworms (e.g., *Bombyx mori*) and spiders (*Nephila clavipes* and *Araneus diadematus*) are the most extensively characterized in the literature. Historically, silk from silkworms has been used by man to produce textiles for thousands of years due to its luster, lightweight, and tear resistance [1], [2]. Additionally, silk fibers in the form of sutures and wound dressings have been used for centuries, have played an important socioeconomic role.

Recently, efforts have been made to expand the socioeconomic role of silks by exploring the underlying physiological and molecular nature of the silk. Silks are fibrous proteins synthesized in epithelial cells that line the luminal surface of specialized glands and secrete a

highly concentrated protein solution into the lumen of the gland, where it is maintained as a liquid crystalline solution before forming fibers [1].

Generally, depending on the source, composition, and protein structure, the properties of silks differ widely. These fibers are evolutionarily tailored to perform vital functions like protecting eggs or larvae, capturing and trapping prey under potentially high impact, supporting the weight of the spider during movement (e.g., dragline), constructing webs, and adhering to diverse substrates. In addition to these diverse ecological functions, silk protein has also demonstrated a combination of commercially useful properties (e.g., biocompatibility, robust mechanical strength in various material formats and controllable rates of degradation to non-toxic byproducts *in vivo*, etc.), leading it to be increasingly considered for various biomedical and drug delivery applications [3], [4], [5]. Although spider silk has not yet been commercialized for biomedical applications due to their cannibalistic nature that precludes farming them and the relatively low levels of production of these silks (despite production throughout their lifecycle) compared to silkworm silk, genetic engineering of spider silk has been actively investigated over the past three decades, since the genetic sequences of the protein were deciphered [3], [6].

Typically, golden orb-weaving spiders can produce seven different types of silks from seven different glands [7]. Among different types of spider silks, dragline silk also called major ampullate silk exhibits the highest tensile strength with moderate elasticity, making it stronger than steel and tougher than other natural and synthetic materials including Kevlar. Dragline silk is comprised of two proteins: major ampullate Spidroin 1 (MaSp1) and major ampullate Spidroin 2 (MaSp2) [6] with distinct amino acid motifs, leading it to be characterized as a natural block copolymer. In fact, the amino acid sequence of dragline silk can be generalized as sets of consensus repeats consisting of two predominant amino acid motifs (1) GPGXX (X = G, Q, Y) and (2) a poly

Ala or poly GA region. In a broader perspective, this relatively simplistic molecular structure consists of extended domains of hydrophobic amino acids, segregated by relatively short and more hydrophilic regions. Furthermore, the domains comprising mainly glycine, alanine, glutamine, serine, and tyrosine organize themselves together into β-sheet crystallites via intramolecular or intermolecular forces including hydrogen bonds, van der Waals forces, and hydrophobic interactions, leading to the formation of highly ordered crystalline regions; whereas, the non-repetitive domains form non-crystalline regions thought to be important for solubilization and fiber formation [5]. The β-sheets formed by the poly Alanine tail with successive alanine residues arranged on alternate sides of the backbone is responsible for the tensile strength of the silk and is poorly hydrated while the GPGXX repeat forms a β-spiral similar to that of elastin and is responsible for the elastic properties of the silk protein [8], [9]. Poly alanine and GPGXX motifs are the primary motifs of Masp2 while poly alanine and GGX are the primary motifs of Masp1. These repetitive motifs control various structural and functional aspects of the protein that control the balance of the fiber's strength and elasticity. Hence, by manipulating the amount and ratio of these motifs, synthetic fibers with different mechanical and elastic properties could be fashioned.

In addition to modifying the ratio of genetic motifs, specific amino acid motifs, correlated with functional properties, can be chemically and/or genetically modified while preserving their intrinsic properties and critical secondary structural features. Both of these modification strategies can lead to the production of recombinant silk polymers that control 1) polymer size, 2) chemical reactivity, 3) biological activity, and 4) bulk material properties [5], [8]. Furthermore, isolated silk spidroin can be fabricated conveniently into various formats (films, fibers, microparticles etc.) due to its versatility in processing (Figure 1). Finally, silk has been shown to support stem cell adhesion, proliferation, and differentiation *in vitro* and promote tissue repair and resist

pathological adhesion *in vivo*. In addition, there is a growing interest in introducing more functionality into silk fibroin proteins for their use in tissue engineering and drug delivery [10]. Low immunogenicity as well as thermal and chemical stability [11]–[13], along with the opportunity to control and manipulate the primary structure/function relationship of spider silk by embedding different functionalities or by altering the ratio of amino acid blocks [14] to produce a mechanically robust and chemically defined biomaterial makes synthetic spider silk proteins an attractive biomaterial for drug delivery and also an intriguing surface coating alternative. The presence of diverse, reactive amino acid groups on the recombinant silk protein can further tune the surface chemistry of the protein and be tailored for different applications. Although the major part of protein consists of non-reactive glycine and alanine, it also contains significant amounts of serine, threonine, aspartic and glutamic acid, and tyrosine, which can be modified easily [15]. Some of the modifications reported in the literature are 1) coupling reactions by carbiidomide, glutaraldehyde and cyanuric chloride 2) amino acid modifications by sulfation/oxidation of tyrosine or azo modified tyrosine 3) grafting reactions by tyrosinase catalyzed grafting and poly methacrylate grafting (Figure 2) [15], [16]. Apart from these modifications, functionalization with various peptides/enzymes have also been explored [17]–[20]. Short peptide sequences when immobilized on biomaterials can improve cell adhesion, cell proliferation and differentiation particularly for bone, teeth and ligament. Some of the functionalization's of spider silk being explored in the lab include 1) increasing cell adhesion and proliferation by chemical attachment of cell binding domains like RGD (Arg-Gly-Asp) [21], [22] 2) antimicrobial peptides including hepsidin [20], [23] and 3) silk modified with fibronectin, antimicrobial peptides and growth factors for wound dressing and skin grafts [24], [25]. Apart from these modifications, silk has also been investigated in drug delivery due to its biocompatibility and relatively slow degradation, which is

useful for modified drug release. The work outlined in this dissertation will describe two different modifications of silk to prevent and treat both infection and thrombosis.

1.2. Relationship between infection and thrombosis

Severe infection is often linked to prothrombotic events, effectively countering resolution with therapeutics, allowing infections and thrombosis to proceed uninterrupted [26]–[28]. Indeed, haemostatic abnormalities are encountered in most cases of infection, ranging from an increase in sensitive markers for coagulation activation to a rise in host factors such as platelets, fibrin and fibronectin that may result in localized thrombotic complications; simultaneously, independent production of thrombi can also provide a rich matrix of fibrils for bacterial adhesion [29], [30]. There are two important manifestations of this complex relation between infection and thrombosis.

i. **Activation of coagulation cascade by the enzymes released from the bacteria:** Hemolytic bacteria, such as *Staphylococcus aureus,* one of the major hospital acquired infection causing agents [31], can release enzymes that can directly act on the coagulation cascade. *S aureus* and other related bacteria secrete coagulase, an enzyme which activates human prothrombin. Prothrombin converts fibrinogen to fibrin, resulting in the clotting of plasma in the vicinity of the bacteria [32], [33]. Apart from its ability to clot the blood, there is extensive experimental evidence linking coagulase and bacterial virulence. Specifically, it was found that coagulase binds tightly to the surface of the bacteria, allowing the microbe to coat its surface with a protective fibrin clot, allowing the bacteria to evade the immune system and leading to increased virulence and resistance [31], [34], [35]. Due its similarity in function to human thrombin, coagulase can be used as a trigger to develop substrates that can respond to the enzyme, ultimately creating an infection responsive drug delivery system.

Figure 1.1. Different morphologies of silk processing (silkworm). Adopted from "chemically modified silk proteins; advanced engineering materials."

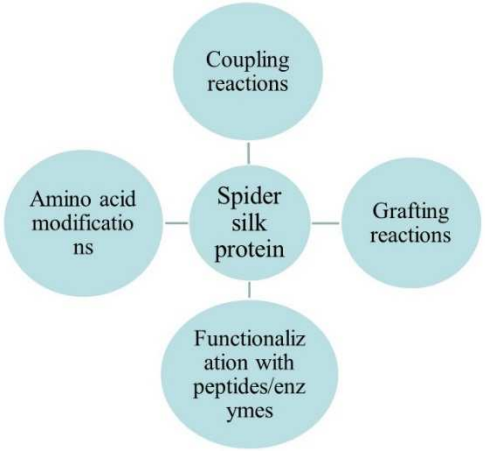

Figure 1.2. Different modifications of spider silk protein.

ii. **Indirect activation by recruiting host factors:** Various mechanisms involved in the interaction between infection and thrombus formation have been elucidated. Initially, it was thought the link only occurred through the direct activation of the contact arm of the coagulation cascade by microorganisms; however, later it became apparent that cytokines

played an important role in the activation of coagulation and subsequent fibrin deposition [27]. This mechanism is of particular importance in cases of CRBSI (catheter-related bloodstream infection) where thrombi lead to microbial surface colonization of catheters or medical devices. Importantly, when bacteria colonize a surface, they often secrete a complex mucopolysaccharide barrier to form a "biofilm", allowing them to corporatize lay escape the host immune response [36]. Either systemic antibiotic administration with antibiotic lock therapy or heparin therapy has been employed separately for the treatment of CRBSI. Unfortunately, such a strategy addresses only one problem at a time and completely ignores this complex relationship.

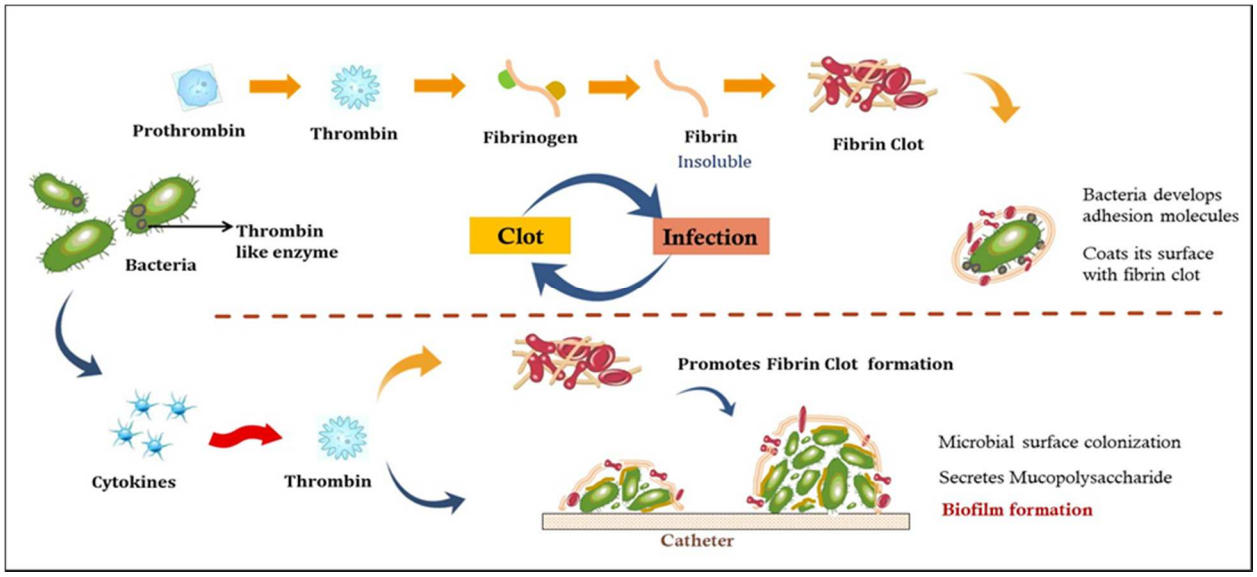

Figure 1.3. Graphical representation of the relation between infection and thrombosis.

By genetically linking non-native, bioinspired, bioactive motifs with a robust silk protein sequence, a tough, biocompatible, self-assembling material can be produced. This observation leads to my global hypothesis: recombinant spider silk protein can be functionalized with a wide range of other biologically-active motifs, including a heparin binding peptide and a thrombin sensitive peptide, which can then be processed as a biopolymer to manipulate the link between

thrombosis and infection. As a corollary, such a biopolymer can be used for both drug delivery and as a surface coating.

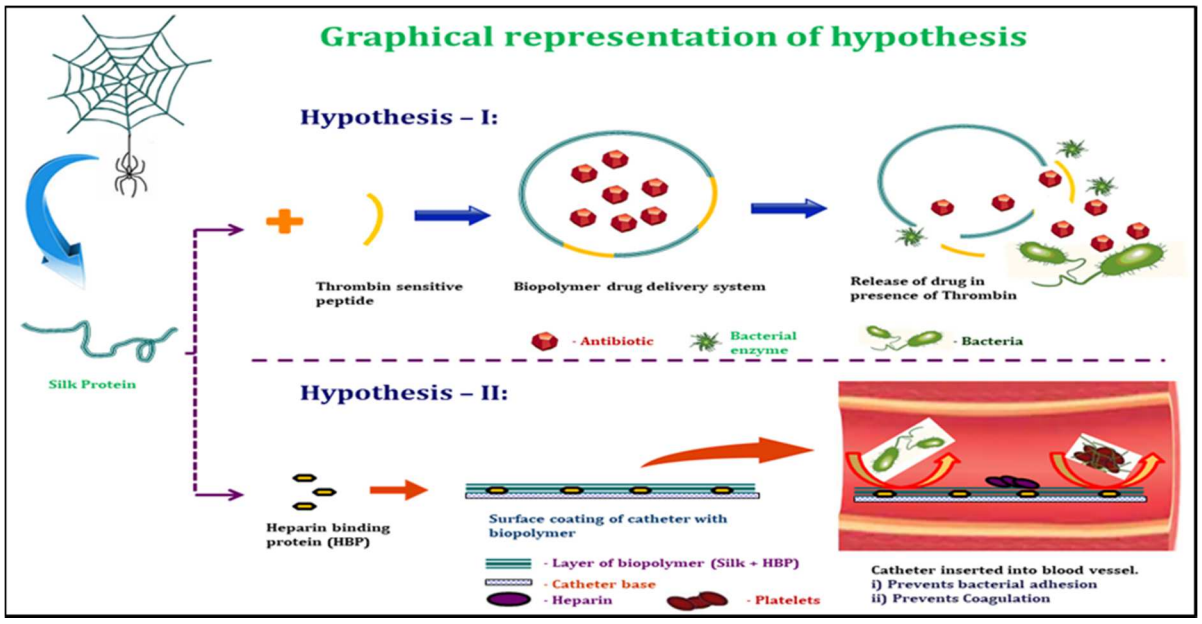

Figure 1.4. Graphical representation of the hypotheses being tested in the thesis.

The dissertation is aimed at investigating following hypothesis and specific aims. Chapter two is focused on chemical modification of spider silk protein for infection responsive delivery of antibiotic. Chapter three is focused on genetic modification of spider silk with heparin binding motif to create a fusion protein for anticoagulant and antimicrobial properties. Chapter four is focused on using the fusion protein as a coating material for catheters.

Hypothesis 1: A synthetic, thrombin-sensitive peptide (TSP) chemically grafted to a recombinant silk peptide will sensitize the silk peptide to thrombin-like cleavage, potentially enhancing the common coagulation pathway, while concurrently providing the basis for a self-assembling, vancomycin-encapsulating nanosphere that will release its drug payload only in the presence of *S. aureus*.

***Specific Aim 1*:** Determine the proteolytic stability of the newly created thrombin-sensitive, silk-based biopolymer to *S. aureus* thrombin-like activity

Specific Aim 2: Characterize the physical (e.g., the size, polydispersity, and encapsulation efficacy) and pharmacokinetic properties of thrombin-sensitive silk micelles in the presence of *S. aureus* exudate.

Specific Aim 3: Determine the efficacy of antibiotic released from thrombin-sensitive silk biopolymer nanoscale micelles (nanospheres) in a rat septic arthritis model.

Hypothesis 2: A recombinant bi-domain protein chimera comprising both a heparin binding peptide $(ARKKAAKA)_n$ and a MaSp2 silk peptide $(GGYGPGQQGPGGYGPGQQGPSGPGSAAAAAAAA)_n$ represents a robust, silk-based, heparin-binding, antimicrobial surface coating that can actively capture endogenous circulating heparins from blood and plasma-based solutions.

***Specific Aim 1*:** Determine the *in vitro* anti-thrombotic, antimicrobial activities of the silk-heparin-binding protein chimera (S4H4).

***Specific Aim 2*:** Assess the anti-thrombotic and antimicrobial properties of a hemodialysis catheter coated with recombinant S4H4.

1.3. References

[1] C. Vepari and D. L. Kaplan, "Silk as a Biomaterial," *Prog Polym Sci*, vol. 32, no. 8–9, pp. 991–1007, 2007.

[2] B. Joseph and S. J. Raj, "Therapeutic applications and properties of silk proteins from Bombyx mori," *Frontiers in Life Science*, vol. 6, no. 3–4, pp. 55–60, Dec. 2012.

[3] G. H. Altman *et al.*, "Silk-based biomaterials," *Biomaterials*, vol. 24, no. 3, pp. 401–416, Feb. 2003.

[4] S. Kapoor and S. C. Kundu, "Silk protein-based hydrogels: Promising advanced materials for biomedical applications," *Acta Biomaterialia*, vol. 31, pp. 17–32, Feb. 2016.

[5] L.-D. Koh *et al.*, “Structures, mechanical properties and applications of silk fibroin materials,” *Progress in Polymer Science*, vol. 46, pp. 86–110, Jul. 2015.

[6] M. B. Hinman and R. V. Lewis, “Isolation of a clone encoding a second dragline silk fibroin. Nephila clavipes dragline silk is a two-protein fiber.,” *J. Biol. Chem.*, vol. 267, no. 27, pp. 19320–19324, Sep. 1992.

[7] B. An *et al.*, “Reproducing Natural Spider Silks’ Copolymer Behavior in Synthetic Silk Mimics,” *Biomacromolecules*, vol. 13, no. 12, pp. 3938–3948, Dec. 2012.

[8] C. Y. Hayashi, N. H. Shipley, and R. V. Lewis, “Hypotheses that correlate the sequence, structure, and mechanical properties of spider silk proteins,” *International Journal of Biological Macromolecules*, vol. 24, no. 2, pp. 271–275, Mar. 1999.

[9] J. Gosline, M. Lillie, E. Carrington, P. Guerette, C. Ortlepp, and K. Savage, “Elastic proteins: biological roles and mechanical properties.,” *Philos Trans R Soc Lond B Biol Sci*, vol. 357, no. 1418, pp. 121–132, Feb. 2002.

[10] Y. Wang, H.-J. Kim, G. Vunjak-Novakovic, and D. L. Kaplan, “Stem cell-based tissue engineering with silk biomaterials,” *Biomaterials*, vol. 27, no. 36, pp. 6064–6082, Dec. 2006.

[11] B. Panilaitis, G. H. Altman, J. Chen, H.-J. Jin, V. Karageorgiou, and D. L. Kaplan, “Macrophage responses to silk,” *Biomaterials*, vol. 24, no. 18, pp. 3079–3085, Aug. 2003.

[12] L. Meinel *et al.*, “The inflammatory responses to silk films in vitro and in vivo,” *Biomaterials*, vol. 26, no. 2, pp. 147–155, Jan. 2005.

[13] K. Spiess, R. Ene, C. D. Keenan, J. Senker, F. Kremer, and T. Scheibel, “Impact of initial solvent on thermal stability and mechanical properties of recombinant spider silk films,” *Journal of Materials Chemistry*, vol. 21, no. 35, pp. 13594–13604, 2011.

[14] “Properties of Synthetic Spider Silk Fibers Based on Argiope aurantia MaSp2 - Biomacromolecules (ACS Publications).” [Online]. Available: https://pubs.acs.org/doi/abs/10.1021/bm701124p. [Accessed: 24-Jul-2018].

[15] A. R. Murphy and D. L. Kaplan, “Biomedical applications of chemically-modified silk fibroin,” *J Mater Chem*, vol. 19, no. 36, pp. 6443–6450, Jun. 2009.

[16] J. Chen, H. Venkatesan, and J. Hu, “Chemically Modified Silk Proteins,” *Advanced Engineering Materials*, vol. 20, no. 7, p. 1700961, Jul. 2018.

[17] K. Numata, M. R. Reagan, R. H. Goldstein, M. Rosenblatt, and D. L. Kaplan, “Spider silk-based gene carriers for tumor cell-specific delivery,” *Bioconjug. Chem.*, vol. 22, no. 8, pp. 1605–1610, Aug. 2011.

[18] T. Deptuch and H. Dams-Kozlowska, “Silk Materials Functionalized via Genetic Engineering for Biomedical Applications,” *Materials (Basel)*, vol. 10, no. 12, Dec. 2017.

[19] D. Huemmerich, U. Slotta, and T. Scheibel, “Processing and modification of films made from recombinant spider silk proteins,” *Appl. Phys. A*, vol. 82, no. 2, pp. 219–222, Feb. 2006.

[20] S. Gomes, I. B. Leonor, J. F. Mano, R. L. Reis, and D. L. Kaplan, “Antimicrobial functionalized genetically engineered spider silk,” *Biomaterials*, vol. 32, no. 18, pp. 4255–4266, Jun. 2011.

[21] G. Vidal *et al.*, "Enhanced cellular adhesion on titanium by silk functionalized with titanium binding and RGD peptides," *Acta Biomaterialia*, vol. 9, no. 1, pp. 4935–4943, Jan. 2013.

[22] E. Bini, C. W. P. Foo, J. Huang, V. Karageorgiou, B. Kitchel, and D. L. Kaplan, "RGD-Functionalized Bioengineered Spider Dragline Silk Biomaterial," *Biomacromolecules*, vol. 7, no. 11, pp. 3139–3145, Nov. 2006.

[23] S. Gomes, J. Gallego-Llamas, I. B. Leonor, J. F. Mano, R. L. Reis, and D. L. Kaplan, "Biological responses to spider silk-antibiotic fusion protein," *J Tissue Eng Regen Med*, vol. 6, no. 5, pp. 356–368, May 2012.

[24] D. Chouhan, N. Thatikonda, L. Nilebäck, M. Widhe, M. Hedhammar, and B. B. Mandal, "Recombinant Spider Silk Functionalized Silkworm Silk Matrices as Potential Bioactive Wound Dressings and Skin Grafts," *ACS Applied Materials & Interfaces*, vol. 10, no. 28, pp. 23560–23572, Jul. 2018.

[25] C. P. Tasiopoulos, M. Widhe, and M. Hedhammar, "Recombinant Spider Silk Functionalized with a Motif from Fibronectin Mediates Cell Adhesion and Growth on Polymeric Substrates by Entrapping Cells During Self-Assembly," *ACS Applied Materials & Interfaces*, vol. 10, no. 17, pp. 14531–14539, May 2018.

[26] H. M. Bos, R. A. de Boer, G. L. Burns, and S. F. Mohammad, "Evidence that bacteria prefer to adhere to thrombus," *ASAIO J.*, vol. 42, no. 5, pp. M881-884, Oct. 1996.

[27] M. Levi, "New insights into pathways that determine the link between infection and thrombosis," vol. 70, no. 3, p. 7, 2012.

[28] S. F. Mohammad, "Enhanced risk of infection with device-associated thrombi," *ASAIO J.*, vol. 46, no. 6, pp. S63-68, Dec. 2000.

[29] V. G. Gavalas, M. J. Berrocal, and L. G. Bachas, “Enhancing the blood compatibility of ion-selective electrodes,” *Anal Bioanal Chem*, vol. 384, no. 1, pp. 65–72, Jan. 2006.

[30] M. J. Berrocal, R. D. Johnson, I. H. A. Badr, M. Liu, D. Gao, and L. G. Bachas, “Improving the Blood Compatibility of Ion-Selective Electrodes by Employing Poly(MPC-co-BMA), a Copolymer Containing Phosphorylcholine, as a Membrane Coating,” *Anal. Chem.*, vol. 74, no. 15, pp. 3644–3648, Aug. 2002.

[31] M. McAdow, D. M. Missiakas, and O. Schneewind, “Staphylococcus aureus Secretes Coagulase and von Willebrand Factor Binding Protein to Modify the Coagulation Cascade and Establish Host Infections,” *J Innate Immun*, vol. 4, no. 2, pp. 141–148, Feb. 2012.

[32] E. Bonar, J. Międzobrodzki, and B. Władyka, “Chapter 7 - The Staphylococcal Coagulases,” in *Pet-To-Man Travelling Staphylococci*, V. Savini, Ed. Academic Press, 2018, pp. 95–102.

[33] J. P. Soulier and O. Prou-Wartelle, “Study of thrombin-coagulase,” *Thromb Diath Haemorrh*, vol. 17, no. 3–4, pp. 321–334, May 1967.

[34] “Coagulase | Encyclopedia.com.” [Online]. Available: https://www.encyclopedia.com/science-and-technology/biology-and-genetics/cell-biology/coagulase. [Accessed: 04-Aug-2018].

[35] P. Phonimdaeng, M. O’Reilly, P. Nowlan, A. J. Bramley, and T. J. Foster, “The coagulase of Staphylococcus aureus 8325-4. Sequence analysis and virulence of site-specific coagulase-deficient mutants,” *Mol. Microbiol.*, vol. 4, no. 3, pp. 393–404, Mar. 1990.

[36] H. Shah, W. Bosch, K. M. Thompson, and W. C. Hellinger, “Intravascular Catheter-Related Bloodstream Infection,” *Neurohospitalist*, vol. 3, no. 3, pp. 144–151, Jul. 2013.

CHAPTER 2. INFECTION RESPONSIVE SMART DELIVERY OF ANTIBIOTICS USING RECOMBINANT SPIDER SILK NANOSPHERES

2.1. Abstract

Frequent and inappropriate usage of antibiotics has changed the natural evolution of bacteria by reducing susceptibility and increasing resistance towards antibacterial agents. New resistance mechanisms evolved in response to host defenses and pharmaceutical interventions are threatening our ability to treat common infections, resulting in increased mortality. In face of this rising epidemic, antibiotic drug discovery, which has long been overlooked by big pharma, is reaching a critical low. Thus, the development of an infection-responsive drug delivery system, which may mitigate multidrug resistance and preserve the lifetime of our current antibiotic arsenal, has garnered the attention of both popular science and funding agencies. The present work describes the development of a thrombin sensitive linker embedded into a recombinant spider silk copolymer to create a nanosphere drug delivery vehicle. Recent studies have suggested that there is an increase in thrombin-like activity during *Staphylococcus aureus* infection; thus, drug release from this new "smart" nanosphere can be triggered in the presence of infection. A thrombin sensitive peptide (TSP) was synthesized and the thrombin cleavage sensitivity was determined by HPLC. The results showed no cleavage of the peptide when exposed to human serum whereas the peptide was cleaved when incubated with *S. aureus* exudate. Subsequently, the peptide was coupled with a silk copolymer via EDC-NHS chemistry and formulated into nanospheres encapsulating antibiotic vancomycin. These nanospheres were evaluated for *in vitro* infection responsive drug release and antimicrobial activity. Finally, the drug responsive nanospheres were assessed for efficacy in an in vivo septic arthritis model. Our study provides evidence that the

protein conjugate was enzyme responsive and can be used to formulate targeted drug release to combat infections against multidrug resistant bacterial strains.

2.2. Introduction

Antibiotics are an essential component of infection treatment and prevention. The care of patients with serious infections both within and outside healthcare settings is increasingly complicated by the high prevalence of resistant or multidrug-resistant (MDR) pathogens. Infections caused by MDR pathogens are usually associated with higher mortality and healthcare costs [1]. Although clinical antimicrobial misuse and overuse are the primary drivers for the development of resistance, poor patient compliance plays an equally important role in promoting spontaneous mutation and horizontal gene transfer that lead to the evolution of resistance. Recent research has also confirmed that sub-lethal concentrations of antibiotics can also convey resistance [2]–[4]. Thus, the necessity to use elevated concentrations of vancomycin, traditionally thought of as an antibiotic of last resort, are now commonplace, prompting concerns that society is reverting to a pre-antibiotic era.

Extending the life of current antibiotics to address the rising tide of resistance requires a paradigm shift away from new drug and small molecule discovery and development toward better delivery systems. Irrespective of the type of resistance mechanism and the spread of resistance, combatting it requires multiple levels of intervention, including new and modified antibiotics, antibiotic conjugates, and cutting-edge drug delivery systems to address this rising global problem. Systemic administration of antibiotics has been the mainstay of antimicrobial therapy for infectious disease control for decades [5]. Unfortunately, systemic delivery suffers from several significant drawbacks (e.g., poor penetration to wound and post-operative tissues, systemic toxicity, poor patient compliance, disruption of the patient's healthy flora, etc.) that limit it as a

stable antibiotic delivery strategy. Furthermore, sub-therapeutic antibiotic concentrations are known to inadvertently promote the development and spread of resistance [6]. Regardless of the underlying cause, multidrug resistant bacteria are quickly outpacing antibiotic discovery and development. As the current pipeline is not adequate to effectively address antibiotic resistance, alternate and better use of our current arsenal may help to mitigate the resistance trend. While many delivery strategies including topical, oral, intravenous etc., facilitate systemic drug bioavailability, local release seeks to provide therapeutic drug concentrations only to intended target sites to produce the desired pharmacological effect. Local delivery systems are frequently considered particularly to address thrombosis, osteomyelitis, periodontitis, biomedical device-related infections and other microbial pathologies, that are refractory to most conventional methods of systemic drug administration [6], [7]. Adding to this, the development of "smart" responsive delivery systems may prove an effective strategy and provide a synergistic effect to extend the effective lifetime of current therapeutics. Targeted nanotechnology-based drug delivery systems that respond to local environments are emerging as an effective approach to: 1) decrease the dose and frequency of administration to improve the therapeutic index, 2) target organ and even intracellular compartments to limit systemic side effects and 3) mitigate resistance that results from sub-therapeutic antibiotic exposure.

Strategies utilizing microenvironments unique to tissues and disease states as a molecular cue to activate drug release has gained widespread attention in the treatment of various diseases like cancer, diabetes and bacterial infections as it increases drug stability and therapeutic efficacy while decreasing toxic side effects at the same time [8]–[11]. Several enzymes were reported to be elevated during infection, including a thrombin-like enzyme in *S. aureus*, myeloperoxidase in *Candida*, and esterases in uropathogens; whereas, the release of bacterial phosphatase and

phospholipase, which are key virulence factors for certain bacteria, are reported in other studies [11]. These enzymes can be used as biomarkers for timely initiation of treatment and also as therapeutic targets for an infection-responsive drug release system. *S. aureus* and *P. aeruginosa* infected wound fluid has been reported to have high thrombin-like enzymatic cleavage activity due to the bacterial enzyme staphylocoagulase [12], [13], [14]. Staphylocoagulase has thrombin like function which activates prothrombin and mediates cleavage of fibrinogen to fibrin. Thrombin, an endogenous human protease also cleaves fibrinogen at the Arg-Gly bonds with a unique substrate specificity and is typically found at approximately 150 mg/L in the blood but is elevated in both *S. aurues* and *P. aeruginosa* infections due to the activity of staphylocoagulase. Thus, it can be used as a trigger to release the antibiotic in the presence of infection. Previous research has optimized the sequence of the substrate (thrombin-sensitive peptide), $GF_DPRGFPAGG$, which demonstrated complete cleavage within 15 minutes, releasing gentamicin linked to a polyvinyl alcohol (PVA) support matrix [15].

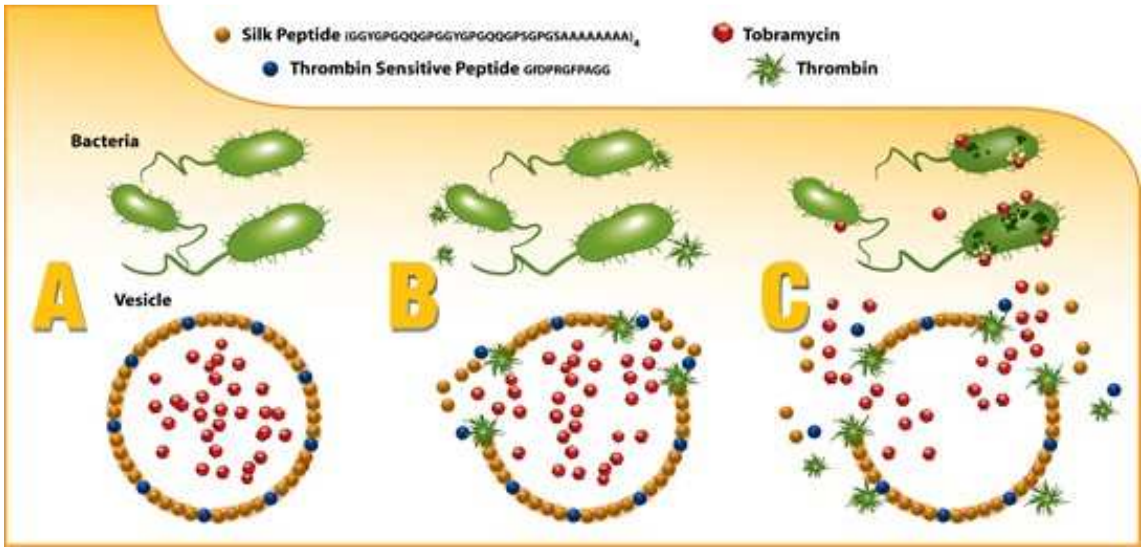

Figure 2.1. Graphical representation of the infection responsive release of the drug triggered by bacterial enzyme.

Spidroins (i.e., spider silk proteins) are natural, structural, block copolymer, with a demonstrated combination of robust mechanical properties, biocompatibility, and tailorable rates of degradation to non-toxic byproducts *in vivo,* leading them to be increasingly considered for various biomedical and drug delivery applications [16], [17], [18]. By capitalizing on this "plug-and-play" motif structure, spidroins can be directly engineered to not only incorporate the thrombin sensitive peptide element but also to promote self-assembly into drug-encapsulating micelles and microcapsules that can release their drug payload only in the presence of infection [19]–[22].

2.3. Methods

2.3.1. Protein expression and purification

The cloned consensus sequence of MaSp2 $(GGYGPGQQGPGGYGPGQQGPSGPGSAAAAAAAA)_2$ was transformed into *E. coli* BL21(DE3) pLysS cells (Promega, USA) for the expression of silk protein (sx2). Briefly, cultures were grown to an OD_{600} between 0.4 and 0.5 after which Isopropyl-β-D-1-thiogalactopyranoside (IPTG, Thermo Fisher Scientific, MA) was added at a final concentration of 0.5 mM to induce the expression. After 4 hours the culture was centrifuged at 4000 rpm for 10 minutes and the cell pellet was collected and resuspended in 100 mM HEPES buffer (1/10 of the final culture volume). To this, 50 μg/ml DNase I (Sigma) is added and sonicated at 60% amplitude for 30 seconds. The cell suspension was centrifuged again at the same conditions and the supernatant containing the protein was collected [23]. Proteins were purified by affinity chromatography using His-Pur Ni-NTA resin and the purified protein was dialyzed against water overnight and lyophilized [24]

2.3.2. Protein characterization

2.3.2.1. Sodium Dodecyl Sulfate Polyacrylamide Gel Electrophoresis (SDS-PAGE)

Lyophilized protein was resuspended in phosphate buffer saline (PBS) for further analysis. SDS-PAGE was performed to check the size and purity of the protein. Each sample was heated with NuPAGE LDS sample buffer (Invitrogen, CA) at 95°C before loading into precast Bis-tris 4-12 % polyacrylamide gradient gel (ThermoFisher, MA). The gel was stained with AcquaStain Protein Gel Stain (Bulldog Bio. Inc) according to the manufacturer's protocol and visualized under white light on a BioRad Chemidoc XRS imaging system.

2.3.2.2. Western Blot

The purified protein was then confirmed by semi dry western blot. Briefly, protein was transferred to a nitrocellulose membrane on a semi-dry blotter (Owl^{TM} semi-dry electroblotting systems, Fisher Scientific, CA) at a constant voltage of 70V for 60 min. After proteins were transferred to the nitrocellulose membrane, the membrane was blocked overnight at 4°C using 5% non-fat milk as blocking agent. The membrane was washed with Tris buffered saline plus Tween 20 (0.05 %) and incubated with a 1:2500 dilution of a HRP-conjugated 6x-His Epitope Tag Polyclonal Antibody (Thermo Scientific, MA1-21315, CA) for one hour. The protein was detected by Western ECL substrate (Promega, WI) according to manufacturer's protocol and the bands were visualized using the Omega Lum^{TM} G gel imaging system (Aplegen Inc, CA).

2.3.2.3. Mass Spectrometry

LC-MS was performed on purified protein samples at the Core Synthesis and Analytical Services Facility (Center for Protease Research, North Dakota State University, USA). Mass spectrometric analysis was performed on a Waters Synapt G2-Si HDMS using ES+ sensitivity mode equipped with Acquity UPLC- I class with Waters C18 (2.1mm X 100mm) column. A linear

gradient was performed with the ratio of A (0.1% formic acid in water) to B (0.1% formic acid in Acetonitrile) from 95:5 over 5 minutes and shifting to (A/B) to 5:95 at a flow rate of 0.2 mL/min. Protein solution (100 µL) was mixed with 200 µL of water in acetonitrile (50/50) and 10 µL was injected at a rate of 0.4 mL/min. with m/z range of 500 Da to 2500 Da. The collected mass spectrum data in continuum format were processed using MaxEnt1 software (Waters Corporation, USA) to obtain the protein mass.

2.3.3. Susceptibility of the Thrombin Sensitive Peptide (TSP) to spent bacterial media

The thrombin-sensitive peptide, HHHHHHDDDDKGF$_D$PRGFPAGG (TSP) was custom synthesized by standard Fmoc synthesis (WatsonBio, TX). The susceptibility of the peptide to the bacterial thrombin-like enzyme was assessed by exposing the peptide to media from an actively growing *S. aureus* culture [12]. Enzymatic activity of the media was initially determined by titrating culture exudate into a fluorogenic thrombin substrate, Boc-Val-Pro-Arg-MCA (Sigma Aldrich, MO) [25]. TSP was then exposed to the media with varying enzymatic activity and incubated at 37^{0}C with shaking. The sample was analyzed with HPLC (mobile phase 0.1% TFA/water (A) 0.1% TFA/Acetonitrile (B), under a gradient flow of 5-90% at a flow rate of 1.0 ml/min) every 12 hours through 48 hours. Protein was detected at a wavelength of 215 nm. A similar experiment was conducted with the recombinant spider silk to check the susceptibility of the silk protein to the bacterial enzyme.

2.3.4. Creation of silk-TSP conjugate

TSP was chemically grafted onto the silk peptide using EDC-NHS chemistry [26]–[28]. Lyophilized silk was dissolved in a reaction buffer (i.e., MES at a pH of 6). It was then activated by adding 100mM EDC [1-ethyl-3-(3-dimethylaminopropyl) carbodiimide hydrochloride] and 200mM excess of NHS (*N*-hydroxy sulfosuccinimide) and allowed to react for 30 minutes at room

temperature. The number of reactive carboxyl groups of silk were calculated and TSP was added to get an equimolar ratio of carboxy groups in silk and amine groups of TSP. The peptides were allowed to react for 3 hours at room temperature (i.e., conjugate). The formed conjugate was then dialyzed to remove the unconjugated TSP. Conjugate was then analyzed by Differential Scanning Calorimetry (DSC) and SDS-PAGE.

2.3.5. Determination of CAC of the silk peptide and the conjugate

Critical aggregation concentration (CAC) of silk was determined by a pyrene fluorescence method [29]. Briefly 24µg/ml (working concentration) of pyrene solution was prepared in acetone and evaporated. Silk peptide in phosphate buffer at different concentrations was then added to pyrene and the mixture was sonicated for 5 minutes and incubated for 1 hour. The fluorescence spectra of the samples was recorded at an excitation of 336 nm and emission from 360 – 450 nm wavelengths. Intensity peaks at 379 nm (I1) and 393 nm (I3) was recorded. The ratio of I1/I3 was plotted against log concentration and the point where a sharp inclination in the graph was noted as the CAC. The formed nanospheres [30], [31] were analyzed for size by zeta sizer and TEM.

2.3.6. Preparation of drug-loaded nanospheres

The model antibiotic drug vancomycin was used to prepare drug loaded nanospheres. A simple dissolution method was used to prepare nanospheres at three different ratios of protein:drug [32], [33]. Briefly, silk solution in phosphate buffer at higher than CAC was added slowly to vancomycin HCl drug solution in PBS and sonicated with probe sonicator for 5 minutes followed by bath sonication for an hour and incubation at room temperature for 1 hour. Drug loaded nanospheres were then analyzed for size by Dynamic Laser Scattering (DLS) and TEM.

To calculate the encapsulation efficiency, nanospheres were centrifuged at 15000 rpm for 1 hr, and the supernatant was analyzed by UV spectrophotometer at a wavelength of 280 nm for

the free drug. Following successful preparation of nanospheres of plain silk, drug loaded conjugate nanospheres were prepared. CAC of the conjugate was determined in the similar manner using pyrene fluorescence method and drug loaded nanospheres were prepared with vancomycin free base to incorporate the drug into the hydrophobic core of the nanospheres and analyzed by SEM.

2.3.7. Antibacterial activity of the conjugated nanospheres

Antibacterial activity of the nanospheres was tested by calculating the Minimum Inhibitory Concentration (MIC) using the microplate method and Kirby Bauer Zone of Inhibition [34], [35]. Briefly, to determine the MIC, a culture of *Staphylococcus aureus* (ATCC 49230) was incubated overnight at 37°C with shaking. The next day, the bacterial cell solution was diluted to 10^7 CFU/mL and different concentrations (ranging from 1ug/ml to 32 ug/ml) of either vancomycin free drug or vancomycin loaded nanospheres were added to the bacterial solution . Two hundred microliters of this bacterial/vancomycin suspension was seeded in a 96-well plate followed by incubation at 37 °C for 24 h. The optical density of each well was recorded on the microplate reader (Epoch, BioTek, VT). Selected concentrations of the particles surrounding the determined MIC were taken and ZOI was conducted by disc diffusion method. Briefly, 6mm discs were placed in 96-well plate and 200 µl of drug loaded particles were added to the wells and the discs were soaked for 24 hrs. After 24 hrs, the discs were dried and plated on S. *aureus* streaked on LB agar plates, and the cleared diameter was measured using digital calipers.

2.3.8. In vitro infection responsive activity

In vitro drug release was determined using a dialysis method in which drug loaded particles were incubated with bacterial growth media in dialysis tube (molecular weight cut off 7 KDa) [36]. The bacterial growth media was obtained from an overnight culture of *Staphylococcus aureus* (ATCC 49230) or *Staphylococcus epidermidis* (ATCC 14990) at 10^7CFU/mL. The culture was

centrifuged at 3000 rpm to separate the bacterial media from the cell pellet and 1.5 ml of each bacterial media was incubated with nanospheres separately. The dialysis tube was placed in a beaker containing PBS as release media under stirring. Release media was collected at predetermined time points and analyzed by UV-vis spectrometer (Spectramax m5, Molecular Devices, Downingtown, PA, USA) at 230 nm to determine the amount of released vancomycin from the nanospheres.

2.3.9. In vitro drug release study

To assess the release profile of the formulations, in vitro drug release was performed by dialysis method following the same protocol described above. The formulation was incubated for 48 hours with the bacterial media extracted from the *S. aureus* culture. The release media was collected for every 3 hours and analyzed for the drug release by UV-vis spectrometer. The amount of the drug release was plotted against time to create a drug release profile.

2.3.10. In vivo septic arthritis model

An initial pilot study was done in a modified induced septic arthritis rat model using a local inoculation of bacteria [37]–[39]. All studies were done under the supervision of the Institutional Animal Care and Use Committee (protocol A19068) at North Dakota State University. Sprague Dawley rats (n=3/cohort) were inoculated with 20µl of *S. aureus* culture (10^2 CFU/ml diluted into sterile PBS) directly injected into the synovial space of right knee joint of the rat under isoflurane anesthesia. Injections were done after shaving the joint and swabbing with betadine and isopropanol to sterile the site. The infection was allowed to develop for 48 hrs during which time the animal was closely monitored and pain was controlled with buprenorphine injections (0.03 mg/kg). Sterile buffer was injected into the other knee to act as a control. Development of disease was monitored by visible erythema and/or swelling of the joint along with hematological analysis

of synovial fluid and histopathological analysis. After 48 hrs, rats were euthanized by isoflurane overdose and synovial fluid was collected from the joint space prior to the disarticulation and further processing of the limb. Synovial fluid was spread on blood agar plates (VWR, Radnor, PA) [40] and incubated overnight at 37^0C. The number of colonies were counted the next day.

After establishing the septic arthritis disease model, treatment with either free drug, drug-loaded conjugate particles, or drug-loaded silk particles was given on day two after bacterial inoculation. Rats were divided into three treatment groups. The first group received drug loaded (14 mg/kg) conjugate nanoparticles in the infected knee locally delivered into the synovial joint space while the uninfected knee was injected with unloaded conjugate nanoparticles. The second group received drug loaded plain silk SX_2 particles into the infected knee while the uninfected knee was injected with unloaded SX_2 particles. The third group received free drug into the infected knee joint and sterile PBS into the uninfected knee. The treatment was continued for 48 hours after which rats were euthanized and limbs were collected for histopathological analysis. Before euthanasia, synovial fluid was collected from the joint space of the infected knee and the control knee and cultured on LB agar plates overnight. After incubation overnight, the number of colonies were counted.

Table 2.1. Cohort chart of animal groups.

Cohort	Bacteria	Formulation	Drug
0	Yes	No	No
1	Yes	Yes (conjugate)	Yes
2	Yes	Yes (SX2)	Yes
3	Yes	No	Yes

2.4. Results

2.4.1. Protein characterization

Two repetitive sequence of recombinant MaSp2 peptide (GGYGPGQQGPGGYGPGQQGPSGPGSAAAAAAAA with a six histidine tag and an enterokinase site N terminal was cloned and expressed in *E.coli*. The recombinant protein was purified using Ni-NTA resin for His-Tag purification and validated by SDS-PAGE, western blot and mass spectrometry. The theoretical molecular weight of the protein was predicted to be 14766 Da which was confirmed by a band on the SDS-PAGE corresponding to 15 kDa (Figure 2.2a). Molecular weight was additionally confirmed by Electro Spray mass spectrometry after running through UPLC and showed a peak at a mass of 14756 Da (Figure 2.2c). Finally, a western blot was performed with anti-His antibody which further validated the production of the recombinant silk protein (Figure 2.2b).

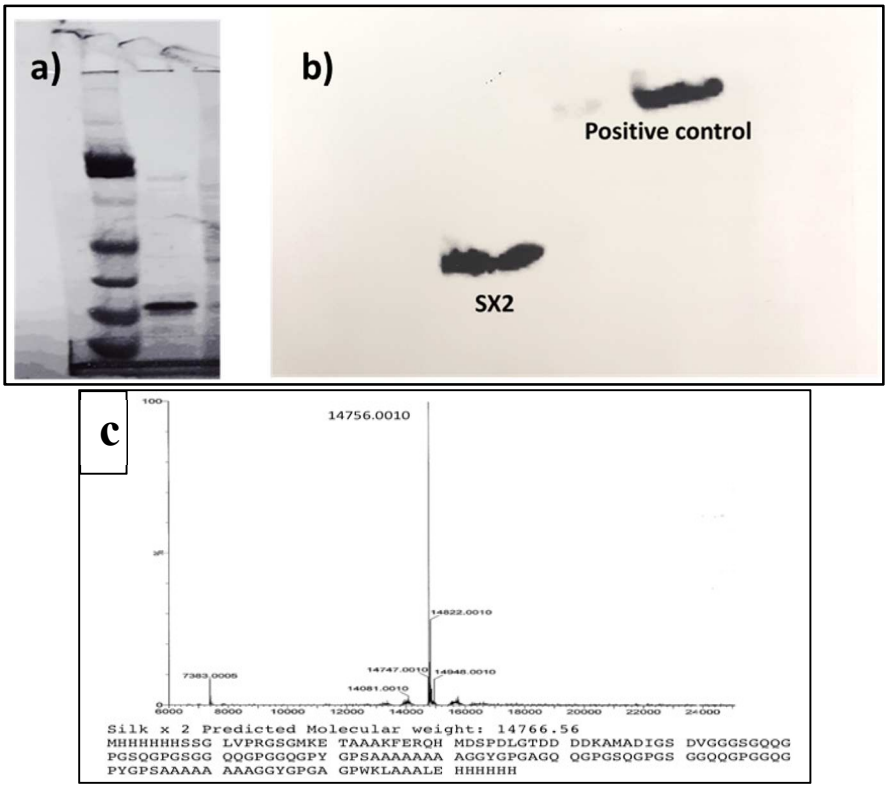

Figure 2.2. a) SDS-PAGE of the purified protein showing the band at 15kDa, b) western blot of the protein against anti-his antibody confirms the production of the protein, c) theoretical mass was predicted to be 14,766 Da while mass spectrometry of the silk protein was determined to be 14,756 Da.

2.4.2. Susceptibility of the thrombin sensitive peptide (TSP) and silk protein to the bacterial media

The susceptibility of the TSP to the bacterial thrombin-like enzyme was assessed by exposing the peptide to media from an actively growing *S. aureus* culture. Enzymatic activity of the bacterial culture was determined by a fluorogenic thrombin substrate, Boc-Val-Pro-Arg-MCA. TSP was initially titrated into media with varying enzymatic activity to determine the amount of enzyme required to cleave the peptide. The enzymatic activity was found to be 23 a.u. HPLC showed that TSP was cleaved within 12 hours of exposure of the peptide to the bacterial media (Figure 2.3a); whereas, the peptide was still intact upon exposure to water or even human thrombin at the same enzymatic activity (data not shown). Subsequently, susceptibility of the silk protein to

the bacterial thrombolytic enzyme was analyzed in a similar manner and showed no significant difference in the degradation of silk even after 48 hours at different concentrations of the media when compared to the control group without spent bacterial media (Figure 2.3b). This shows that TSP can be readily cleaved by the bacterial enzyme; whereas, silk protein is stable.

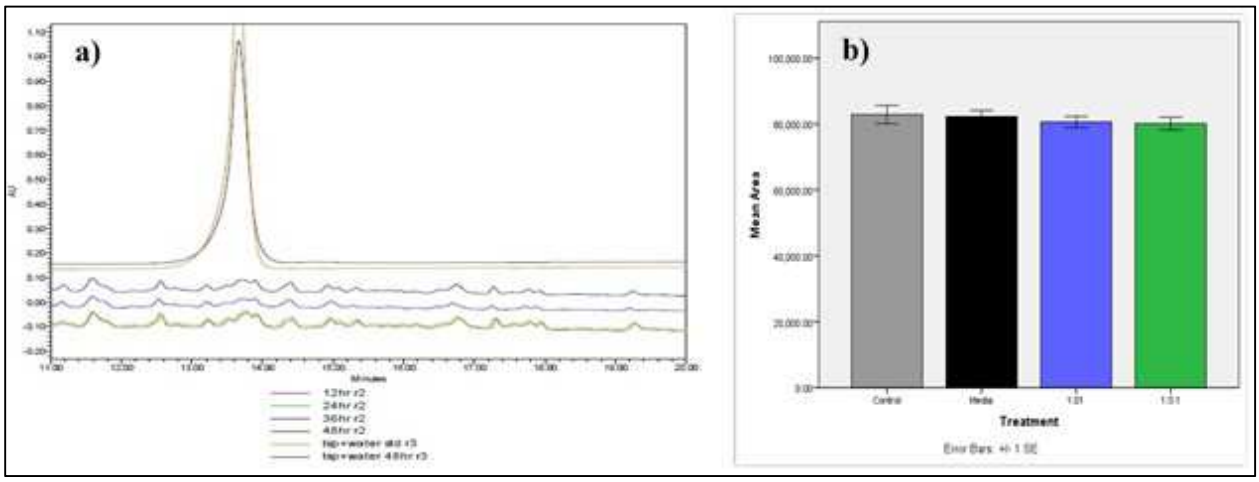

Figure 2.3. a) HPLC analysis of TSP exposed to the bacterial media from *S. aureus* culture shows cleavage of the peptide within 12 hrs of exposure to the media, b) analysis of silk peptide exposed to the bacterial media shows the stability of the peptide even after 48 hrs.

2.4.3. Creation of silk-TSP conjugate

Amide coupling by EDC/sulfo-NHS is one of the most commonly used strategies for cross-linking biomolecules. TSP was chemically grafted onto the silk peptide using EDC-NHS chemistry and confirmed by gel electrophoresis, which shows a shift in the band due to a slight increase in the molecular weight after conjugation (Figure 2.4a). It was also confirmed by DSC (Figure 2.4b) which produced an additional peak after conjugation that is different from both the reacting species.

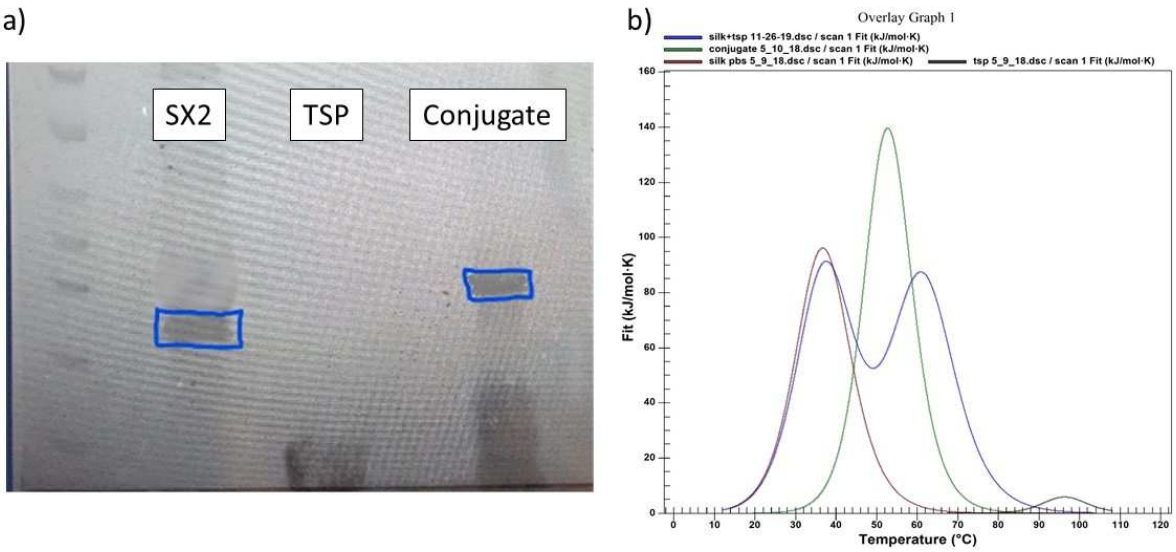

Figure 2.4. a) SDS PAGE showing the molecular weight difference between silk and the conjugate, b) DSC graph of silk, TSP and the conjugate showing increase in enthalpy of the conjugate.

2.4.4. Determination of CAC of the silk peptide and the conjugate and preparation of drug loaded nanospheres

Due to the amiphilic nature of the spidroins, they have the inherent ability to self assemble and form nanospheres. The CAC of plain silk was determined to be 1.2mg/ml (81µM) by pyrene fluorescence. The formed nanospheres were determined to be 164.3 ± 10.92 nm with a Poly Dispersity Index (PDI) of 0.3 ± 0.02 and Zeta potential of -16 (Figure 2.5). The size of the particles (less than 1µm) is not anticipated to impact the delivery of the particles. Vancomycin HCl was loaded into nanospheres at three different ratios of drug:protein using a dissolution method. Among different formulations, the first formulation containing drug:protein of 1:1 was found to have highest encapsulation efficiency of 56% with a size 184.2±11.9 nm (Table 2.2).

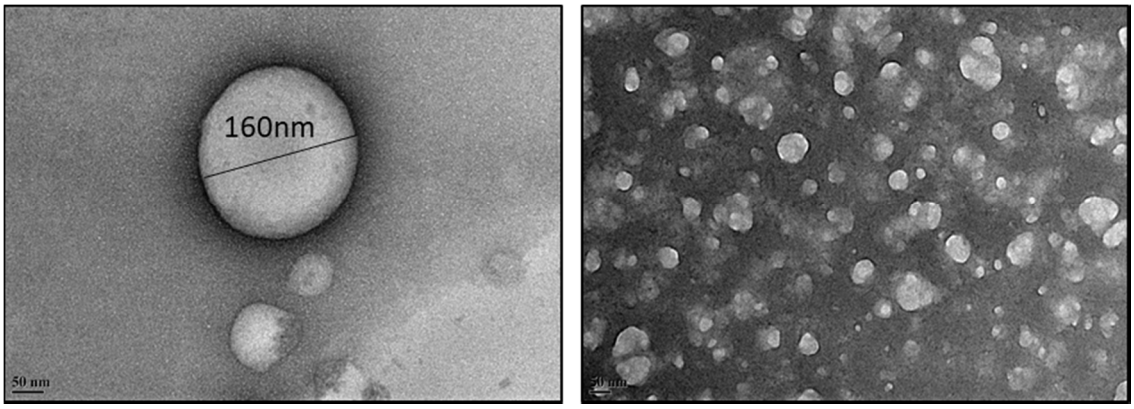

Figure 2.5. TEM images of silk nanospheres.

Table 2.2. Drug loading efficiency of silk micelles.

Protein : drug	EE (%)	Size (nm)	PDI
1:1	56	184.2 ± 11.9	0.29 ± 0.12
1:2	53.2	195.9 ± 3.9	0.4 ± 0.07
1:3	52.4	254.5 ± 12.8	0.4 ± 0.06

Drug loaded conjugate nanospheres were prepared in a similar manner. Prior to preparing the nanospheres, the CAC of the conjugate was determined by pyrene fluorescence and was found to be approximately 53.7 μM. Vancomycin free base was derived from vancomycin HCl, making the the drug hydrophobic and allowing it to be incorporated into the inner core. SEM of the conjugate micelles (Figure 2.6) confirmed the spherical architecture of the nanospheres. The highest encapsulation of the conjugate was found to be with 2mg of Vancomycin free base, which showed an encapsulation of 60% of the drug (data not shown). This increase in encapsulation of free base drug can also suggest that the drug is incorporated inside the core of the particle when compared to the hydrophilic form of the drug.

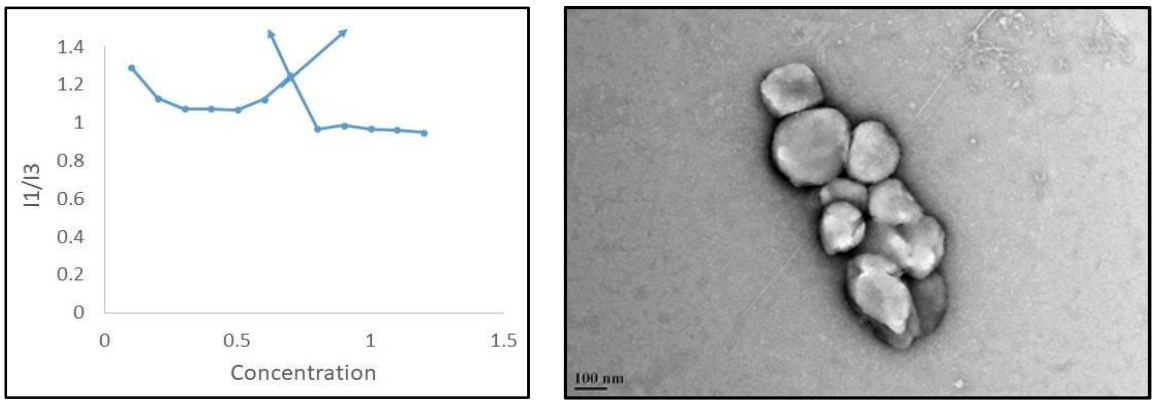

Figure 2.6. a) CAC of the conjugate as determined by pyrene fluorescence method, b) TEM mages of drug loaded conjugate nanospheres.

2.4.5. Antibacterial activity of the conjugate nanospheres

To explore the potential efficacy of this delivery system for the treatment of *S.aureus* septic arthritis, the antibacterial effect of Vancomycin-loaded nanospheres was first tested in vitro on *Staphylococcus aureus*. The Minimum Inhibitory Concentration (MIC) of Vancomycin free drug was determined to be 2µg/ml, while the MIC of the drug loaded nanospheres was found to be 16 µg/ml based on their OD values. Once the MIC was established, antibacterial activity was tested by a Kirby Bauer Zone of Inhibition assay. ZOI of the nanospheres was found to be 19.1mm (Figure 2.7) when compared to empty micelles, which is in accordance with the standard ZOI values of the free drug (>12mm) for SA.

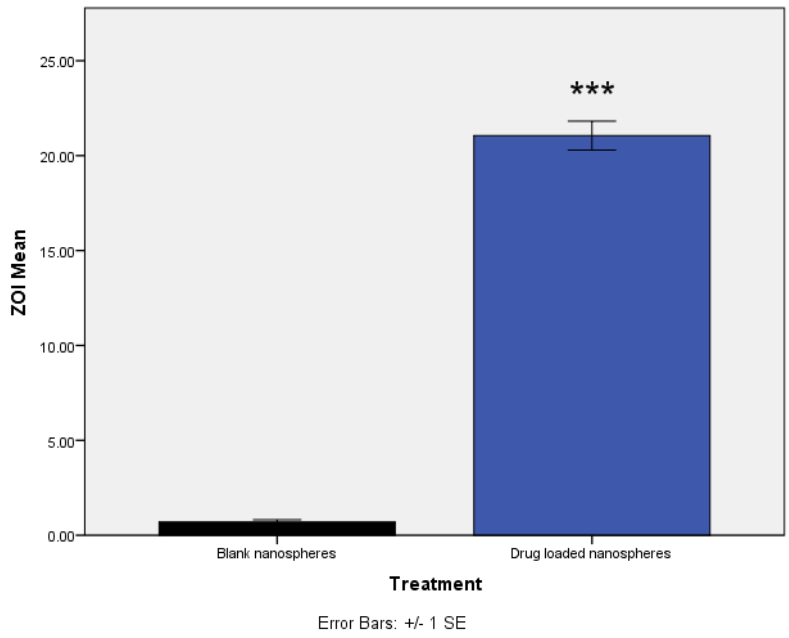

Figure 2.7. a) ZOI of drug loaded conjugate micelles at different concentrations b) ZOI of blank micelles and drug loaded micelles at MIC.

2.4.6. In vitro infection responsive activity

The release profile of the drug loaded (2mg) nanospheres under various conditions was recorded to evaluate infection responsive drug release. After 24 hrs of incubation, cumulative release of drug from the silk/TSP conjugate particles was recorded as 84.4% when exposed to the media from *Staphylococcus aureus*. The cumulative release from conjugate particles in the absence of media was found to be 18.9%. Plain silk particles showed a release of 15.6% and 17.5% when exposed to the media from SA and buffer respectively (Figure 2.8), indicating that although the silk particles do not show infection responsive release, they do seem to be leaky. In order to confirm the infection responsive release in the presence of SA specific enzymes, the release profile of conjugate particles was also determined in the presence of media from *S. epidermidis*. Drug release in response to *S. epidermidis* was found to be 20.8%, which is slightly greater than control particles.

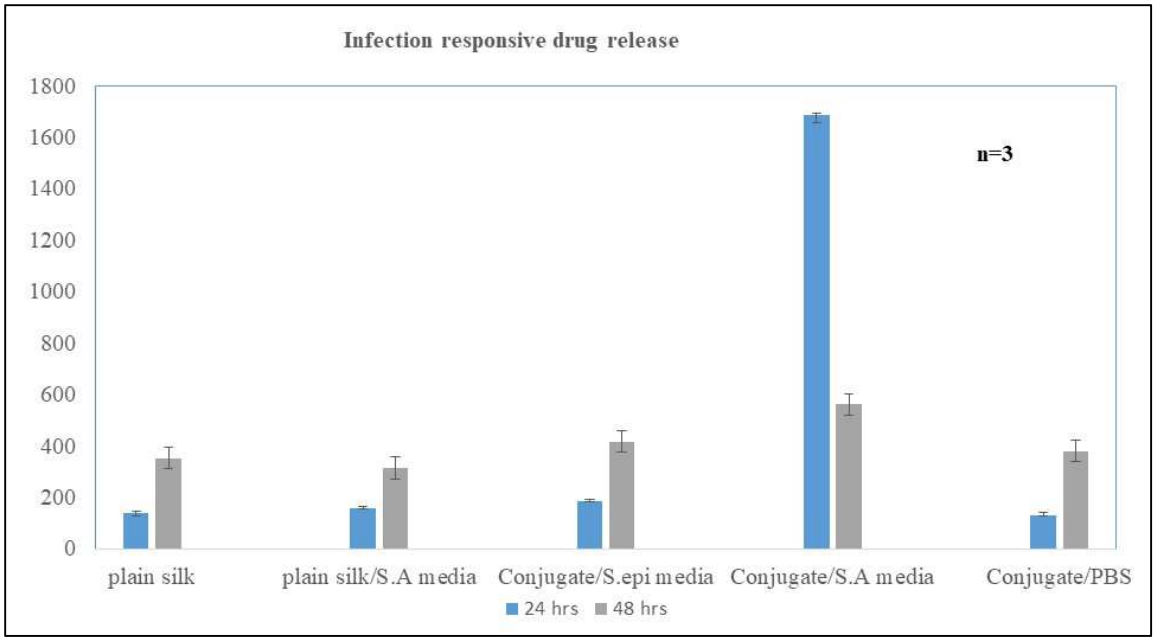

Figure 2.8. In vitro infection responsive release of the drug loaded particles against different media.

2.4.7. In vitro drug release study

Using a dialysis method an infection responsive drug release curve was established, showing maximum release of the drug (85%) was achieved within 12 hours with the release slowly declining over time, giving an almost bell shaped curve (Figure 2.9).

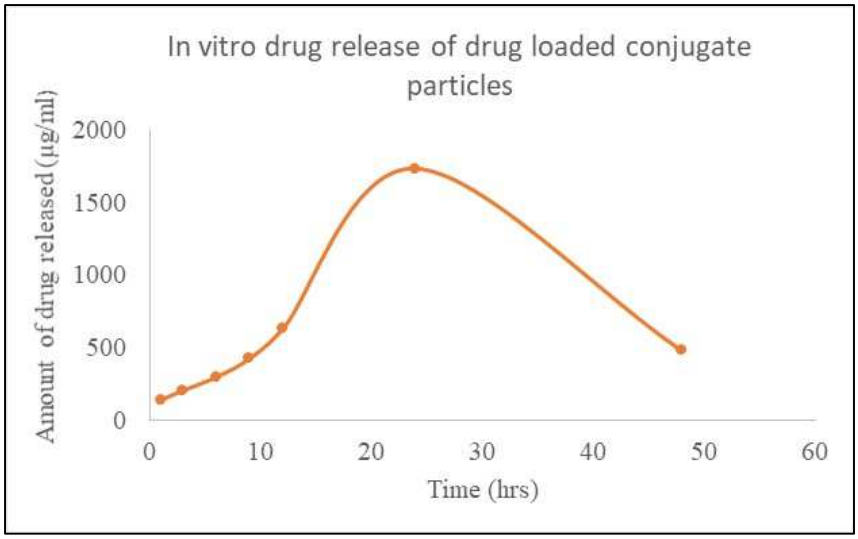

Figure 2.9. In vitro drug release profile of the drug loaded conjugate nanospheres in the presence of bacterial media.

2.4.8. In vivo drug release in septic arthritis model

The disease model was established by inoculating the bacteria at a concentration of 10^2 CFU/ml directly into the knee joint. After 48 hrs, synovial fluid was collected from both the infected and uninfected knee joints prior to collecting the joints. An overnight culture of the synovial fluid from the infected showed a lawn of bacteria while the uninfected knee did not grow any bacteria. The knees were also visually inspected for erythema and inflammation which further confirms the development of septic arthritis. Treatment was given on day two. Bacterial culture from group one drug loaded conjugate particles showed an average of 40 CFU/ml whereas group two containing drug loaded SX2 particles showed 810 CFU/ml on an average (Figure 2.10). This confirms in vivo infection responsive release of the drug.

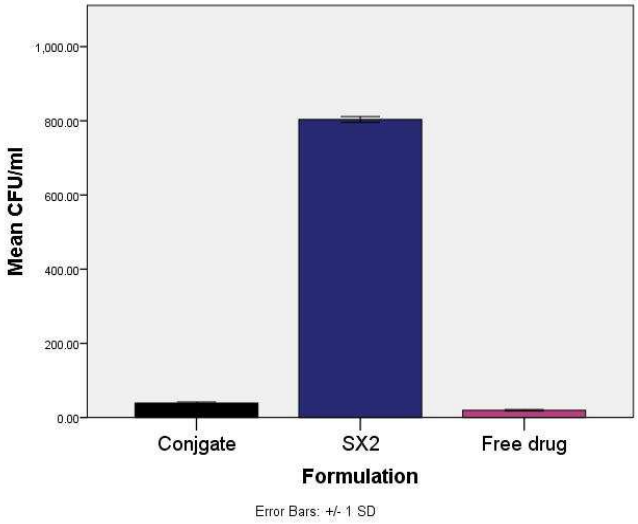

Figure 2.10. Colony count assay on synovial culture of the infected knee after treatment.

2.5. Discussion

Development of smart drug delivery systems as an alternative to new drug discovery is essential to address the rising tide of resistance. Advances in drug delivery are lagging behind more traditional approaches to expand current drug classifications to address resistance; an emphasis should be placed on disease-responsive, local drug delivery systems. Disease-responsive

elements might be integrated into characterized block copolymer biomimetics such as silk. Compared to systemic antibiotic administration, local drug delivery can decrease antibiotic dosing, avoid issues of patient compliance, and limit systemic side effect. Despite these advantages, clinical implementation and efficacy of many local antibiotic delivery systems (e.g. antibiotic loaded bone cement, etc.) is limited by a bolus jettison of drug followed by sub-therapeutic antibiotic leaching [41]. A better strategy may lie in microenvironment triggered local drug release systems capable of providing disease or tissue targeted local drug delivery with the potential to overwhelm drug resistance mechanisms [9], [42]. Tissue targeting, half-life, and pharmacokinetics are all aspects of controlled drug delivery systems that can be customized by modifying the drug delivery/encapsulating matrix. Molecularly manipulating bioinspired polymers that have defined structure activity relationships (SARS) allows the design of smart biomaterials with embedded "protease switches" to act as an environmentally responsive drug delivery system. Spider silk mimicking MaSp2 peptides can be designed to include not only a balance of hydrophobic and hydrophilic amino acid blocks suitable for self-assembling nanosphere formation but also a protease-responsive element in a single innovative biopolymer drug delivery system.

Creating the recombinant silk peptide with an integrated thrombin-sensitive element required 1) the chemical synthesis of a thrombin-sensitive peptide and 2) the expression and purification of a recombinant silk peptide. The thrombin-sensitive peptide, was commercially synthesized using standard Fmoc synthesis and confirmed by HPLC (data not shown) and mass spectrometry. Concurrently, a recombinant MaSp2 peptide $(GGYGPGQQGPGGYGPGQQGPSGPGSAAAAAAAA)_2$ with a six histidine tag and an enterokinase site N terminal to the silk like peptide was cloned and expressed in *E.coli*. The susceptibility of the peptide to the bacterial thrombin-like enzyme was assessed by exposing the

TSP/silk conjugate to media from an actively growing *S. aureus.* TSP was cleaved within 12 hours of exposure to the bacterial media but was intact even after 24 hours of exposure to the human thrombin or water controls and showed minimal degradation in human thrombin after 48 hours (n=3, Figure 2.3a). The proteolytic stability of the silk peptide still shows the presence of stable peptide (Figure 2.3b), indicating that TSP was selectively cleaved by the enzyme. Subsequently, TSP was chemically grafted onto the silk peptide using EDC-NHS chemistry. The conjugate was analyzed initially by SDS-PAGE (Figure 2.4a), which showed a band slightly higher than the SX_2. Since TSP is a very small peptide, gel electrophoresis is not precise in indicating the difference between conjugate and silk protein. Therefore, conjugate was further analyzed by Differential Scanning Calorimetry (DSC) (Figure 2.4b). Notice that silk without TSP is shown in the dashed line, TSP alone is shown as a solid blue line (smallest peak) while the conjugate (solid black line) showed a shift in transition temperature in between that of silk and TSP and an increased intensity. After confirming that the conjugate was produced, the silk/TSP conjugate peptide was allowed to self-assemble into nanospheres. Unlike many other protease drug release systems that use a protease sensitive linker peptide to tether their drug payload to an insoluble matrix, spider silk peptides can be directly engineered to not only incorporate a protease sensitive element but also to promote self assembly via salting out [21], [43] into micelles and microcapsules [20], allowing direct encapsulation of bioactive drug. From the pyrene fluorescence method, the CAC for silk was determined to be 1.2 mg/ml and formed nanospheres were characterized by Zetasizer, which showed an average size of the particles to be 184.2 ± 11.9 nm with a negative zeta potential (Table 2.1) as expected for the amino acid sequence of Masp2. After establishing the self assembly of silk particles, CAC of the conjugate was also determined in the similar manner and drug loaded conjugate nanospheres were prepared (Figure 2.6a). SEM of the conjugate nanospheres (Figure

2.6b) confirmed the spherical architecture of the nanospheres. TSP did not form nanospheres in the absence of silk. The formed nanospheres were analyzed for size using both a zeta sizer and TEM and was found to be 164.3 ± 10.92 nm.

After forming the nanospheres, antibacterial activity of the formulation was evaluated by determining the MIC of the drug loaded formulation and compared with the free drug. MIC of the nanospheres was 16 μg/mL, which showed a ZOI of 19.1 mm, corresponding to standard ZOI values for the unencapsulated drug (Figure 2.7a). Blank formulations did not show any ZOI suggesting that the drug is released from the encapsulated nanospheres to show antimicrobial activity (Figure 2.7b). Infection responsive release was assessed by exposing the formulations to different types of media. When exposed to the media from *S. aureus* the conjugate showed a release of 85% and silk without TSP showed 15% (Figure 2.8), suggesting that TSP was cleaved by the bacterial enzyme to burst the nanospheres and release the drug whereas, plain silk was unable to rupture in the presence or absence of the enzyme. Furthermore, to confirm the specificity of the enzymatic release, drug loaded formulations were also exposed to the media from *S. epidermidis*, which showed release similar to PBS, suggesting that vancomycin release was specific to enzyme secreted from *S. aureus*. The drug release profile was established in the same manner of dialysis to assess whether the formulation showed an immediate release profile and the duration of release. It showed that drug release reached maximum in 24 hrs (Figure 2.9) and started to decline throughout the remainder of the study. The release also corelates with the antibiotic release reported in the literature which showed maximum release of antibiotic within 24 hrs of incubation [12]. This is again in correspondence with the initial HPLC evaluation of susceptibility of TSP, which showed that the TSP was cleaved within 12 hrs although the formulation showed only 75% of release potentially due to the saturation of the enzyme in the media.

Finally, to assess the efficacy of the infection-triggered drug release system, the nanospheres were evaluated in a septic arthritis model. Septic arthritis is an inflammatory disease of the joints commonly caused by *Staphylococcus aureus* [39]. Typically, it is considered a secondary infection since the bacteria escapes from the blood stream and localizes in one large joint such as the knee or hip but can also affect any other joint. Although systemic bacterial inoculation represents the accurate way to simulate disease development, it takes roughly about 21 days for the disease to develop in animal models [38]. In order to hasten the disease development, septic arthritis was induced by local inoculation of the bacteria into the joint space. Systemic antibiotic therapy for 2 – 6 weeks [44] is the usual prescribed treatment for septic arthritis. In cases like septic arthritis, local delivery of the antibiotic appears to be a better approach than the systemic delivery. Therefore, the septic arthritis model selected to test the local release of the drug from the formulations in the presence of infection was appropriate since it is a localized infection. Although systemic bacterial inoculation represents the accurate way to simulate disease development, it takes roughly about 21 days for the disease to develop in animal models [39]. In order to hasten the disease development, septic arthritis was induced by local inoculation of the bacteria into the joint space. Septic arthritis was developed within 24 hrs of infection as confirmed by synovial culture and visual inspection of the knee joint. After the treatment, drug loaded conjugate particles showed significantly more bacterial clearing than drug loaded plain silk SX2 particles (Figure 2.10.). Some bacterial clearing was also observed with SX2 which suggests leakiness of the particles.

2.6. Conclusion

Systemic administration of antibiotics is a common practice for wound infections and infections after hip or knee replacement surgeries. Apart from long duration of treatment, systemic

administration causes unnecessary toxicity and poor penetration into the tissues may require higher doses. Lower concentrations at the disease site also augment development of resistance by the bacteria. In such cases localized delivery is more advantageous in terms of dosing and also frequency of administration. Thus, we developed infection responsive spider silk nanospheres which can release the drug only at the site of infection. Use of spider silk as a drug carrier provides the advantage of encapsulating large amount of drug without leaching due to elastic and mechanical properties. Local delivery of these particles also ensures that the particles can release required concentration of the drug at the disease site. This study also paves way to develop other disease specific drug release models by developing peptide linkers sensitive to specific enzymes related to the disease.

2.7. Acknowledgements

This research was supported by NIH grant R03 111418 We thank Jayma and Scott Payne for their help with the SEM and TEM imaging. Funding for the Core Synthesis and Analytical Services Facility used in this publication was made possible by NIH Grant P30 GM103332 (NIGMS). Manuscript contents are solely the responsibility of the authors and do not necessarily represent the official views of the NIH.

2.8. References

[1] D. J. Rosenberg, “Infections, bacterial resistance, and antimicrobial stewardship: the emerging role of hospitalists,” *J. Hosp. Med.*, vol. 7 Suppl 1, pp. S34-43, 2012.

[2] A. Rodríguez-Rojas, J. Rodríguez-Beltrán, A. Couce, and J. Blázquez, “Antibiotics and antibiotic resistance: A bitter fight against evolution,” *Int. J. Med. Microbiol.*, vol. 303, no. 6, pp. 293–297, Aug. 2013.

[3] B. D. Brooks and A. E. Brooks, “Therapeutic strategies to combat antibiotic resistance,” *Adv. Drug Deliv. Rev.*, vol. 78, pp. 14–27, Nov. 2014.

[4] N. Woodford and M. J. Ellington, “The emergence of antibiotic resistance by mutation,” *Clin. Microbiol. Infect.*, vol. 13, no. 1, pp. 5–18, Jan. 2007.

[5] A. Budimir, “Fighting Antimicrobial Resistance,” p. 414.

[6] P. Wu and D. W. Grainger, “Drug/device combinations for local drug therapies and infection prophylaxis,” *Biomaterials*, vol. 27, no. 11, pp. 2450–2467, Apr. 2006.

[7] D. Gomes, M. Pereira, and A. F. Bettencourt, “Osteomyelitis: an overview of antimicrobial therapy,” *Braz. J. Pharm. Sci.*, vol. 49, no. 1, pp. 13–27, Mar. 2013.

[8] J. Zhou, A. L. Loftus, G. Mulley, and A. T. A. Jenkins, “A Thin Film Detection/Response System for Pathogenic Bacteria,” *J. Am. Chem. Soc.*, vol. 132, no. 18, pp. 6566–6570, May 2010.

[9] M.-H. Xiong, Y.-J. Li, Y. Bao, X.-Z. Yang, B. Hu, and J. Wang, “Bacteria-Responsive Multifunctional Nanogel for Targeted Antibiotic Delivery,” *Adv. Mater.*, vol. 24, no. 46, pp. 6175–6180, Dec. 2012.

[10] R. de la Rica, D. Aili, and M. M. Stevens, “Enzyme-responsive nanoparticles for drug release and diagnostics,” *Adv. Drug Deliv. Rev.*, vol. 64, no. 11, pp. 967–978, Aug. 2012.

[11] “Enzyme-responsive materials for wound infection diagnosis,” *Biotechnol. Bioeng.*, vol. 113, no. 12, pp. 2534–2534, Dec. 2016.

[12] M. Tanihara, Y. Suzuki, Y. Nishimura, K. Suzuki, Y. Kakimaru, and Y. Fukunishi, “A novel microbial infection-responsive drug release system,” *J. Pharm. Sci.*, vol. 88, no. 5, pp. 510–514, May 1999.

[13] Y. Suzuki, M. Tanihara, Y. Nishimura, K. Suzuki, Y. Kakimaru, and Y. Shimizu, "A new drug delivery system with controlled release of antibiotic only in the presence of infection," *J. Biomed. Mater. Res.*, vol. 42, no. 1, pp. 112–116, Oct. 1998.

[14] P. Panizzi, R. Friedrich, P. Fuentes-Prior, K. Richter, P. E. Bock, and W. Bode, "Fibrinogen Substrate Recognition by Staphylocoagulase·(Pro)thrombin Complexes," *J. Biol. Chem.*, vol. 281, no. 2, pp. 1179–1187, Jan. 2006.

[15] M. Tanihara, Y. Suzuki, Y. Nishimura, K. Suzuki, and Y. Kakimaru, "Thrombin-sensitive peptide linkers for biological signal-responsive drug release systems," *Peptides*, vol. 19, no. 3, pp. 421–425, 1998.

[16] G. H. Altman *et al.*, "Silk-based biomaterials," *Biomaterials*, vol. 24, no. 3, pp. 401–416, Feb. 2003.

[17] S. Kapoor and S. C. Kundu, "Silk protein-based hydrogels: Promising advanced materials for biomedical applications," *Acta Biomater.*, vol. 31, pp. 17–32, Feb. 2016.

[18] L.-D. Koh *et al.*, "Structures, mechanical properties and applications of silk fibroin materials," *Prog. Polym. Sci.*, vol. 46, pp. 86–110, Jul. 2015.

[19] Y. Wang, H.-J. Kim, G. Vunjak-Novakovic, and D. L. Kaplan, "Stem cell-based tissue engineering with silk biomaterials," *Biomaterials*, vol. 27, no. 36, pp. 6064–6082, Dec. 2006.

[20] K. D. Hermanson, D. Huemmerich, T. Scheibel, and A. R. Bausch, "Engineered Microcapsules Fabricated from Reconstituted Spider Silk," *Adv. Mater.*, vol. 19, no. 14, pp. 1810–1815, Jul. 2007.

[21] U. K. Slotta, S. Rammensee, S. Gorb, and T. Scheibel, "An Engineered Spider Silk Protein Forms Microspheres," *Angew. Chem. Int. Ed.*, vol. 47, no. 24, pp. 4592–4594.

[22] O. S. Rabotyagova, P. Cebe, and D. L. Kaplan, "Self-Assembly of Genetically Engineered Spider Silk Block Copolymers," *Biomacromolecules*, vol. 10, no. 2, pp. 229–236, Feb. 2009.

[23] Y. Hsia, E. Gnesa, R. Pacheco, K. Kohler, F. Jeffery, and C. Vierra, "Synthetic spider silk production on a laboratory scale," *J. Vis. Exp. JoVE*, no. 65, p. e4191, Jul. 2012.

[24] F. Teulé *et al.*, "A protocol for the production of recombinant spider silk-like proteins for artificial fiber spinning," *Nat. Protoc.*, vol. 4, no. 3, pp. 341–355, 2009.

[25] T. Morita, H. Kato, S. Iwanaga, K. Takada, T. Kimura, and S. Sakakibara, "New Fluorogenic Substrates for α-Thrombin, Factor Xa, Kallikreins, and Urokinase," *J. Biochem. (Tokyo)*, vol. 82, no. 5, pp. 1495–1498, Nov. 1977.

[26] D. Bartczak and A. G. Kanaras, "Preparation of Peptide-Functionalized Gold Nanoparticles Using One Pot EDC/Sulfo-NHS Coupling," *Langmuir*, vol. 27, no. 16, pp. 10119–10123, Aug. 2011.

[27] M. J. E. Fischer, "Amine Coupling Through EDC/NHS: A Practical Approach," in *Surface Plasmon Resonance*, vol. 627, N. J. Mol and M. J. E. Fischer, Eds. Totowa, NJ: Humana Press, 2010, pp. 55–73.

[28] N. Zegers, K. Gerritse, C. Deen, W. Boersma, and E. Claassen, "An improved conjugation method for controlled covalent coupling of synthetic peptides to proteins using glutaraldehyde in a dialysis method," *J. Immunol. Methods*, vol. 130, no. 2, pp. 195–200, Jul. 1990.

[29] G. Basu Ray, I. Chakraborty, and S. P. Moulik, "Pyrene absorption can be a convenient method for probing critical micellar concentration (cmc) and indexing micellar polarity," *J. Colloid Interface Sci.*, vol. 294, no. 1, pp. 248–254, Feb. 2006.

[30] G. Gaucher, M.-H. Dufresne, V. P. Sant, N. Kang, D. Maysinger, and J.-C. Leroux, "Block copolymer micelles: preparation, characterization and application in drug delivery," *J. Controlled Release*, vol. 109, no. 1, pp. 169–188, Dec. 2005.

[31] "The method of purifying bioengineered spider silk determines the silk sphere properties | Scientific Reports." [Online]. Available: https://www.nature.com/articles/srep28106. [Accessed: 29-Jul-2018].

[32] K. Cholkar, A. Patel, A. D. Vadlapudi, and A. K. Mitra, "Novel Nanomicellar Formulation Approaches for Anterior and Posterior Segment Ocular Drug Delivery," *Recent Pat. Nanomedicine*, vol. 2, no. 2, pp. 82–95, 2012.

[33] A. Mandal, R. Bisht, I. D. Rupenthal, and A. K. Mitra, "Polymeric micelles for ocular drug delivery: From structural frameworks to recent preclinical studies," *J. Control. Release Off. J. Control. Release Soc.*, vol. 248, pp. 96–116, Feb. 2017.

[34] J. A. Lepe, J. Domínguez-Herrera, J. Pachón, and J. Aznar, "Determining accurate vancomycin MIC values for methicillin-resistant Staphylococcus aureus by the microdilution method," *J. Antimicrob. Chemother.*, vol. 69, no. 1, pp. 136–138, Jan. 2014.

[35] A. F. Radovic-Moreno, T. K. Lu, V. A. Puscasu, C. J. Yoon, R. Langer, and O. C. Farokhzad, "Surface Charge-Switching Polymeric Nanoparticles for Bacterial Cell Wall-Targeted Delivery of Antibiotics," *ACS Nano*, vol. 6, no. 5, pp. 4279–4287, May 2012.

[36] Y. Cong *et al.*, "Alendronate-decorated biodegradable polymeric micelles for potential bone-targeted delivery of vancomycin," *J. Biomater. Sci. Polym. Ed.*, vol. 26, no. 11, pp. 629–643, 2015.

[37] W. Reizner, J. G. Hunter, N. T. O'Malley, R. D. Southgate, E. M. Schwarz, and S. L. Kates, "A systematic review of animal models for Staphylococcus aureus osteomyelitis," *Eur. Cell. Mater.*, vol. 27, pp. 196–212, Mar. 2014.

[38] F. dos S. Batista, O. Malafaia, J. M. Ribas Filho, N. G. Czeczko, and J. C. D. Repka, "Model of septic arthritis by intravenous inoculation of Staphylococcus aureus in Wistar rats," *Acta Cir. Bras.*, vol. 19, no. suppl 1, pp. 42–50, Dec. 2004.

[39] P. M. Colavite and A. Sartori, "Septic arthritis: immunopathogenesis, experimental models and therapy," *J. Venom. Anim. Toxins Trop. Dis.*, vol. 20, p. 19, May 2014.

[40] A. Heininger, M. Binder, S. Schmidt, K. Unertl, K. Botzenhart, and G. Döring, "PCR and Blood Culture for Detection of Escherichia coli Bacteremia in Rats," *J. Clin. Microbiol.*, vol. 37, no. 8, pp. 2479–2482, Aug. 1999.

[41] H. S. Gold and R. C. Moellering, "Antimicrobial-Drug Resistance," *N. Engl. J. Med.*, vol. 335, no. 19, pp. 1445–1453, Nov. 1996.

[42] B. F. Gilmore, "Proteases As Selective Activators Of Triggered Drug Release: A Potential Answer To The Problem Of Biomaterial-Associated Infections?," *J. Biotechnol. Biomater.*, vol. 02, no. 05, 2012.

[43] A. Lammel, M. Schwab, U. Slotta, G. Winter, and T. Scheibel, "Processing Conditions for the Formation of Spider Silk Microspheres," *ChemSusChem*, vol. 1, no. 5, pp. 413–416.

[44] "Septic arthritis - Diagnosis and treatment - Mayo Clinic." [Online]. Available: https://www.mayoclinic.org/diseases-conditions/bone-and-joint-infections/diagnosis-treatment/drc-20350760. [Accessed: 08-Aug-2019].

CHAPTER 3. A RECOMBINANT HEPARIN-BINDING MAJOR AMPULLATE SPIDROIN 2 (MASP2) SILK PROTEIN

3.1. Abstract

Peptide units comprising major ampullate spider silk like peptide confer a balance of strength and extensibility governed by established structure-property relationships. Small peptides correlated to specific functionalities can be recombined within these units to create designer silk fibers with new hybrid properties. In this study, a small basic peptide (ARKKAAKA) known to both bind heparin and mimic an antimicrobial peptide, was genetically linked to a protease-resistant, mechanically robust silk like peptide, MaSp2, endowing spider silk with new heparin-binding and antimicrobial capabilities. Purified fusion proteins (four silk domains and four heparin-binding peptide repeats) were expressed in E. coli. Successful fusion of a MaSp2 spider silk peptide with this heparin-binding motif was shown with analytical assays. Furthermore, the ability of the fusion peptide to bind heparin and inhibit bacterial growth was also assessed. Using this strategy, we were able to link two individual genetic motifs to create a designer recombinant silk like protein with improved blood compatibility and antimicrobial properties.

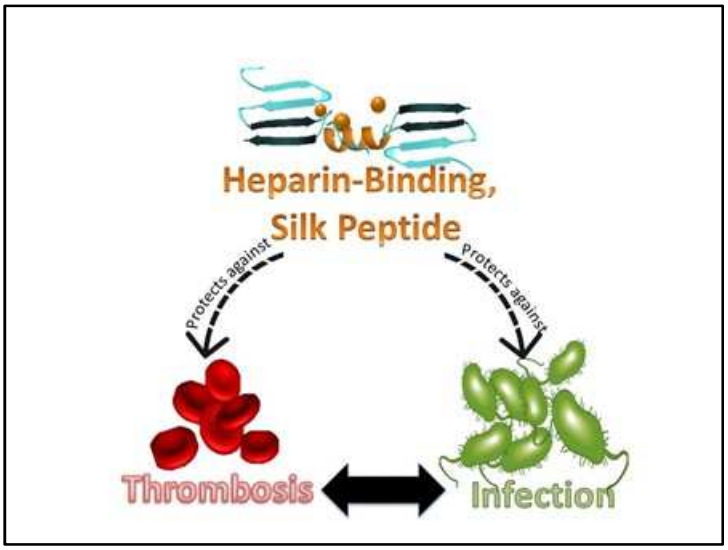

Figure 3.1. Infection and thrombosis are intimately connected. This is of particular concern for hemodialysis catheters and other blood-contacting medical devices. The heparin-binding motif (HBM) can both bind heparin to influence blood contact activation cascades and also elicit antimicrobial properties. Thus, genetically linking heparin-binding motif with a protease-resistant silk protein to bind heparin, both from solution as well as at a surface could be used as a medical device coating to improve blood compatibility and limit infection risks.

3.2. Introduction

Major ampullate spider silk's intrinsic balance of dichotomous mechanical properties, unrivaled strength and impressive recoverable deformation, is provided by structural hierarchy rooted in the biochemical composition of two proteins, MaSp1 and MaSp2 [1], [2]. Phylogenetic analyses of these major ampullate sequences revealed an evolutionarily conserved sequence of repetitive amino acid motifs thought to correlate to specific structural and functional features [3]. The component amino acid motifs of major ampullate spider silk have been well-studied by producing clones of simplistic monomer motifs [4–7] to identify and establish overarching structure-property relationships [3], [8]. In addition to mechanical properties that can be manipulated by genetically combining motifs correlated with specific properties [1,3], several recombinant spider silk fusion proteins have been explored to date (i.e., silk-uranium binding proteins [9], silk-antibiotic [10], silk-silica binding proteins [11], [12], silk-bone sialoprotein [13],

silk-elastin [14] etc.), providing additional biological functions. Silk was also recently complexed with heparin and chitosan to create an anticoagulant, antimicrobial, dual functional protein [15]. This manuscript describes a new genetic modification of silk designed to exploit a peptide sequence repeat encoded to not only capture circulating heparin, facilitating repeated heparin-surface association and disassociation, but also to endow silk with intrinsic antimicrobial properties.

Heparin, a hydrophilic, highly sulfonated negatively charged polysaccharide copolymer comprised of glucosamine and glucuronic acid, is endogenously found in the human body (approximately 20 μg/ml in adult plasma) and commonly used as an extracorporeal anticoagulant at therapeutic concentrations over 50 nM [8], [16], [17]. Importantly, heparin is naturally bound by a diverse family of heparin-binding proteins [18]–[20], based on electrostatic interactions where positively charged, basic amino acid residues in the Heparin Binding amino acid Motif (HBM) of these proteins interact through ionic and hydrogen bonds with the strongly negatively charged sulfate and carboxylate groups on the heparin polysaccharide [18], [21]. Furthermore, the tertiary structure of the HBM is analogous to an antimicrobial peptide (AMP) [22], [23], with the overall structure XBBBXXBX (X – hydrophobic or uncharged amino acid, B – basic amino acid). Previous work has sought to exploit surface-bound HBM to create heparinized surfaces [24], [25]. These efforts were able to successfully bind solution-phase heparin, with the best binding affinity based on four concatenated repeats of the synthetic motif (ARKKAAKA, 42 ± 15 nm) [25]. This peptide is analogous to the LL-37 antimicrobial peptide, which can be proteolytically degraded by human neutrophil-produced elastase as well as P.aeruginosa elastase and S.aureus V8 metalloproteinase and aureolysin [26]. Accordingly, bound heparin bioactivity was shown to be reduced by proteolytic cleavage [24], [27]. Therefore, utilizing a heparin-binding motif as a surface

capture agent for circulating heparin necessitates embedding the protease-susceptible peptide into a protective polymer background. A biological and structural biopolymer fusion, such as using major ampullate spider silk with HBMs, may provide such a suitable background to permit heparin capture and stability for possible further technological use in biomaterials.

In this context, we sought to genetically embed a small heparin-binding amino acid motif (HBM) into a recombinant protease-resistant silk like protein [28], [31], to ultimately create a chimera with new biomaterials properties as conceptually described in figure 3.1.

Although many other silk fusion proteins have been explored [32] (e.g., antibiotics [10], [33], chitosan [15], elastin [14], silica [11], [12], [34], RGD [35], this recombinant fusion protein seeks to uniquely combine silk's recognized mechanical properties with HBM's known biological activity, creating a robust, naturally heparin-binding, antimicrobial biomaterial. By genetically embedding four concatenated repeats of the heparin-binding motif, ARKKAAKA, in a background of MaSp2 amino acid motifs (GPGXX and A), a mechanically robust new protein material capable of both (1) binding biologically active heparin and (2) resisting pathogen colonization is produced, potentially allowing both anticoagulation and anti-infectivity during in vivo applications [36]. Here we report the design, production, and characterization of a new recombinant silk fusion protein with the ability to bind heparin, endowing it with limited anticoagulant and in vitro antimicrobial properties.

3.3. Methods

3.3.1. Protein expression and purification

The complete genetic sequence (two repeats of silk (SX2), two repeats of silk linked with four repeats of HBM (S2H4) and four repeats of silk linked with four repeats of HBM (S4H4)) was synthesized and cloned directly into pET 30a by GenScript (USA).

All proteins were expressed in E.coli BL21(DE3) pLysS cells (Promega, USA). Cultures were grown in 37°C LB medium containing 100µg/ml Kanamycin with shaking to an OD600 between 0.8 and 1.0. Isopropyl-β-D-1-thiogalactopyranoside (IPTG, Sigma-Aldrich, USA) was added at a final concentration of 1mM to induce the expression. After 2 hours, the culture was centrifuged at 8000 rpm for 10 minutes and the media was decanted. Cell pellets were resuspended in 100mM HEPES buffer (1/10 of the final culture volume). To achieve better yields and higher purity, 50 µg/ml DNase I (Sigma) and 1 µL of protease inhibitor cocktail (Sigma-Aldrich, USA) per 100µL of harvested expression culture was added prior to sonication (30 seconds at 40% power) and purification. Proteins were purified using nickel affinity chromatography. To identify the highest yield clones from each construct, the Maxwell® 16 Polyhistidine Protein Purification system (Promega, USA) was used according to the manufacturer's instructions for the prefilled nickel affinity reagent cartridge (Promega, USA) [37]. Purified protein was dialyzed against water overnight and lyophilized [38].

3.3.2. Protein characterization

3.3.2.1. Sodium Dodecyl Sulfate Polyacrylamide Gel Electrophoresis (SDS-PAGE)

Sodium Dodecyl Sulfate Polyacrylamide Gel Electrophoresis (SDS-PAGE) - Purified proteins were analyzed for size and purity by SDS-PAGE. Importantly, solution from each well of the Maxwell purification cartridge was also analyzed on SDS-PAGE to assess the efficacy of the purification. Each sample was heated with NuPAGE LDS sample buffer (Invitrogen) briefly (<5 minutes) at 95°C and then loaded into a precast Bis-tris 4-12 % Polyacrylamide gradient gel (Invitrogen, USA). Protein bands were visualized under white light on a BioRad Chemidoc XRS imaging system after AcquaStain Protein Gel Stain (Bulldog Bio. Inc, USA).

3.3.2.2. Western Blot

The identity of purified protein products was confirmed via western blotting. Purified proteins were run on a denaturing SDS-PAGE and transferred to a nitrocellulose membrane at 40V for 60 minutes using a standard transfer protocol [39]. After proteins were transferred to the nitrocellulose membrane using Invitrogen's XCellTM Blot Module, the SNAPi.d. protein detection system (Millipore, USA) was used for immune detection with a 1:4000 dilution of a HRP-conjugated 6x-His Epitope Tag Polyclonal Antibody (PA1-23024, Thermo,USA) in Tris buffered saline plus Tween 20 (0.05%) (Fisher,USA TBST, ionic strength = 175mM). Amersham™ ECL™ Prime Western blotting detection reagent (GE Healthcare Life Sciences, USA) was used as detection reagent according to manufacturer concentration and the bands were visualized using the Bio-Rad ChemiDoc™ XRS camera under varying exposure.

3.3.2.3. Mass Spectrometry (MS)

Mass spectrometry was performed at the Core Synthesis and Analytical Services Facility (Center for Protease Research, North Dakota State University, USA) on purified protein samples. Briefly, the intact mass analyses of the specific silk like proteins was performed after desalting them through a desalting cartridge followed by LC-MS analysis on a Waters Synapt G2-Si HDMS (Waters Corporation, USA). UPLC was performed on an Acquity UPLC- I class with Waters BEH C18 (2.1mm X 100mm) 1.7 µm column. The column was maintained at 35°C throughout the analyses. A linear gradient was performed over 7 minutes shifting the ratio of A (0.1% formic acid in water) to B (0.1% formic acid in Acetonitrile) shifted from 90/10 (A/B) to 10/90 (A/B). The total gradient run was 13 minutes. Desalted protein solution (100 µL) was mixed with 200 µL of 0.1% TFA in Water/Acetonitrile (50/50) and 10 µL was injected at a rate of 0.5 mL/min. Mass spectrometric analysis was performed on a Waters Synapt G2-Si HDMS. The collected mass

spectrum data in continuum format were processed using MaxEnt1 software (Waters Corporation, USA) to obtain the protein mass. The peak width parameter used to obtain the result was between 0.45 Da to 0.6 Da depending on the sample. Spectra were processed between 5000 to 50,000 Da at 1 Da/channel.

3.3.3. Heparin-binding characterization

3.3.3.1. Heparin Affinity Column Chromatography

Affinity column chromatography was performed with HyperD resin (Pall, USA) according to the manufacturer's protocol to determine the affinity of each protein for heparin. Briefly, the column was washed with five column volumes of wash buffer (20 mM Tris HCl, 0.3 M NaCl, pH 7.4, ionic strength 0.32 mol/L) prior to application of the protein. Based on the binding capacity of the column, approximately 100 µg of protein in a 2 ml volume of Maxwell elution buffer (500mM Imidazole and 100mM HEPES, pH 7.5, ionic strength ≈ 0.73M [40] was applied to the column and allowed to elute drop-wise (flow-through fraction). The column was then washed with 3 column volumes (6 ml) of wash buffer followed by 2 column volumes of elution buffer (20 mM Tris HCl, 2 M NaCl, pH 7.4, ionic strength 4.04 mol/L). Each chromatography fraction was collected separately for analysis. ATIII and IL-2 were used as positive controls for heparin binding [41], and BSA as a negative control.

3.3.3.2. Heparin Affinity Dot Blot

Purified proteins (10 µl at approximated 100µg/µl) were applied to a nitrocellulose membrane (Sigma-Aldrich, USA) and allowed to adsorb for 30 minutes. The membrane was blocked on a rotating platform for an hour in block solution (5% solution of non-fat instant milk (Carnation, USA) in Tris buffered saline plus Tween 20 (0.05%) (Fisher, USA TBST) ionic strength = 0.175M). The membrane was subsequently probed with a biotinylated heparin (Sigma-

Aldrich; from porcine intestinal mucosa, mw: 15000 Da, purity: >97%) ligand diluted at 1:100 in the blocking solution for one hour on a rotating platform. After washing the membrane three times for 15 minutes each in TBST (approximately 75 ml), the blot was probed with horseradish peroxidase(HRP)-tagged streptavidin (Fisher Scientific, USA) at a 1:100 dilution in the blocking solution for one hour on a rotating platform. The membrane was washed again three times for 15 minutes each in TBST (approximately 75 ml), and reacted with enhance chemiluminescence reagents (Pierce, USA) for 5 minutes prior to imaging on an Aplegen Omega Lum G over 5 minutes, acquiring images at varying exposure times. An equivalent amount of IL-2 (PeproTech, USA) was spotted as a positive control and while BSA was spotted as a negative control. Additionally, a blot was probed with secondary streptavidin–HRP (Horseradish Peroxidase) (ThermoFisher Scientific, USA) only using an analogous protocol without the addition of biotinylated heparin.

3.3.3.3. Heparin Affinity ELISA

An indirect ELISA was performed on the protein sample with BSA and plain silk (SX2) as negative controls. Polystyrene microtiter plate wells (n=3) were incubated with 100µl of protein samples at a concentration of 100ug/ml in Tris buffer (pH 7.5) for 2 hours. After incubation, the wells were washed three times using TBST (0.05% Tween) and blocked using 5% milk in TBS for another hour. Plates were rinsed again with TBST three times. Subsequently, 100µl of biotinylated heparin (heparin-biotin sodium salt, MW 15000 Da, Sigma Aldrich, USA) at a concentration of 45µg/ml diluted in TBST was added to each well and incubated for 1 hour. Wells were washed again with TBST three times before adding Streptavidin conjugated with HRP at a dilution of 1:1000 as the secondary ligand and incubated for 1 hour. Wells were again washed, and 100µL of TMB substrate (Fisher Scientific, USA) was added and allowed to incubate for 20

minutes at which time the reaction was stopped using 1M HCl according to the manufacturer's instructions for the TMB substrate. Sample optical absorbance was read at 480 nm on an Epoch plate reader (Biotek, USA).

3.3.3.4. APTT Coagulation Assay

An activated partial Thromboplastin time (aPTT) assay, which assess the rate at which the complex of plasma clotting factors assembles to convert prothrombin to thrombin prior to clot formation, (APTT XL Pacific Homeostasis Assay, Thermo Fischer, USA) was performed to indirectly assess blood coagulation in the presence of SX2 or S4H4 according to the manufacturer's protocol. Whole blood for the assay was collected from euthanized rats via cardiac puncture into a sodium citrate (4% w/v) solution and immediately stored at -80°C for use. Blood was centrifuged at 2000 RPM for 10 minutes to separate the plasma. Initially, heparin was titrated into plasma to determine the amount needed to prevent citrate-treated plasma from clotting in the presence of calcium. Briefly, different concentrations of aqueous heparin (heparin sodium porcine mucosa, Sigma Aldrich, USA) (200µL per well), ranging from 50 µg/mL to 200 µg/mL (diluted in Tris buffered saline (TBS)) was incubated with plasma (0.1 mL) in each well (n=2) for 2 hours at room temperature with shaking. Subsequently, 0.1 mL of APTT-XL reagent was added, and the reaction was incubated for 5 min. Calcium chloride solution (0.1 mL of 0.02 M) was added to initiate clot-like formation and the time required for the formation of clot was recorded. Clot-like formation was visually assessed as an optical change in the transparency of the solution. Based on its ability to prevent clot formation during the titration, 100 µg/mL of heparin was used for all additional assessments. A similar protocol was followed to assess the coagulation of plasma in the presence of SX2 and S4H4 with the exception that the wells (n=4) were incubated with either these proteins at a concentration of 200 µg/mL prior to the addition of heparin and/or plasma. After

allowing the protein to attach to the surface for 2 hours, the protein-depleted solution was removed from the wells and the wells were rinsed with PBS three times or five times and blocked with 0.5% milk in TBS for 30 minutes. The wells were not allowed to completely dry. Subsequently, all wells were rinsed again three times with PBS, and 200 μL of heparin (100 μg/mL in TBS) and incubated for another 2 hours. After incubation, the wells were rinsed with PBS and thromboplastin time was assessed using the APTT-XL assay by adding clarified plasma (0.1 mL) and the APTT-XL reagent (0.1 mL). Silk and S4H4 without heparin were used as controls.

3.3.4. Antibacterial activity

3.3.4.1. Kirby Bauer Zone of Inhibition Assay (ZOI)

Maxwell-purified S4H4 and SX2 protein solutions (300 □l of 20 mg/mL, ~90% purity) were spotted on the surface of an LB agar plate previously (within 15 minutes) streaked with E. coli(ATCC 12435). An equivalent amount of BSA was applied as a negative control. Only one protein was applied to a single agar plate with each protein spotted on 3 independent plates. The plates were incubated at 37°C overnight and the diameter of the zone of inhibition (ZOI) was measured using digital calipers.

3.3.4.2. Prevention of Biofilm Formation

The prevention of biofilm formation was characterized for E. coli (ATCC 12435) using a multi-well plate testing methodology described previously [42], [43]. Prior to bacterial inoculation, 0.5 mL of protein solution (1 mg/ml) was added to four wells of a tissue culture 24-well polystyrene plate for 1 h and rinsed three times with 1.0 mL of PBS. Subsequently, an overnight culture of E. coli prepared in LB broth was rinsed three times in PBS, harvested via centrifugation, and diluted in PBS to an OD600 of 0.4. The resulting resuspension was used to prepare 107 – 108 cells/ml suspensions in minimal media M63 (10g of (NH4)2SO4, 68g of

KH2PO4, 2.5mg of FeSO4 7H2O, 254mg of MgSO4 7H2O, pH - 7) supplemented with 2g/L dextrose. This bacterial suspension (1 ml) was added to well plates pretreated for 1 h with either S4H4 or SX2 protein solutions and incubated statically for 24 h at 37°C (PBS and blank plate were used as controls). The wells were rinsed three times with 1.0 mL of PBS and stained with 0.5 ml of crystal violet (CV) solution dye (Bioworld, TX) for 15 min at ambient laboratory conditions. Excess CV dye was removed by rinsing three times with 1.0 mL of water and the wells were dried for 1 hour. The CV dye was extracted in 33% glacial acetic acid for 15 min to solubilize the dye bound to the biofilm. An aliquot of 150µl of the acetic acid extracts were transferred to a 96-well plate and the absorbance of dye was measured at 600 nm using a multi-well plate spectrophotometer, Tecan Safire 2 (Tecan US Inc, North Carolina).

3.4. Results

Exploiting the molecular hierarchy, the repetitive sequence for Argiope aurantia major ampullate spidroin 2 (MaSp2), one of the key structural spider silk proteins, was genetically linked with the consensus sequence for binding heparin (HBM) (Figure 3.2). MaSp2 (silk) and HBM sequences were designed and engineered in a cloning plasmid not only to optimize expression in E. coli, but also to facilitate the genetic linkage and polymerization of each gene individually using a compatible non-regenerable cloning strategy (Figure 3.2A-C). All produced clones were screened via colony PCR (Figure 3.2D) and sequence confirmed by the University of Utah core sequencing facility.via colony PCR (Figure 3.2D) and sequence confirmed by the University of Utah core sequencing facility.

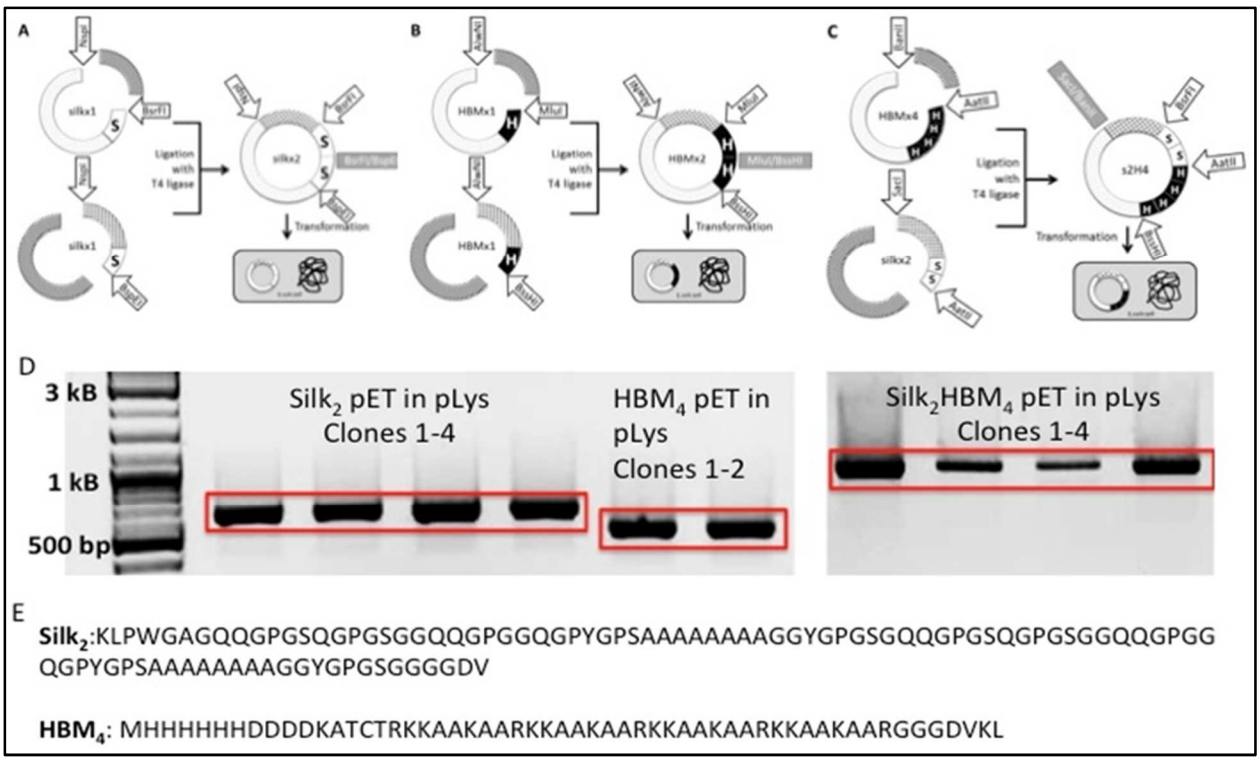

Figure 3.2. Schematic showing the compatible non-regenerable cloning design used to genetically polymerize the A) *Argiope aurantia* MaSp2 consensus repeat motif using BsrFI and BspEI to produce compatible ends, which after being ligated together cannot be cleaved by either BsrFI or BspEI; B) HBM consensus repeat motif using MluI and BssHI to produce compatible ends, which after being ligated together cannot be cleaved by either MluI or BssHI; C) the *Argiope aurantia* MaSp2 consensus repeat motif concatenated with the HBM consensus repeat motif using BanII and SacI. D) Agarose gel electrophoresis showing the successful linkage of $silk_2$ and HBM_4. Bands of interest are highlighted by the boxes. Each band represents a different clone. E) Amino acid sequences for each clone. Note that a 6xHis tag was included in each construction for purification and detection. SX2 was predicted to be 14,766 Da while S4H4 was predicted to be 16,355 Da.

Subsequently, genes were PCR-cloned into pET30a for protein expression. After constructs were transferred into pET30a, expression was induced in BL21-DE3 E. coli using IPTG. Alternatively, (S4H4) fusion constructs were synthesized and cloned into pET30a by GenScript. Fusion protein production was confirmed by: (1) the slight shift in molecular weight upon addition of the HBM4 peptide (SX2= 14766 Da, S2H4= 15146 Da, S4H4= 16355 Da Figure 3.2), (2) the reaction with an anti-histidine antibody (Figure 3.3), and mass spectrometry (Figure 3.4).

Additionally, HPLC was also done on S2H4 to show a shift in the peak retention time compare to SX2 alone.

Following confirmation that the HBM4 peptide was in fact attached (Figures 3.3 and 3.4), functional assays were used to determine the capability of the fusion peptide to bind heparin on both a solid phase column (Figure 3.5) and from solution as a surface-bound protein (Figure 3.6).

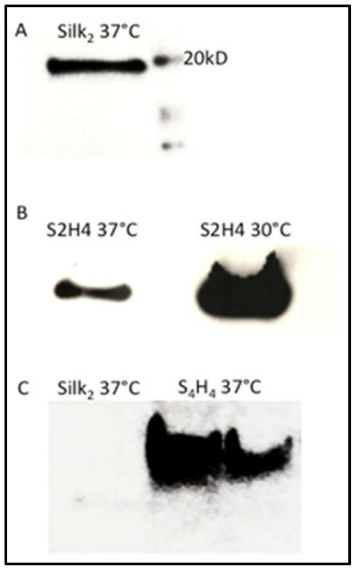

Figure 3.3. Western blots for (A) silk2 protein, (B) S2H4, and (C) S4H4 (2 clones) using a HRP-conjugated anti-His antibody. Only in the $silk_2$ blot can the molecular weight marker be seen. (all gels were non-reducing).

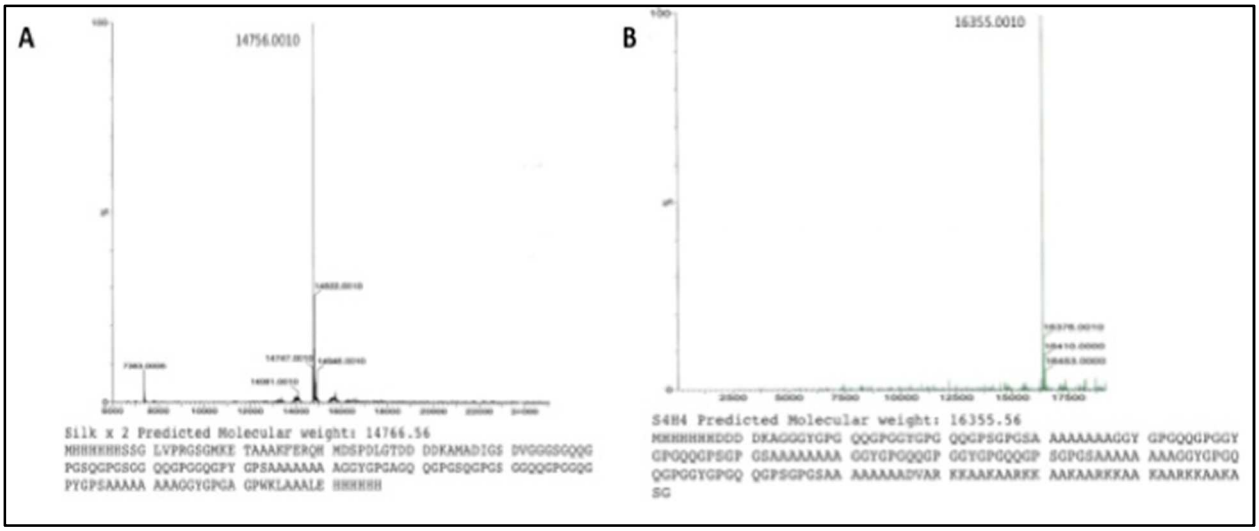

Figure 3.4. Mass spectrometric validation of the desired recombinant modified silk fusion protein sequences. (A) Based on the amino acid sequence shown for SX2, predicted to be 14766.56, the SX2 protein was confirmed. (B) Based on the amino acid sequence shown for S4H4, predicted to be 16355.56, the S4H4 protein was confirmed.

In each assay, bovine serum albumin (BSA) was used as negative control, having no reported ability to bind heparin [41,44,45]. HyperD heparin affinity resin has heparin covalently bound to the column's solid phase, allowing interaction with recombinant proteins under flow through the column. The presence of non-HBM containing silk protein in the eluted, unbound wash fraction (Figure 5) confirms that recombinant silk solution alone has limited affinity for immobilized heparin. Alternatively, when HBM was genetically linked to silk repeats, the resulting fusion protein was seen in the elution fraction, reflecting the dramatically increased ability of this recombinant protein to bind immobilized heparin on the column.

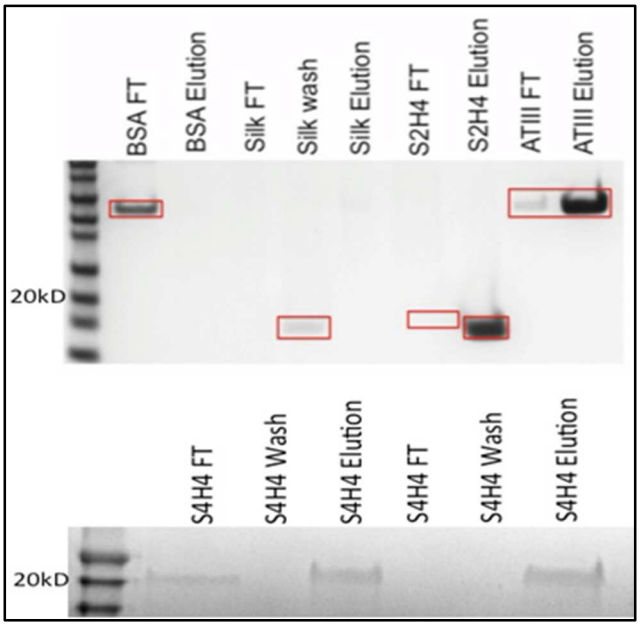

Figure 3.5. SDS PAGE demonstrating a solid phase functional assay using heparin affinity chromatography. Increased ability of both the recombinant S2H4 and S4H4 proteins to bind heparin as indicated by its elution in the high salt buffer. Two clones of S4H4 are shown. Bands of interest are highlighted by the boxes.

Despite this result, anomalous, non-specific protein affinity interactions can occur during heparin affinity column chromatography due to charge-charge interactions; therefore, a dot blot assay on nitrocellulose was used to confirm the ability of surface-adsorbed, silk-HBM fusion protein to bind biotinylated heparin (Figure 3.6A).

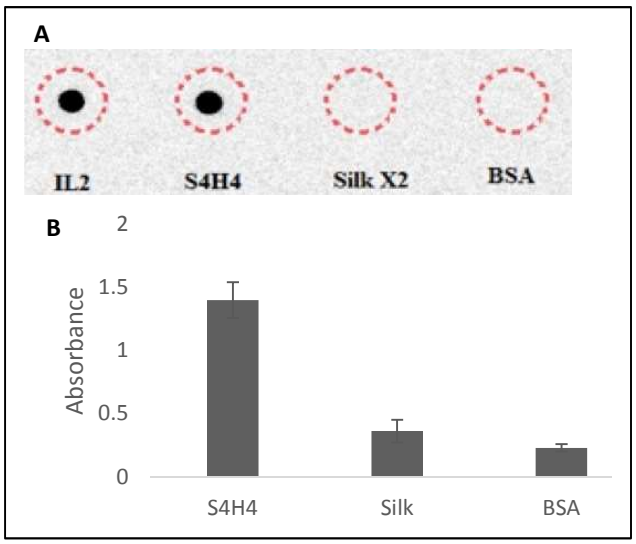

Figure 3.6. (A) S4H4 spotted on nitrocellulose binds heparin similar to the positive control IL-2. SX2 was unable to bind heparin, similar to the BSA negative control. Areas where each test protein was spotted are indicated by a dashed circle. (B) ELISA to detect the interaction of S4H4, SX2 and BSA (negative control) with heparin; n=4, $p<0.05$.

The fusion protein S4H4 was detected by biotinylated heparin; whereas, heparin did not bind to either the SX2 or the BSA negative control. An analogous blot was probed with secondary streptavidin–HRP only (data not shown). Unfortunately, this assay format exhibited limited sensitivity: approximately 0.3 mg of protein applied to each 10µl spot was required for subsequent heparin detection. Thus, an Enzyme Linked Immunosorbent Assay (ELISA) was conducted to validate the dot blot and support binding sensitivity. The ELISA was able to confirm that biotinylated heparin bound approximately 3-fold better to S4H4 than to SX2 or BSA (Figure 3.6B).

One powerful aspect of this unique fusion is the ability of the heparin-binding motif to not only bind heparin but also to act as an antimicrobial peptide. To assess the ability of S4H4 to inhibit bacterial growth, a standard Kirby Bauer zone of inhibition study was performed against planktonic *E.coli*. Silk without the heparin-binding motif (SX2) did not show a zone of clearing nor did BSA; however, S4H4 produced a clear zone of inhibition (Figure 3.7). Significantly, no proteins were complexed with heparin in this experiment.

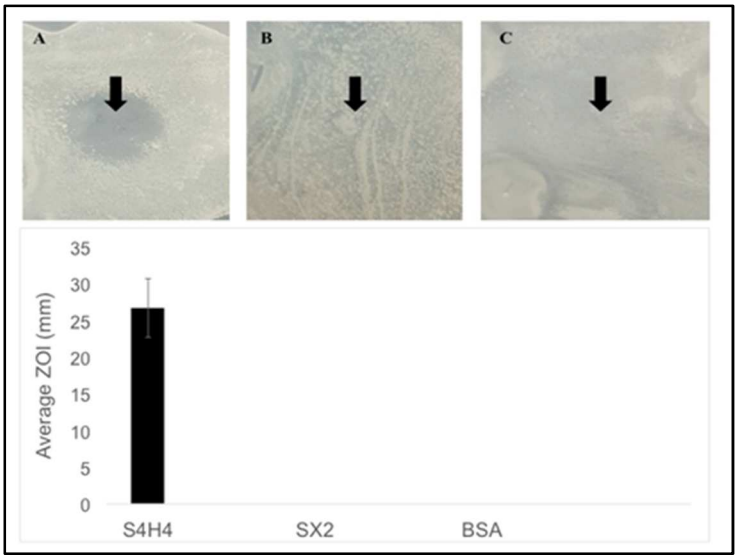

Figure 3.7. ZOI against E. coli of silk with (A) and without (B) the heparin-binding motif. BSA (C) is included as a negative control. Note that the same amount of protein was spotted (indicated by the arrow) for each sample. The average (n=3) zone of inhibition is shown in the bar graph below the representative images. No zone of inhibition was observed for either silk or BSA controls.

In addition to the antibacterial effect on planktonic E.coli indicated in the ZOI assay, the fusion protein in the absence of heparin also prevented the growth of an E. coli biofilm (Figure 3.8) when compared to both PBS-treated and blank plate (i.e., TCPS) controls. ATCC E. coli strain 12435 is a validated biofilm forming strain [45]. The control groups show a clear formation of biofilm with the presence of a glycocalyx as indicated by the crystal violet (CV) blue color in the well (images in Figure 3.8); whereas CV absorbance (600 nm), a standard measure of biofilm formation [46], in the presence of S4H4 is below the detectable limit of the assay and the spectrophotometer (L.O.D. 0 - 4 OD) and seems to have effectively prevented biofilm in the wells.

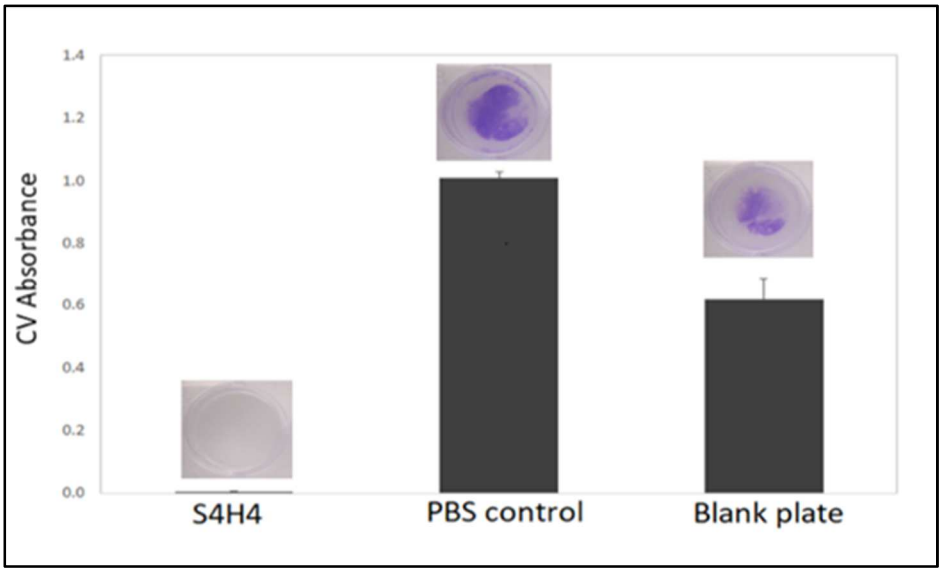

Figure 3.8. Crystal violet assay for biofilm formation showing that wells coated with S4H4 do not support biofilm formation. Alternatively, wells rinsed with PBS or blank clearly evidenced biofilm (as indicated by absorbance at 600 nm and presence of purple color. (n=3).

While both dot blot and ELISA provide evidence that heparin can bind to S4H4, bioactivity of the bound heparin must also be assessed. A validated assay to determine the activated partial thromboplastin time (aPTT) as an indirect measure of clot-like formation in vitro, was performed on SX2 and S4H4 proteins. Time to visualise clot formation elicited by the calcium ion addition was confirmed as a decrease in the optical transparency of the aPTT solution reaction and formation of a clot (Figure 3.9). When silk conjugated to heparin-binding motif (S4H4) was surface coated and exposed to heparinized plasma, no clot was detected by the aPTT assay after 24 hours, similar to an uncoated microwell surface when soluble heparin only was added. However, when heparin was added to wells coated with silk alone (SX2), clotting was merely delayed (13±5 minutes) when compared to silk-coated control wells without heparin addition (9±3 min) (Table 3.1). Regardless of the surface coating, in the absence of heparin, SX2, S4H4, or plasma all showed similar clotting times of approximately 9 minutes.

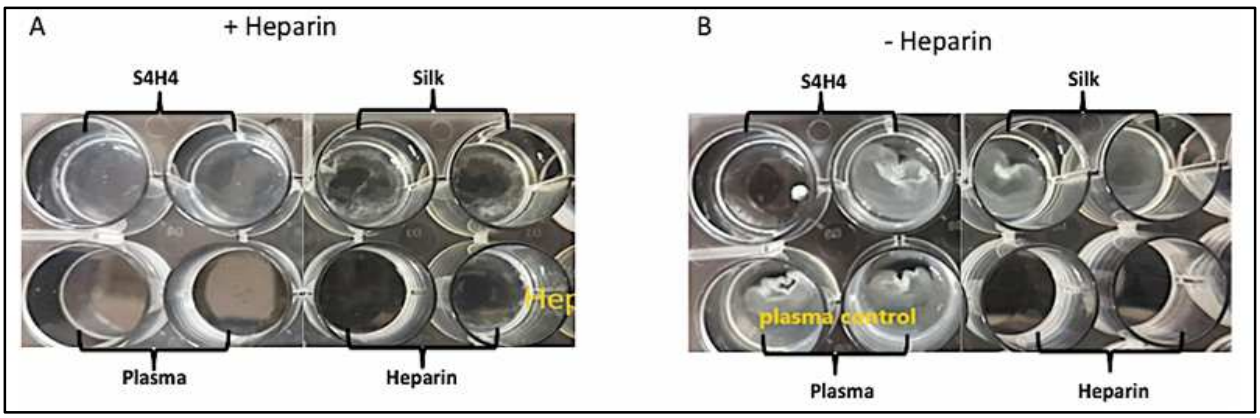

Figure 3.9. A visual representation of the APTT coagulation assay endpoints. (A) heparin added to the assay produced noticeable lack of clotting in both S4H4 and the plasma as anticipated by their ability to bind heparin, comparable to the heparinized controls shown in the bottom right two wells. The silk-coated surface shows evidence of clot-like formation. (B) absence of heparin produced a strong clotting response in all wells with the exception of heparinized wells (bottom right) (n=3).

Table 3.1. aPTT assay clotting times for coated microwells with or without the presence of heparin. In the absence of heparin, baseline clotting times remain relatively consistent (n=3).

Sample	Heparin added	Clotting time (min)
Heparin	+	No clot
S4H4	+	No clot
Silk	+	13±5
Plasma only	+	30±6
S4H4		9±4
Silk		9±3
Plasma only		8±3

3.5. Discussion

Tailored surface coatings have been used for over four decades to improve material performance in blood, tissue or biological milieu [47]. Historically, several strategies either actively or passively by pharmaceutical have been exploited specifically to combat either material-associated thrombosis or infection [48]. For over 30 years, heparin's use as a surface-immobilized bio-active agent has been reported in many commercial forms (e.g., Carmeda BioActive Surface, BioInteractions Biba-Hepcoat technology (Tyco Healthcare) licensed by Medtronic) to improve hemocompatibility [49]–[51] in vitro and in vivo on numerous commercial medical devices [52],

[53]. The relative success of chemically defined polymer surface coatings in providing a versatile platform for pharmaceutical immobilization is a driving force behind the use of either biomimetic [54]–[56] or synthetic polymers [57], [58] as surface coatings [59]. Among these synthetic and biopolymers, silk's genetic and structural hierarchy has made it an attractive alternative platform. Several groups have explored heparin-silk complexes by covalently linking heparin to silkworm silk (a more readily available yet mechanically inferior silk) or via blending/mixing prior to processing by electrospinning or film casting [60]–[62]. Recently, heparin grafted either electrostatically or covalently [63] to silk-based vascular scaffolds, showed that heparin grafted at a density of 1.48 ± 0.19 mg/cm^2 was able to improve the *in vitro* anticoagulant effect of the silk for up to 12-weeks [64] with clotting assays reported to be (151.5 ± 11.7 s for APTT and 85.6 ± 9.1 s for PT); however, *in vivo* activity is suspected to be much less since these surfaces were assayed in the absence of serum proteins [51]. A "self-renewing" multi-functional heparinizable coating, created using the silk-based fusion protein described here and relying on biological mechanisms and thrombosis signaling pathways, offers an alternative [65].

Using a compatible non-regenerable cloning strategy [38], [39], [66] silk2 and HBM4 constructs were created and genetically linked to create the S2H4 fusion protein (Figure 3.2); S4H4was directly synthesized in pET30a for expression. Based on anticipated intermolecular hydrogen bonding [67], two polymerized MaSp2 silk monomers were predicted to provide a sufficient mechanical background to embed repeated heparin-binding motifs and subsequently bind heparin with minimal steric hindrance. Additionally, in this silk background, the heparin-binding motif may also produce both anticoagulant and antimicrobial effects based on its AMP-like residues and structure. Traditionally, AMPs are proposed to exert antimicrobial effects on bacteria by disrupting microbial outer membranes or by creating pores; however, until recently,

the primary mode of AMP action when surface-bound remained unknown [68], [69]. In 2018, Xiao and colleagues used a sum frequency generation microscope technique to probe the mechanism of AMP action, noting that when bacteria contacted a surface-immobilized AMP, the AMP changes shape and kills the bacteria [69]. Additionally, it is unclear the minimum length of the AMP necessary for such activity. Liu et al. investigated influence of AMP length on the hemolytic and antimicrobial activity of an Arg-Trp (RW) and found that $(RW)_3$, a 6 amino acid peptide had an optimal length [70]; inclusion of lysine in such a structure is predicted to enhance its efficacy. Importantly, while Alanine and Arginine can promote heparin binding, the presence of Proline, prominent in the repetitive silk motif, is disruptive (although it may enhance the efficacy of the AMP functionality), [68] further necessitating a minimal silk component in the AMP-mimicking silk fusion protein [25].

Additionally, recombinant E.coli production of cationic proteins [71], such as the heparin-binding motif, is often limited. Using only two silk repeats was insufficient to incorporate greater than four heparin-binding repeats. Fusion protein yields could potentially be increased by addition of a periplasmic localization signal [72]. Antimicrobial peptides, such as LL-37 have recently received substantial research interest amidst the rising tide of antimicrobial resistant bacteria [68], and their recombinant production, like most peptides, is cost effective in E.coli. However, their yield is generally compromised due to their bacterial toxic nature [71]. Therefore, successful recombinant production of an AMP requires stabilization with a fusion partner, to mask its lethal effects and provide proteolytic stability [71], [73]. Interestingly, natural production of AMPs seem to be essential for innate immunity in mammalian systems [74] and have even been identified in several bacterial species [75]. Nevertheless, expression of the HBM peptide alone in the absence of the MaSp2 silk peptide in any measurable quantity was not feasible (data not shown), likely due

to the high molar percent of lysine in the peptide and the specific bacteria's innate ability to respond to this AMP [71], [76]. Thus, the HBM peptide was expressed only as a fusion stabilized by silk. Notably, the production of S2H4 was hampered, which may be a reflection of the necessary length of the fusion partner. Such a hypothesis should be further explored to increase the recombinant protein yield. Yang et al. produced a cecropin AD (a cationic AMP) elastin like peptide (ELP) fusion protein similar to that reported in this study and demonstrated the link between the length of the ELP sequence and the yield of the fusion [77]–[79].

In addition to using a larger fusion tag or additional silk repeats to increase the yield of the heparin-binding motif, evidence suggests that promoting the sequestration of the recombinant cationic fusion protein, may occur when using a periplasmic signal peptide, and also improve the yield. A lower induction temperature was also found to improve expression (Figure 3.4). Contrary to Luan et al. who recently demonstrated the ability of E.coli to recombinantly express AMPs as a self-cleaving fusion that was sequestered as aggregates [73], the HBM silk fusion was not sequestered in inclusion bodies in any measurable amount (data not shown) and did not appear to aggregate and subsequently precipitate when dissolved in water or PBS even at concentrations up to 20 mg/ml. Surprisingly, this may have been detrimental to efficient AMP recombinant protein production as Zorko et al. recently demonstrated the ability to produce large quantities of recombinant AMP by forcing sequestration in inclusion bodies [76]. Future work will modify the ratio of the MaSp2 silk to heparin-binding motifs in attempts to optimize both mechanical and biological properties while increasing recombinant protein yield.

Based on previous reports of heparin's dissociation constant determined using radio labelled heparin in a reducing, affinity co-electrophoresis with the ARKKAAKA peptide in a 1% agarose gel (KD = 42±15 nM, Mr = 3318),[25] four uninterrupted heparin-binding motifs (each 8

amino acids long) were used to optimize possible heparin complexing interactions. Kinetics of heparin binding in our silk system are expected to be very different based on the media ionic strength. Importantly, when concatenated with the silk sequence repeats, the molecular weight of the recombinant protein was only shifted by approximately 1600 Da, likely because the molecular weight of the silk construct was artificially inflated by the presence of two histidine tags and additional downstream cloning sites that were not included in the concatenated construct. Heparin affinity chromatography (Figure 3.5) as well as a dot blot and an indirect ELISA probed with a biotinylated heparin ligand (Figure 3.6) confirmed that heparin was only able to bind to the recombinant protein that included the heparin-binding motif, supporting the functionality of the genetic construct.

Although the genetic sequence of the S2H4 clone was confirmed and the peptide appeared to be the correct size (Figure 3.3) and able to bind heparin (Figure 3.5), mass spectrometry and amino acid analysis were unable to confirm the S2H4 protein identity. This could potentially be attributed to poor recombinant protein concentrations resulting from pre-column processing prior to injection. After derivatizing recombinant proteins with o-phthaldehyde, HPLC of S2H4 showed the emergence of a new peak, indicating an increase in the number of primary amine groups, such as is evident with the addition of the heparin-binding motif. Nevertheless, this analysis was not considered sequence confirmation of S2H4, but merely evidence of changes in the silk peptide. Alternatively, S4H4 protein identity was confirmed via mass spectrometry (Figure 3.3) and was carried forward for all functional assays.

After producing and confirming the identity of the recombinant silk and silk-heparin fusion proteins, the ability of the fusion protein to bind bioactive heparin when adsorbed to a surface was assessed. The silk protein was adsorbed from aqueous solution to a model polystyrene (PS) plastic

surface and heparin was added prior to exposure to fresh rat plasma. Activated partial thromboplastin time (aPTT) assay provided an indirect measure of coagulation (Figure 3.9 and Table 3.1). Plasma coagulation times were altered for S4H4, similar to when the plasma was treated with heparin in the absence of any protein. As heparin is expected to associate and disassociate with HBM (4 repeats), (disassociation constant of 42 nM in a 1% agarose gel matrix as previously described [80]), this provides a rudimentary qualitative assessment of heparin's stability with the coated protein on the surface. The wash time following heparin adsorption was varied, revealing that the ability of heparin to prevent clot formation in the aPTT assay was lost with more rigorous washing (3 times for 1 minute each). To verify if the protein was lost from the surface with washing, x-ray photoelectron spectroscopy (XPS) was performed on the plates before and after washing, showing an increase in the presence of nitrogen both before and after washing compared to the uncoated PS control although the percent nitrogen decreased from 14 to 10% after washing (data not shown). Nitrogen presence on the surface of coated wells, both before and after washing, indicates not only protein presence on the surface after rigorous washing but also that heparin is dissociating from its molecular binding partner under those same wash conditions. Conversely, the rinse/wash steps used in the current protocol allowed heparin's anticoagulant activity to be retained (Table 3.1), indirectly indicating that heparin remained bound to the coated protein under these conditions. Moreover, the ELISA assay using heparin as the primary ligand (Figure 3.6B) provides further evidence that the heparin-binding silk protein remains surface-bound and capable of binding heparin. Importantly, the ability to bind biotinylated heparin was not evident with adsorbed silk or BSA negative controls (Figure 3.6B). Antithrombin III (ATIII) or interleukin-2 (IL2), both documented to bind heparin [44], were used as positive controls for the HyperD heparin affinity column (Figure 3.5) and the dot blot (Figure 3.6) respectively, while

BSA, with no documented ability to bind heparin, was used as the negative control for all assays [81], [82]. IL-2 binding of heparin did not yield a positive result in ELISA (data not shown). Surface-bound heparin on the HyperD heparin affinity resin was shown capable of retaining S2H4 and S4H4 (Figure 3.5), although the S2H4 fusion did not appear capable of binding heparin with the same robustness as its natural binding partner, ATIII[81]. Additionally, endpoint ELISA indicated a significant difference in heparin binding capacity of S4H4 compared to the silk2 negative control (Figure 3.6). Heparin bound with very little non-specific binding to silk2, (Figure 3.5 and 3.6).

Determining the kinetics of heparin binding remains challenging. The challenge is two-fold: (1) heparin is an anionic polyelectrolyte, (2) electrostatic binding to heparin is not a specific interaction, and (3) purification of heparin includes multiple, varied molecular weights. Previous indirect efforts using labeled heparin have been used successfully; however, direct label-free kinetic determination is challenging at best [41], [83], [84], [84]. To decipher and determine kinetic heparin binding profiles, two designs were evaluated via kinetic ELISAs, in which heparin was either the capture ligand and the protein was added in solution, or the protein was the capture molecule and heparin was added in solution. Unfortunately, while this design produced confirmation that the HBM-modified silk can complex heparin, the complex disassociation constant could not be determined. Additionally, heparin interacts with many proteins through charge/charge interactions similar to an ion exchange resin, and not specifically through site saturation, a key principle for label-free affinity measurements.

Regardless of the technique used to determine protein ligand affinity, the ionic strength of the various buffers, particularly for heparin-binding experiments, could potentially reduce or disrupt the predominant electrostatic interactions [85] between negatively charged heparin and its

positively charged binding partners (i.e., silk and silk fusion constructs) and must be considered during analyses. Substantial ionic strength of blood seems to control natural heparin engagement specifically with over 20,000 different non-specific blood proteins and a 320 mOsm solute concentration [86], [87]. This may indicate a level of specificity governs the interaction of heparin beyond mere electrostatic interactions; a theory that was recently explored [88]. Nevertheless, the ionic strength of the buffer, particularly the wash buffer used in all immunoassays (i.e., dot blot and ELISA) and label-free affinity measurements, should provide sufficient stringency to prevent non-specific background interactions. Thus, TBS Tween (ionic strength of 0.175M), well below the concentration used to disrupt non-specific electrostatic interactions in the HyperD heparin column (4.04 mol/L), was used to reduce non-specific background interactions sufficiently at pH 7.5 as evidenced by the minimal or absent signal in the silk alone and the BSA negative control, and the overall low background of the blot (Figure 3.6A). ELISAs were also run with both desalted and buffered (Maxwell elution buffer, 500mM imidazole, 100mM HEPES, pH 7.5) samples with no significant differences in assay performance (data not shown), indicating that ionic strength based on buffer composition did not alter heparin-silk complex interactions. Importantly, as Promega's Maxwell 16 protein purification system required elution in the Maxwell elution buffer, we were concerned that this buffer's ionic strength (500mM imidazole, 100mM HEPES, pH 7.5) may interfere or provide artifactual results. Therefore, the ELISA was run with desalted samples resuspended in PBS. Furthermore, the Maxwell elution buffer ionic strength is well below the manufacturer's recommended elution buffer for the HyperD heparin column (I=2M). As a zwitterion, HEPES is proposed not to contribute to solution ionic strength [89]. Imidazole, is partially protonated at pH 7.4, indicating that at physiological pH it has limited contribution to ionic strength and is used primarily to stabilize proteins [90]. Therefore, although buffer

interference by ionic screening of heparin electrostatic interactions with stationary phase binding agents cannot be completely discounted, experimental and theoretical evidence would suggest that such an effect is limited, and consistent for each assay.

Evidence from affinity chromatography (Figure 3.5), dot blot (Figure 3.6A), and ELISA (Figure 3.6B), support that adding the heparin-binding motif allows silk to interact with heparin. However, these interaction experiments were unable to determine if the bound heparin could still function as an anti-coagulant. The ability to do so is critical for any surface application. Thus, an assay to determine activated thromboplastin time was performed (Figure 3.9 and Table 3.1). Regardless of the protein, in the absence of heparin, optical transparency, reflecting clot formation, was lost approximately 9 minutes after the addition of calcium chloride to the assay to chelate the sodium citrate anticoagulate used during collection. However, in the presence of heparin, S4H4 did not show a clot, similar to heparin alone; whereas, in the presence of unmodified silk peptide, clotting was only slightly delayed from 9 minutes (unheparinized condition) to 13 minutes (Table 3.1), indicating that heparin remained bioactive when surface bound, at least in the intrinsic and common coagulation pathways.

In addition to providing heparin-binding ability to a silk peptide, addition of the HBM sequence also produced some activity analogous to an antimicrobial peptide. Initially, it seems counterintuitive that a surface- bound AMP could be bactericidal, based on the classic proposed mechanism of action, permeating the cytoplasmic membrane without specific target [91], which necessitates a soluble, ampholytic species. Model AMPs such as LL37exemplify this general mechanism. Notably, soluble heparin binding motifs with a structure similar to that used in this study exhibited roughly equivalent activity to LL-37 [91]. LL37 and its counterions are influxed into the periplasmic space, effectively extracting water from the cytoplasm to reduce turgor

pressure in the cell. Subsequently, LL37 is thought to interfere with peptidoglycan biosynthesis, thereby exerting its bactericidal effects [68]. Notably, it has been suggested that HBM includes a common motif component (XBBXBX (where X represents hydrophobic or uncharged amino acids, and B represents basic amino acids) that folds as an amphipathic helical structure with approximately 20Å between basic amino acids [91]. Alternatively, c-WFW, a potent cyclic hexapeptide studied, never permeated the cytoplasmic membrane of E. coli but instead disrupted the lipid organization of the membrane [68]. Thus, more recent evidence suggests not only a diversity of mechanisms based on the peptide sequence of the AMP but also AMP/bacterial pairings [68], [92]. The proposed mechanism based on hydrophobic and hydrophilic regions with imperfect amphiphilicity to facilitate disruption of the bacterial membrane leads to the prediction that surface bound HBM may prove more effective against sessile bacterium than planktonic. However, such structural and mechanistic studies remain to be done with the silk fusion peptide. Nevertheless, based on a standard Kirby Bauer zone of inhibition assay (Figure 3.7) as well as a crystal violet biofilm assay (Figure 3.8), silk modified with HBM both in solution phase and as a surface coating reduces the proliferation of both planktonic (Figure 3.7) and biofilm (Figure 3.8) E.coli bacteria.

Embedding the heparin-binding motif in a silk peptide, was meant to endow the silk peptide with the ability to bind heparin and prevent bacterial colonization of a surface; however, silk was also meant to impart mechanical robustness to the heparin-binding motif. Thus, fibers were wet spun from either unmodified or HBM modified silk. Subsequent mechanical testing revealed that the presence of HBM decreased the breaking stress from 41 MPa to 11 MPa, but increased the breaking strain from 4.4% to 7.1 %. This may be a reflection of the fiber thickness as it is known that thicker diameter fibers impart extensibility while thinner diameters are associated with

strength [93]. Nevertheless, optimizing the ratio of HBM to silk may be necessary to preserve mechanical integrity.

3.6. Conclusions

A new protein fusion comprising spider silk-derived MaSp2 peptides fused with a consensus heparin-binding peptide was cloned, expressed, purified and shown to bind heparin both at surfaces and in buffer solutions. While fusion protein affinity for complexing soluble heparin was demonstrated under certain in vitro conditions, the precise complex stoichiometry and binding kinetics remain undetermined. However, bound heparin appeared to be bioactive in an aPTT assay as an indirect measurement of coagulation as well as providing antimicrobial activity against both planktonic and biofilm E.coli. Utility of this protein as a biomaterial material, exploiting both the recombinant protein-bound heparin and also the intrinsic antimicrobial potential based on its AMP-like structure, represents the next application for this newly engineered recombinant chimera.

3.7. Acknowledgements

This research was supported by NIH grant R21 DK088426-01 and by start-up funds provided to A. Brooks from North Dakota State University Department of Pharmaceutical Sciences. We thank Dr. R. Campbell (Utah) for his input on using biotinylated heparin, K. Hill (NDSU) for assistance with protein production, J. Bahr for XPS study and B. Hoffmann for assistance with mechanical testing. Funding for the Core Synthesis and Analytical Services Facility used in this publication was made possible by NIH Grant P30 GM103332 (NIGMS). Manuscript contents are solely the responsibility of the authors and do not necessarily represent the official views of the NIH.

3.8. References

[1] A. E. Brooks *et al.*, "Distinct contributions of model MaSp1 and MaSp2 like peptides to the mechanical properties of synthetic major ampullate silk fibers as revealed in silico," *Nanotechnol. Sci. Appl.*, vol. 1, pp. 9–16, Aug. 2008.

[2] M. B. Hinman, J. A. Jones, and R. V. Lewis, "Synthetic spider silk: a modular fiber," *Trends Biotechnol.*, vol. 18, no. 9, pp. 374–379, 2000.

[3] C. Y. Hayashi, N. H. Shipley, and R. V. Lewis, "Hypotheses that correlate the sequence, structure, and mechanical properties of spider silk proteins," *Int. J. Biol. Macromol.*, vol. 24, no. 2–3, pp. 271–275, Apr. 1999.

[4] M. S. Creager *et al.*, "Solid-state NMR comparison of various spiders' dragline silk fiber," *Biomacromolecules*, vol. 11, no. 8, pp. 2039–2043, Aug. 2010.

[5] G. P. Holland, J. E. Jenkins, M. S. Creager, R. V. Lewis, and J. L. Yarger, "Solid-state NMR investigation of major and minor ampullate spider silk in the native and hydrated states," *Biomacromolecules*, vol. 9, no. 2, pp. 651–657, Feb. 2008.

[6] K. Yazawa, E. Yamaguchi, D. Knight, and T. Asakura, "13 C solid-state NMR study of the 13 C-labeled peptide, (E)8 GGLGGQGAG(A)6 GGAGQGGYGG as a model for the local structure of Nephila clavipes dragline silk (MaSp1) before and after spinning," *Biopolymers*, vol. 97, no. 6, pp. 347–354, Jun. 2012.

[7] K. Ohgo, F. Bagusat, T. Asakura, and U. Scheler, "Investigation of structural transition of regenerated silk fibroin aqueous solution by Rheo-NMR spectroscopy," *J. Am. Chem. Soc.*, vol. 130, no. 12, pp. 4182–4186, Mar. 2008.

[8] H. Xiao, S. J. Miller, N. U. Bang, and W. P. Faulk, “Protein-bound heparin/heparan sulfates in human adult and umbilical cord plasma,” *Haemostasis*, vol. 29, no. 4, pp. 237–246, 1999.

[9] S. T. Krishnaji and D. L. Kaplan, “Bioengineered chimeric spider silk-uranium binding proteins,” *Macromol. Biosci.*, vol. 13, no. 2, pp. 256–264, Feb. 2013.

[10] S. Gomes, J. Gallego-Llamas, I. B. Leonor, J. F. Mano, R. L. Reis, and D. L. Kaplan, “Biological responses to spider silk-antibiotic fusion protein,” *J. Tissue Eng. Regen. Med.*, vol. 6, no. 5, pp. 356–368, May 2012.

[11] L. L. S. Canabady-Rochelle, D. J. Belton, O. Deschaume, H. A. Currie, D. L. Kaplan, and C. C. Perry, “Bioinspired silicification of silica-binding peptide-silk protein chimeras: comparison of chemically and genetically produced proteins,” *Biomacromolecules*, vol. 13, no. 3, pp. 683–690, Mar. 2012.

[12] C. Wong Po Foo *et al.*, “Novel nanocomposites from spider silk-silica fusion (chimeric) proteins,” *Proc. Natl. Acad. Sci. U. S. A.*, vol. 103, no. 25, pp. 9428–9433, Jun. 2006.

[13] S. Gomes, K. Numata, I. B. Leonor, J. F. Mano, R. L. Reis, and D. L. Kaplan, “AFM study of morphology and mechanical properties of a chimeric spider silk and bone sialoprotein protein for bone regeneration,” *Biomacromolecules*, vol. 12, no. 5, pp. 1675–1685, May 2011.

[14] J. Scheller, D. Henggeler, A. Viviani, and U. Conrad, “Purification of spider silk-elastin from transgenic plants and application for human chondrocyte proliferation,” *Transgenic Res.*, vol. 13, no. 1, pp. 51–57, Feb. 2004.

[15] J. Wang, W. Hu, Q. Liu, and S. Zhang, “Dual-functional composite with anticoagulant and antibacterial properties based on heparinized silk fibroin and chitosan,” *Colloids Surf. B Biointerfaces*, vol. 85, no. 2, pp. 241–247, Jul. 2011.

[16] H. Yu, E. M. Munoz, R. E. Edens, and R. J. Linhardt, “Heparin Regulation of the Complement System,” in *Chemistry and Biology of Heparin and Heparan Sulfate*, Oxford, UK: Elsevier, 2005, pp. 313–343.

[17] D. Diekjürgen and D. W. Grainger, “Polysaccharide matrices used in 3D in vitro cell culture systems,” *Biomaterials*, vol. 141, pp. 96–115, Oct. 2017.

[18] H. Edward Conrad, “Chapter 1 - Heparin vs Heparan Sulfate,” in *Heparin-Binding Proteins*, H. E. Conrad, Ed. San Diego: Academic Press, 1998, pp. 1–5.

[19] H. Edward Conrad, “Chapter 8 - Heparin-Binding Proteins in Hemostasis,” in *Heparin-Binding Proteins*, H. E. Conrad, Ed. San Diego: Academic Press, 1998, pp. 239–300.

[20] H. Edward Conrad, “Chapter 4 - Structural Modification of Heparinoids,” in *Heparin-Binding Proteins*, H. E. Conrad, Ed. San Diego: Academic Press, 1998, pp. 115–136.

[21] H. Edward Conrad, “Chapter 6 - Heparinoid/Protein Interactions,” in *Heparin-Binding Proteins*, H. E. Conrad, Ed. San Diego: Academic Press, 1998, pp. 183–202.

[22] A. D. Cardin and H. J. Weintraub, “Molecular modeling of protein-glycosaminoglycan interactions.,” *Arterioscler. Thromb. Vasc. Biol.*, vol. 9, no. 1, pp. 21–32, Jan. 1989.

[23] M. Pasupuleti, A. Schmidtchen, and M. Malmsten, “Antimicrobial peptides: key components of the innate immune system,” *Crit. Rev. Biotechnol.*, vol. 32, no. 2, pp. 143–171, Jun. 2012.

[24] M. C. L. Martins, S. A. Curtin, S. C. Freitas, P. Salgueiro, B. D. Ratner, and M. A. Barbosa, “Molecularly designed surfaces for blood deheparinization using an

immobilized heparin-binding peptide," *J. Biomed. Mater. Res. A*, vol. 88, no. 1, pp. 162–173, Jan. 2009.

[25] A. Verrecchio, M. W. Germann, B. P. Schick, B. Kung, T. Twardowski, and J. D. San Antonio, "Design of peptides with high affinities for heparin and endothelial cell proteoglycans," *J. Biol. Chem.*, vol. 275, no. 11, pp. 7701–7707, Mar. 2000.

[26] M. Malmsten, G. Kasetty, M. Pasupuleti, J. Alenfall, and A. Schmidtchen, "Highly selective end-tagged antimicrobial peptides derived from PRELP," *PloS One*, vol. 6, no. 1, p. e16400, 2011.

[27] J.-Y. Lee *et al.*, "Characterization of the surface immobilized synthetic heparin binding domain derived from human fibroblast growth factor-2 and its effect on osteoblast differentiation," *J. Biomed. Mater. Res. A*, vol. 83, no. 4, pp. 970–979, Dec. 2007.

[28] C. Vepari, D. Matheson, L. Drummy, R. Naik, and D. L. Kaplan, "Surface modification of silk fibroin with poly(ethylene glycol) for antiadhesion and antithrombotic applications," *J. Biomed. Mater. Res. A*, vol. 93, no. 2, pp. 595–606, May 2010.

[29] X. Wang, X. Zhang, J. Castellot, I. Herman, M. Iafrati, and D. L. Kaplan, "Controlled release from multilayer silk biomaterial coatings to modulate vascular cell responses," *Biomaterials*, vol. 29, no. 7, pp. 894–903, Mar. 2008.

[30] B. Panilaitis, G. H. Altman, J. Chen, H. J. Jin, V. Karageorgiou, and D. L. Kaplan, "Macrophage responses to silk," *Biomaterials*, vol. 24, no. 18, pp. 3079–3085, Aug. 2003.

[31] Y. Wang, H.-J. Kim, G. Vunjak-Novakovic, and D. L. Kaplan, "Stem cell-based tissue engineering with silk biomaterials," *Biomaterials*, vol. 27, no. 36, pp. 6064–6082, Dec. 2006.

[32] M. Nagaoka, H.-L. Jiang, T. Hoshiba, T. Akaike, and C.-S. Cho, “Application of recombinant fusion proteins for tissue engineering,” *Ann. Biomed. Eng.*, vol. 38, no. 3, pp. 683–693, Mar. 2010.

[33] S. C. Gomes, I. B. Leonor, J. F. Mano, R. L. Reis, and D. L. Kaplan, “Antimicrobial functionalized genetically engineered spider silk,” *Biomaterials*, vol. 32, no. 18, pp. 4255–4266, Jun. 2011.

[34] D. J. Belton, A. J. Mieszawska, H. A. Currie, D. L. Kaplan, and C. C. Perry, “Silk-silica composites from genetically engineered chimeric proteins: materials properties correlate with silica condensation rate and colloidal stability of the proteins in aqueous solution,” *Langmuir*, vol. 28, no. 9, pp. 4373–4381, Mar. 2012.

[35] E. Bini, C. W. P. Foo, J. Huang, V. Karageorgiou, B. Kitchel, and D. L. Kaplan, “RGD-functionalized bioengineered spider dragline silk biomaterial,” *Biomacromolecules*, vol. 7, no. 11, pp. 3139–3145, Nov. 2006.

[36] P. Appelgren, U. Ransjö, L. Bindslev, F. Espersen, and O. Larm, “Surface heparinization of central venous catheters reduces microbial colonization in vitro and in vivo: results from a prospective, randomized trial,” *Crit. Care Med.*, vol. 24, no. 9, pp. 1482–1489, Sep. 1996.

[37] N. Betz, C. Cowan, S. Krueger, S. Fly, J. Stevens, and M. Bjerke, “Maxwell® 16 Polyhistidine Protein Purification Kit: Automated Protein Purification with Maximum Performance and Convenience,” *Promega Notes*, vol. 95, pp. 12–15.

[38] F. Teulé *et al.*, “A protocol for the production of recombinant spider silk-like proteins for artificial fiber spinning,” *Nat. Protoc.*, vol. 4, no. 3, pp. 341–355, 2009.

[39] A. E. Brooks, S. M. Stricker, S. B. Joshi, T. J. Kamerzell, C. R. Middaugh, and R. V. Lewis, “Properties of synthetic spider silk fibers based on Argiope aurantia MaSp2,” *Biomacromolecules*, vol. 9, no. 6, pp. 1506–1510, Jun. 2008.

[40] R. K. Scopes, *Protein Purification: Principles and Practice*. Springer Science & Business Media, 2013.

[41] S. Najjam, R. V. Gibbs, M. Y. Gordon, and C. C. Rider, “Characterization of human recombinant interleukin 2 binding to heparin and heparan sulfate using an ELISA approach,” *Cytokine*, vol. 9, no. 12, pp. 1013–1022, Dec. 1997.

[42] A. J. Kugel *et al.*, “Combinatorial materials research applied to the development of new surface coatings XII: Novel, environmentally friendly antimicrobial coatings derived from biocide-functional acrylic polyols and isocyanates,” *J. Coat. Technol. Res.*, vol. 6, no. 1, pp. 107–121, Mar. 2009.

[43] S. Stafslien, J. Daniels, B. Chisholm, and D. Christianson, “Combinatorial materials research applied to the development of new surface coatings III. Utilisation of a high-throughput multiwell plate screening method to rapidly assess bacterial biofilm retention on antifouling surfaces,” *Biofouling*, vol. 23, no. 1, pp. 37–44, Jan. 2007.

[44] S. Najjam, B. Mulloy, J. Theze, M. Gordon, R. Gibbs, and C. C. Rider, “Further characterization of the binding of human recombinant interleukin 2 to heparin and identification of putative binding sites,” *Glycobiology*, vol. 8, no. 5, pp. 509–516, May 1998.

[45] H. Wu, C. Moser, H.-Z. Wang, N. Høiby, and Z.-J. Song, “Strategies for combating bacterial biofilm infections,” *Int. J. Oral Sci.*, vol. 7, no. 1, pp. 1–7, Mar. 2015.

[46] V. O. Adetunji and T. O. Isola, “Crystal Violet Binding Assay for Assessment of Biofilm Formation by Listeria monocytogenes and Listeria spp on Wood, Steel and Glass Surfaces,” p. 5, 2011.

[47] “Research and Markets: The Market For Drug Eluting Coronary Stents Is Exhibiting Clear Evidence of Recovery with Average Annual PCI Volumes Rising by 5% in the US and 4% in Europe | Business Wire,” 23-Feb-2009. [Online]. Available: http://www.businesswire.com/news/home/20090223005750/en/Research-Markets-Market-Drug-Eluting-Coronary-Stents. [Accessed: 12-Feb-2016].

[48] J. Gunn and D. Cumberland, “Stent coatings and local drug delivery,” *Eur Heart J*, vol. 20, pp. 1693–1700, 1999.

[49] K. Christensen, R. Larsson, H. akan Emanuelsson, G. Elgue, and A. Larsson, “Improved blood compatibility of a stent graft by combining heparin coating and abciximab,” *Thromb. Res.*, vol. 115, no. 3, pp. 245–253, 2005.

[50] E.-M. Hietala *et al.*, “Platelet responses and coagulation activation on polylactide and heparin–polycaprolactone-L-lactide-coated polylactide stent struts,” *J. Biomed. Mater. Res. A*, vol. 67, no. 3, pp. 785–791, 2003.

[51] R. Biran and D. Pond, “Heparin coatings for improving blood compatibility of medical devices,” *Adv. Drug Deliv. Rev.*, vol. 112, pp. 12–23, Mar. 2017.

[52] P. L. Foley, C. H. Barthel, and H. R. Brausa, “Effect of covalently bound heparin coating on patency and biocompatibility of long-term indwelling catheters in the rat jugular vein,” *Comp. Med.*, vol. 52, no. 3, pp. 243–248, 2002.

[53] X. M. Mueller, H. T. Tevaearai, D. Hayoz, and L. K. von Segesser, "Morphometric analysis of heparin coated versus standard intra-aortic balloons.," *ASAIO J.*, vol. 44, no. 5, pp. M401–M404, 1998.

[54] L. K. Kairaitis and T. Gottlieb, "Outcome and complications of temporary haemodialysis catheters.," *Nephrol. Dial. Transplant.*, vol. 14, no. 7, pp. 1710–1714, 1999.

[55] M. Stigter, J. Bezemer, K. de Groot, and P. Layrolle, "Incorporation of different antibiotics into carbonated hydroxyapatite coatings on titanium implants, release and antibiotic efficacy," *J. Control. Release Off. J. Control. Release Soc.*, vol. 99, no. 1, pp. 127–137, Sep. 2004.

[56] G. M. Harbers *et al.*, "Functionalized poly (ethylene glycol)-based bioassay surface chemistry that facilitates bio-immobilization and inhibits nonspecific protein, bacterial, and mammalian cell adhesion," *Chem. Mater.*, vol. 19, no. 18, pp. 4405–4414, 2007.

[57] S. K. Hendricks, C. Kwok, M. Shen, T. A. Horbett, B. D. Ratner, and J. D. Bryers, "Plasma-deposited membranes for controlled release of antibiotic to prevent bacterial adhesion and biofilm formation," *J. Biomed. Mater. Res.*, vol. 50, no. 2, pp. 160–170, 2000.

[58] I. A. Rojas, J. B. Slunt, and D. W. Grainger, "Polyurethane coatings release bioactive antibodies to reduce bacterial adhesion," *J. Control. Release Off. J. Control. Release Soc.*, vol. 63, no. 1–2, pp. 175–189, Jan. 2000.

[59] H. Ghandehari, "Recombinant biomaterials for pharmaceutical and biomedical applications," *Pharm. Res.*, vol. 25, no. 3, pp. 672–673, 2008.

[60] M. F. Elahi, G. Guan, L. Wang, X. Zhao, F. Wang, and M. W. King, "Surface modification of silk fibroin fabric using layer-by-layer polyelectrolyte deposition and

heparin immobilization for small-diameter vascular prostheses," *Langmuir ACS J. Surf. Colloids*, vol. 31, no. 8, pp. 2517–2526, Mar. 2015.

[61] M. Cestari, V. Muller, J. H. da S. Rodrigues, C. V. Nakamura, A. F. Rubira, and E. C. Muniz, "Preparing silk fibroin nanofibers through electrospinning: further heparin immobilization toward hemocompatibility improvement," *Biomacromolecules*, vol. 15, no. 5, pp. 1762–1767, May 2014.

[62] F. P. Seib, M. Herklotz, K. A. Burke, M. F. Maitz, C. Werner, and D. L. Kaplan, "Multifunctional silk-heparin biomaterials for vascular tissue engineering applications," *Biomaterials*, vol. 35, no. 1, Jan. 2014.

[63] Z. Liu *et al.*, "Silk fibroin-based woven endovascular prosthesis with heparin surface modification," *J. Mater. Sci. Mater. Med.*, vol. 29, no. 4, p. 46, Apr. 2018.

[64] M. Zamani, M. Khafaji, M. Naji, M. Vossoughi, I. Alemzadeh, and N. Haghighipour, "A Biomimetic Heparinized Composite Silk-Based Vascular Scaffold with sustained Antithrombogenicity," *Sci. Rep.*, vol. 7, Jun. 2017.

[65] S. R. Bailey and others, "Coating of endovascular stents," *Textb. Interv. Cardiol.*, vol. 2, pp. 754–765, 1994.

[66] M. Hinman, Z. Dong, M. Xu, and R. V. Lewis, "Spider silk: a mystery starting to unravel," *Results Probl. Cell Differ.*, vol. 19, pp. 227–254, 1992.

[67] T. P. Knowles *et al.*, "Role of Intermolecular Forces in Defining Material Properties of Protein Nanofibrils," *Science*, vol. 318, no. 5858, pp. 1900–1903, Dec. 2007.

[68] H. Choi, N. Rangarajan, and J. C. Weisshaar, "Lights, Camera, Action! Antimicrobial Peptide Mechanisms Imaged in Space and Time," *Trends Microbiol.*, vol. 24, no. 2, pp. 111–122, Feb. 2016.

[69] M. Xiao, J. Jasensky, L. Foster, K. Kuroda, and Z. Chen, "Monitoring Antimicrobial Mechanisms of Surface-Immobilized Peptides in Situ," *Langmuir*, vol. 34, no. 5, pp. 2057–2062, Feb. 2018.

[70] Z. Liu *et al.*, "Length Effects in Antimicrobial Peptides of the (RW)n Series," *Antimicrob. Agents Chemother.*, vol. 51, no. 2, pp. 597–603, Feb. 2007.

[71] Y. Li, "Recombinant production of antimicrobial peptides in Escherichia coli: A review," *Protein Expr. Purif.*, vol. 80, no. 2, pp. 260–267, Dec. 2011.

[72] H. Sletta *et al.*, "The Presence of N-Terminal Secretion Signal Sequences Leads to Strong Stimulation of the Total Expression Levels of Three Tested Medically Important Proteins during High-Cell-Density Cultivations of Escherichia coli," *Appl. Environ. Microbiol.*, vol. 73, no. 3, pp. 906–912, Feb. 2007.

[73] C. Luan *et al.*, "Recombinant expression of antimicrobial peptides using a novel self-cleaving aggregation tag in Escherichia coli," *Can. J. Microbiol.*, vol. 60, no. 3, pp. 113–120, Mar. 2014.

[74] K.-Y. Huang *et al.*, "Identification of natural antimicrobial peptides from bacteria through metagenomic and metatranscriptomic analysis of high-throughput transcriptome data of Taiwanese oolong teas," *BMC Syst. Biol.*, vol. 11, no. Suppl 7, Dec. 2017.

[75] M. Hassan, M. Kjos, I. F. Nes, D. B. Diep, and F. Lotfipour, "Natural antimicrobial peptides from bacteria: characteristics and potential applications to fight against antibiotic resistance," *J. Appl. Microbiol.*, vol. 113, no. 4, pp. 723–736, Oct. 2012.

[76] M. Zorko and R. Jerala, "Production of Recombinant Antimicrobial Peptides in Bacteria," in *Antimicrobial Peptides*, A. Giuliani and A. C. Rinaldi, Eds. Humana Press, 2010, pp. 61–76.

[77] K. Yang, Y. Su, J. Li, J. Sun, and Y. Yang, “Expression and purification of the antimicrobial peptide cecropin AD by fusion with cationic elastin-like polypeptides,” *Protein Expr. Purif.*, vol. 85, no. 2, pp. 200–203, Oct. 2012.

[78] D. W. Lim, K. Trabbic-Carlson, J. A. MacKay, and A. Chilkoti, “Improved Non-chromatographic Purification of a Recombinant Protein by Cationic Elastin-like Polypeptides,” *Biomacromolecules*, vol. 8, no. 5, pp. 1417–1424, May 2007.

[79] Y. Shen, H.-X. Ai, R. Song, Z.-N. Liang, J.-F. Li, and S.-Q. Zhang, “Expression and purification of moricin CM4 and human β-defensins 4 in Escherichia coli using a new technology,” *Microbiol. Res.*, vol. 165, no. 8, pp. 713–718, Oct. 2010.

[80] A. Verrecchio, M. W. Germann, B. P. Schick, B. Kung, T. Twardowski, and J. D. S. Antonio, “Design of Peptides with High Affinities for Heparin and Endothelial Cell Proteoglycans,” *J. Biol. Chem.*, vol. 275, no. 11, pp. 7701–7707, Mar. 2000.

[81] S. A. V. Raghavan and M. Dikshit, “Recent advances in the status and targets of antithrombotic agents,” *Drugs Future*, vol. 27, no. 7, p. 669, 2002.

[82] T. Hattori, K. Kimura, E. Seyrek, and P. L. Dubin, “Binding of bovine serum albumin to heparin determined by turbidimetric titration and frontal analysis continuous capillary electrophoresis,” *Anal. Biochem.*, vol. 295, no. 2, pp. 158–167, Aug. 2001.

[83] H. Yu, E. M. Muñoz, R. E. Edens, and R. J. Linhardt, “Kinetic studies on the interactions of heparin and complement proteins using surface plasmon resonance,” *Biochim. Biophys. Acta*, vol. 1726, no. 2, pp. 168–176, Nov. 2005.

[84] R. I. W. Osmond, W. C. Kett, S. E. Skett, and D. R. Coombe, “Protein-heparin interactions measured by BIAcore 2000 are affected by the method of heparin immobilization,” *Anal. Biochem.*, vol. 310, no. 2, pp. 199–207, Nov. 2002.

[85] E. M. Muñoz and R. J. Linhardt, “Heparin-Binding Domains in Vascular Biology,” *Arterioscler. Thromb. Vasc. Biol.*, vol. 24, no. 9, pp. 1549–1557, Sep. 2004.

[86] E. A. Ponomarenko *et al.*, “The Size of the Human Proteome: The Width and Depth,” *Int. J. Anal. Chem.*, vol. 2016, 2016.

[87] “Osmolarity - an overview | ScienceDirect Topics.” [Online]. Available: https://www.sciencedirect.com/topics/immunology-and-microbiology/osmolarity. [Accessed: 15-Mar-2019].

[88] M. C. Z. Meneghetti *et al.*, “Heparan sulfate and heparin interactions with proteins,” *J. R. Soc. Interface*, vol. 12, no. 110, Sep. 2015.

[89] E. Stellwagen, J. D. Prantner, and N. C. Stellwagen, “Do zwitterions contribute to the ionic strength of a solution?,” *Anal. Biochem.*, vol. 373, no. 2, pp. 407–409, Feb. 2008.

[90] J. Zheng, A. Wexler, and G. H. Pollack, “Effect of buffers on aqueous solute-exclusion zones around ion-exchange resins,” *J. Colloid Interface Sci.*, vol. 332, no. 2, pp. 511–514, Apr. 2009.

[91] E. Andersson, V. Rydeng\a ard, A. Sonesson, M. Mörgelin, L. Björck, and A. Schmidtchen, “Antimicrobial activities of heparin-binding peptides,” *Eur. J. Biochem.*, vol. 271, no. 6, pp. 1219–1226, 2004.

[92] B. Bechinger and S.-U. Gorr, “Antimicrobial Peptides: Mechanisms of Action and Resistance,” *J. Dent. Res.*, vol. 96, no. 3, pp. 254–260, 2017.

[93] B. Hoffmann, C. Gruat-Henry, P. Mulinti, L. Jiang, B. D. Brooks, and A. E. Brooks, “Using hydrodynamic focusing to predictably alter the diameter of synthetic silk fibers,” *PLOS ONE*, vol. 13, no. 4, p. e0195522, Apr. 2018.

CHAPTER 4. SYNTHESIS AND EVALUATION OF NOVEL HEPARIN BINDING FUNCTIONALIZED MODIFIED SPIDER SILK COATING FOR CATHETER PROVIDING DUAL ANTIMICROBIAL AND ANTICOAGULANT PROPERTIES

4.1 Abstract

Tailored surface coatings have been used for decades to improve material performance in blood. Among different approaches, heparin based biomedical coatings have found great success in the commercial catheter market. However, they have their own limitations. Coating of a vascular device with a heparin binding peptide (HBP), which can sequester the circulating heparin, presents numerous advantages over both systemic heparin therapy and direct heparin bound surfaces. Embedding HBP in a silk biopolymer provides the mechanical integrity necessary under dynamic flow conditions to both insert the catheter and maintain proper blood flow. Furthermore, due to the similarity in structure of HBP with antimicrobial peptides, it is predicted that the fusion protein will also show antimicrobial property, a critical and unique aspect to combat catheter related blood stream infections and extend the longevity of hemodialysis catheters. To assess this hypothesis, a recombinant fusion protein (S_4H_4) containing both silk amino acid motifs and HBP was assessed as a coating on a silicone surface. After validating that, the protein was deposited on the surface via XPS, Raman spectroscopy, ATR and SEM imaging, antimicrobial and anticoagulant activities were evaluated. The coating was able to prevent not only planktonic bacterial growth but also prevented the growth of a biofilm. Finally, the coating had both antibacterial and anticoagulant effect simultaneously. This study proves the successful production of a silk-based biopolymer that can be embedded with a heparin-binding functionality to create a dual functional device coating that can prevent infection and thrombosis together.

4.2. Introduction

Thrombosis (formation of a blood clot) and infection are frequently inextricably connected, effectively countering resolution with single pathology therapeutics, allowing both pathologies to proceed unabated [1]–[3]. Indeed, hemostatic abnormalities are encountered in most cases of infection, ranging from an increase in sensitive markers for active coagulation to a rise in host factors such as platelets, fibrin and fibronectin that may result in localized thrombotic complications; simultaneously, independent production of thrombi can also provide a rich matrix of fibrils for bacterial adhesion [4], [5]. This mechanism is of particular importance in cases of CRBSI (catheter-related bloodstream infection) where thrombi lead to microbial surface colonization of catheters or medical devices [6]. Importantly, when bacteria colonize a surface, such as an in dwelling biomedical device, they often secrete a complex mucopolysaccharide barrier to form a "biofilm", allowing them to not only escape the host immune response but also to thwart many pharmaceutical interventions and enhance their virulence [7], [8].

There are 5 main clinical interventions for thrombosis- related flow problems: forceful catheter flush, fibrinolytic enzymes, mechanical thrombus removal, catheter exchange, and percutaneous fibrin-sheath stripping [9], [10]. Systemic anticoagulation therapy and heparin-based biomedical coatings have been used for decades to improve material performance in the blood and biological milieu; however, heparin therapy can simultaneously promote and treat the thrombosis [11], [12]. Systemic therapy may cause Heparin-induced thrombocytopenia (HIT) as a potential complication that can lead to a non-immune mediated transient decrease in platelet count but a rise in levels of fibrinogen. In addition, studies evaluating catheter surface treatments to reduce infection have provided inconsistent results in reducing CRBSIs. Traditionally, either systemic antibiotic administration with antibiotic lock therapy or heparin therapy has been employed

separately for the treatment of CRBSI. The major drawback of the antibiotic lock therapy is the development of antibiotic resistance by the bacteria in the biofilm due to subtherapeutic exposure of bacteria to the antibiotics while only eliminating the intraluminal source of infection [13], [14]. Furthermore, such a strategy addresses only one problem at a time and completely ignoring the complex relationship between infection and thrombosis, either of which can limit the number of in dwelling catheter days.

Alternatively, recent advances in catheter materials and the relative success of chemically defined polymer surface coatings have proved promising carriers for pharmaceutical immobilization to treat CRBSI. Surface modification and coating of the catheter material can be done via either a passive approach by changing the surface chemistry or physical structure of the device or by a bioactive approach by locally releasing a pharmacological agent to inhibit coagulation. Heparin has been employed in various forms as a covalently immobilized surface coating or a prophylactic agent to improve hemocompatibility of medical devices [15], [16]. Unfortunately, the lifetime of these surface modifications can be limited by the natural foreign body response, which can lead to fibrous capsule formation. This necessitates a resilient and durable strategy to provide improved device resistance to biofouling and device longevity at the same time. A “self-renewable” multi-functional coating relying on biological mechanisms and the coagulation-signaling cascade may prove an effective, alternative strategy.

In addition to biological longevity, mechanical integrity under dynamic flow conditions is a key factor for coating materials. Although many current catheter bulk materials possess sufficient mechanical function, the coatings lack the strength and flexibility necessary to resist delamination during insertion of the catheter while the bulk material maintains proper blood flow. In this context,

genetically modified silk protein, which can capture endogenous heparin tethering it to the device surface, provides an attractive opportunity as a biomaterial coating.

Silk fibroin has demonstrated a combination of excellent properties including biocompatibility, robust mechanical strength in various material formats and controllable rates of degradation to non-toxic byproducts *in vivo*, leading it to be increasingly considered for various biomedical and drug delivery applications [17], [18]. Additionally, the ability to manipulate the primary structure/function relationship of spider silk by embedding different functional amino acid blocks or by altering the ratio of amino acid blocks [19], [20] to produce a mechanically robust and chemically defined biomaterial makes synthetic spider silk proteins an attractive biomaterial. One such attractive target amino acid block to endow new biological function to a recombinant silk peptide is found in the heparin binding region of a variety of endogenous biomolecules (e.g., growth factors). Homology modeling of heparin binding regions reveals a structural prerequisite and consensus amino acid sequence, XBBBXXBX, where B is a basic residue (arginine) and X represents a hydrophobic or uncharged amino acid (alanine) [21], [22]. Interestingly, this consensus sequence has several tertiary structures analogous to antimicrobial peptides and is thought to also be antibacterial [21], [23], [24]. The heparin binding peptide (HBP) (ARKKAAKA) can be either covalently attached to the silk peptide or genetically linked to the silk sequence. This fusion protein is proposed to mitigate both device-centered thrombosis and bacterial biofouling using naturally occurring immobilized amino acid motifs. In this paper, we report the use of this fusion protein as a silicone material coating to prevent both coagulation and bacterial adhesion.

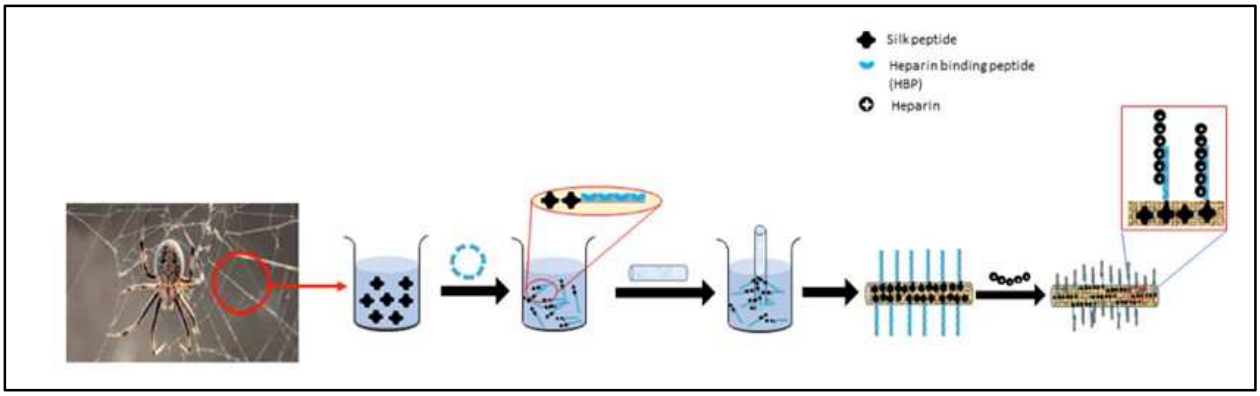

Figure 4.1. Graphical representation of Hypothesis. Spider silk is functionalized with heparin binding peptide (HBP) and coated on catheter tubing which can capture endogenous heparin to make it anti-infective and anti-thrombotic surface.

4.3. Methods

4.3.1. Protein synthesis

The genetic sequence of the fusion protein containing four repeats of a general MaSp2 like monomer ($GPGXXA_8$ where X = G, Q, Y [25]) and four repeats of heparin binding (ARKKAAKA) motif (S_4H_4) was synthesized and cloned into pET 30a (Genscript, Piscataway, NJ). The recombinant protein was expressed in E. coli (New England Biolabs) and purified by nickel affinity chromatography. The heparin capturing ability was determined by heparin affinity chromatography using HyperD heparin resin. Each chromatography fraction was collected separately for analysis. ATIII and IL-2 were used as positive controls for heparin binding [26], and BSA as a negative control. Molecular weight of the purified protein was further confirmed by mass spectrometry. The purified protein was dialyzed for further purification and lyophilized.

4.3.2. Coating preparation

Silicone sheets (USP class VI Silicone, thickness – 0.01", Specialty Manufacturing inc, Saginaw, MI) were used as to mimic the bulk catheter material. The silicone sheet was cut into square shaped coupons (25mm × 25mm) and subsequently activated by plasma treatment prior to coating. The plasma etching process was performed on Trion Phantom RIE Plasma Etcher (Trion

Technology, Clearwater, FL) at 50mTorr with 20 sccm oxygen flow for 90 seconds [27]. The activated silicone coupons were immediately dip coated in the S_4H_4 protein solution (in PBS at 300μM) manually for about ten times with intermittent air drying for 5 minutes in between dipping.

4.3.3. Coating characterization

4.3.3.1. Contact Angle

Static contact angles of coated and uncoated silicone sheets were measured using FTÅ 125 Contact Angle/Surface Tension Analyzer (First Ten Angstroms, Portsmouth VA) to determine the wettability of the surface. Deionized water (10ul) was dispensed onto the surface capturing the image of the water drop using a charged coupled device (CCD) camera. Images were analyzed using an Fta32 V2.0 image analysis software.

4.3.3.2. X-ray Photoelectron Spectroscopy (XPS)

A K-Alpha™ X-ray Photoelectron Spectrometer (Thermo Scientific, MA) was used for elemental analysis to determine the surface chemistry of both coated and uncoated silicone surfaces. Survey spectra were obtained from -10 to 1350 eV with a pass energy of 200 eV and 1 eV energy step size. High resolution (HR) analyses with pass energy of 40 eV were performed at a take-off angle of 90° to determine elemental atomic percent composition. HR scans were performed at 50 eV pass energy for Oxygen (O 1s), Carbon (C 1s), and Nitrogen (N 1s) scans.

4.3.3.3. Scanning Electron Microscopy (SEM) Imaging

The thickness of the coating was analyzed using SEM. Coated and uncoated sheets were cut using a razor blade and the samples (n=3) were attached to cylindrical aluminum mounts using colloidal silver paint (Structure Probe Inc., West Chester, Pennsylvania). Subsequently, the samples were coated with a conductive layer of carbon in a high-vacuum evaporative coater (Cressington 208c, Ted Pella Inc., Redding, California). Images were obtained with a JEOL JSM-

7600F scanning electron microscope (JEOL USA Inc., Peabody, Massachusetts) operating at 2 kV.

4.3.3.4. Attenuated Total Reflection (ATR)

ATR spectra of the coated and uncoated silicone tube were obtained with a Nicolet 6700 FTIR-ATR Spectrometer operated with OMNIC software [28]. The crystal used was a polished diamond. The silicone sheets were placed on the diamond crystal and the spectra were scanned from 400 to 4000 cm^{-1}. Spectra were recorded with 64 scans and 4 cm^{-1} resolution with data spacing of 0.964 cm^{-1}. All spectra were reported without smoothing the output.

4.3.3.5. Raman Spectroscopy

Confocal Raman spectra were obtained from Horiba Jobin Yvon's Raman Spectrometer on LabRAM Aramis software equipped with He-Ne laser source emitting at 532nm [29]. The sample was scanned at a constant speed with 2µm step size. The radiation was focused in the Raman-shift range of 3500-300 cm^{-1} and scattered radiation was collected with a confocal aperture of 600µm and a slit aperture of 150µm.

4.3.4. Characterization of antimicrobial properties

4.3.4.1. ATP Assay

An overnight *S. aureus* (ATCC 49230) culture was prepared in LB broth (Fischer Scientific, Hampton, NH). To create a biofilm, the overnight bacterial culture was taken and diluted into LB broth to get an OD_{600}=0.5. Later, S_4H_4 coated and non-coated silicone sheets (40.92 mm^2 area) were placed in the wells of a 24-well plate and 1.5 mL of diluted bacterial culture was added to the well. The plates were incubated for 24 hours at 37 C with shaking. After incubation, the silicone coupons were collected and washed in 1X Phosphate Buffered Saline PBS, three times. The silicone coupons were wiped with a sterile cotton swab, which was subsequently immersed in

PBS and vortexed to make a bacterial suspension. The ATP assay was performed using the BacTiter Glo kit (Promega, WI, USA) according to the manufacturer's protocol. Briefly, the bacterial suspension in PBS was equilibrated to room temperature (25 C) and 100 µL of the bacterial suspension was put in an opaque 96 well plate. BacTiter Glo reagent (100 µL) was added and mixed followed by incubation at 25 C for 5 minutes. After the incubation, luminescence was measured using SpectraMax5 spectrometer at a wavelength of 560nm.

4.3.4.2. Colony Assay

Antibacterial activity was evaluated by colony assay. Bacterial biofilm was allowed to develop on the coated and uncoated silicone tubing (ID 3mm × OD 4mm, length 3cm, GoFlow systems, Amazon, Seattle, WA) in a method analogous to that for the silicone coupons as described above. After 24 hour incubation, the tubing was rinsed gently to remove any unadhered bacteria. The tubing samples were then vortexed and serial dilutions of the vortexed solution were plated on an agar and incubated overnight at 37 C. The number of colonies were counted the next day.

4.3.4.3. Simultaneous Evaluation of Antimicrobial Anti-coagulant Properties

An overnight culture of *S. aureus* was prepared in LB broth. To create a biofilm, OD_{600} of 0.5 bacterial culture was prepared from the overnight culture. Protein coated and non-coated silicone coupons (40.92 mm^2 area) were placed in a 24 well plate and 1.5 mL of bacterial culture was added to the well. The plates were incubated for 24 hours at 37 C in an incubator. After incubation, the bacterial suspension was removed and the edges of the coupon were wiped with a sterile cotton swab to remove any unadhered bacteria. Subsequently, the coupons were rinsed gently with PBS, and 200 µL of heparin (100 µg/mL in TBS) was added and incubated for 2 hours. The wells were again gently rinsed with PBS. Subsequently, the bacterial and heparin exposed coupons were used for the aPTT (APTT XL Pacific Homeostasis Assay, Thermo Fischer, USA)

assay to check the clot formation. Briefly, 0.1 mL of APTT-XL reagent was added to the well with a silicone coupon, and the reaction was incubated for 5 min. Calcium chloride solution (0.1 mL of 0.02 M) was then added to initiate clot-like formation and clot-like formation was assessed by measuring OD_{600} to determine the change in optical density of the solution.

4.3.4.4. Statistical Analysis

SPSS 23 was used to perform statistical analysis. Student t-test was used to determine the significance difference between coated and uncoated samples. Statistical significance was defined by $p<0.01$ for colony assay and ATP assay, and $p<0.001$ for simultaneous evaluation of anticoagulant and antimicrobial properties.

4.4. Results

4.4.1. Validation of protein

Agarose gel electrophoresis was performed to confirm the successful cloning of silk motif with HBP motif. Slight increase in the base pairs after cloning with HBP motif lead to shift in the molecular weight on the gel. To determine the heparin binding functionality, heparin chromatography was performed which shows the elution of the protein form the column with the elution buffer (Figure 4.2). S_2H_4 was synthesized initially as a control but it did not show any further activity regarding heparin binding. $Silk_2$ was predicted to be 14766 Da while S_4H_4 was predicted to be 16355 Da which was further confirmed by mass spectrometry (data not shown).

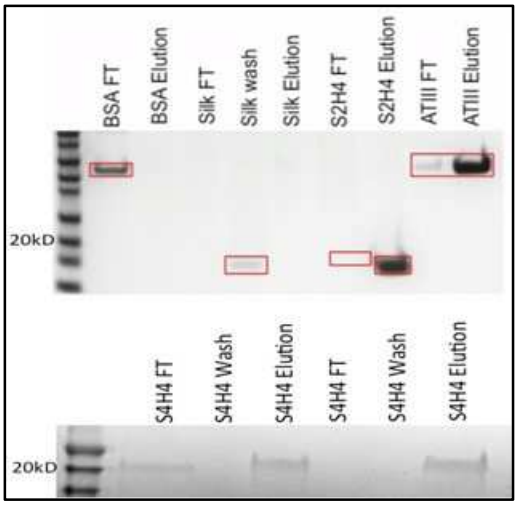

Figure 4.2. SDS PAGE demonstrating a solid phase functional assay using heparin affinity chromatography. Increased ability of both the recombinant S_2H_4 and S_4H_4 proteins to bind heparin as indicated by its elution in the final high salt buffer. Two clones of S_4H_4 are shown. $Silk_2$ was predicted to be 14,766 Da while S_4H_4 was predicted to be 16,355 Da.

4.4.2. Characterization of coating

Once the protein was synthesized and validated, it was solubilized in PBS at a concentration of 300µM. This protein solution was used to coat the silicone sheets by dip coating.

4.4.2.1. Contact Angle

To determine the presence of the S4H4 coating on the surface of hydrophobic silicone, the surface wettability of the coated silicone coupon, the static water contact angle of the coated and uncoated samples was measured. The contact angle of the uncoated silicone sheet was found to be $103.35^0 \pm 2.3^0$ while the protein coated sheets showed a reduced contact angle of $19.6^0 \pm 3.4$ (Fig 4.3), indicating a significant shift from hydrophobicity to hydrophilicity.

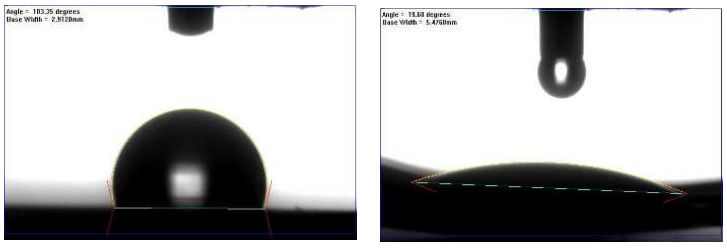

Figure 4.3. Contact angle measurement of uncoated sheet (left), and coated sheet (right) by sessile drop.

4.4.2.2. X-ray Photoelectron Spectroscopy (XPS) Measurements

A shift in the hydrophobic nature of the silicone sheet indicates a change in the surface, likely attributed to the presence of the protein; however, increased specificity was obtained by analyzing the chemical composition of the surface using XPS spectra. Both coated and uncoated silicone sheets show similar percentage composition for C1s, O1s while percentage of N1s increased from 1.56% to 6.1%. Importantly the percentage of silicone also decreased from 2.26% to 0.91% after coating (Table 4.1), further suggesting the presence of protein on the coated sheet.

Table 4.1. XPS survey of the coated and uncoated silicone sheets with atomic percentages.

	Atomic %	
Name	coated	non coated
C1s	71.25	77.75
O1s	16.58	14.86
N1s	6.12	1.57
Cl2p3	3.4	3.18

4.4.2.3. Raman Spectroscopy

A shift in the chemical composition of silicone sheet surface was evidence of2protein coating; however, the coating of tube structure similar to a catheter was assessed by comparing the Raman spectra of both uncoated and the coated tubing. In comparison to the uncoated tubing, Raman spectra of the coated tubing resulted in additional prominent peaks corresponding to Raman shifts at 788, 857, 1261, 1406, and 2795 cm-1 (Figure 4.4). The presence of doublet peaks at 788, 857 cm-1 confirms the presence of a protein with tyrosine as a key aromatic amino acid in the sequence. Similarly, the peak at 1261 cm-1 resulted from the amide linkage that is part of the α-helix structure of protein macromolecule confirming that coating has been deposited on the silicone sheet.

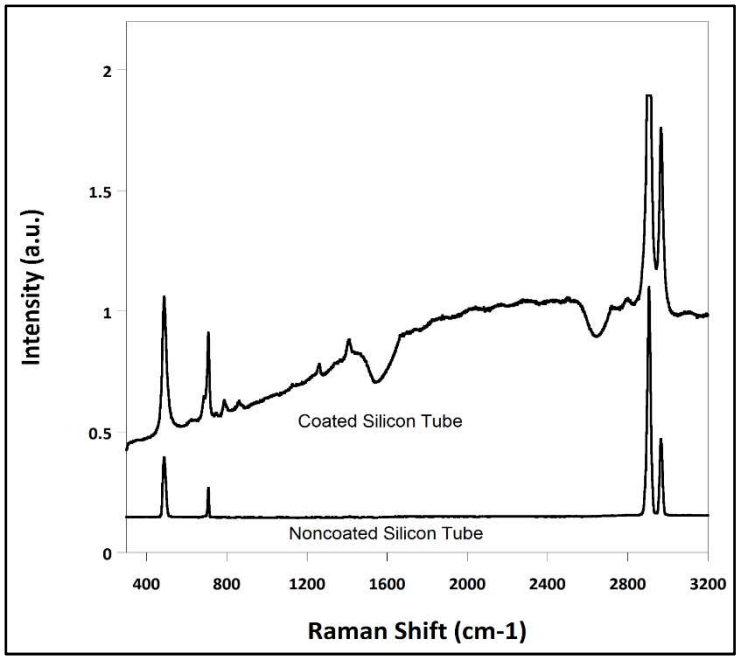

Figure 4.4. Confocal Raman spectra of the coated silicone sheet showing the Raman shifts for tyrosine at 788 and 857 cm-1; Raman shift at 1261 cm-1 due to amide bond compared to the uncoated silicone sheet.

4.4.2.4. Attenuated Total Reflection (ATR)

Presence of the coating on the silicone tube can be augmented for the data obtained from ATR. As compared to the non-coated silicone tube, coated silicone tube resulted detectable peaks at wavenumbers 3268 and 1724 cm^{-1} corresponding to the -OH (stretch), C=O (Stretch) (Figure 4.5) of tyrosine and glutamine. Reflectance peaks at 1632, and 1532 cm^{-1} confirms the presence of aromatic C=C bond. Overall, ATR data further concludes that the coating was deposited on the silicone surface.

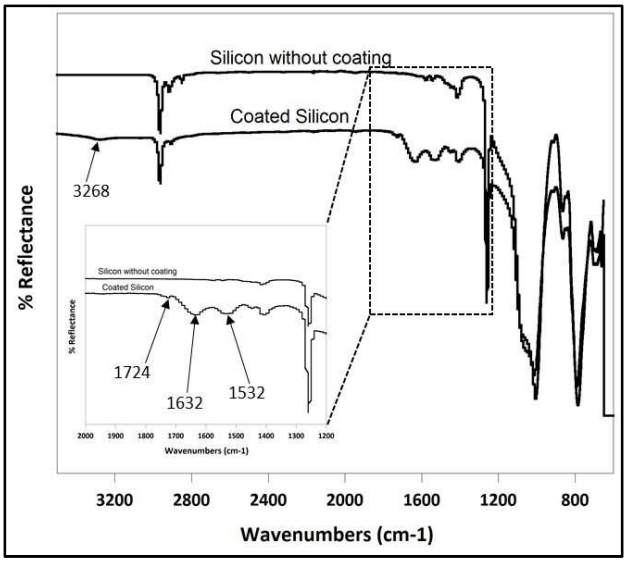

Figure 4.5. ATR spectra of the coated silicone sheet showing the -OH (stretch), C=O (Stretch) and aromatic C=C bond.

4.4.2.5. SEM Imaging

Finally, the uniformity in coating and the thickness of the coating was examined by SEM imaging (Figure 4.6). Based on the imaging, the protein was found to be non-uniformly distributed, although it was clearly present. The thickness was found to be 10.2±3µm as measured from the surface of the sheet.

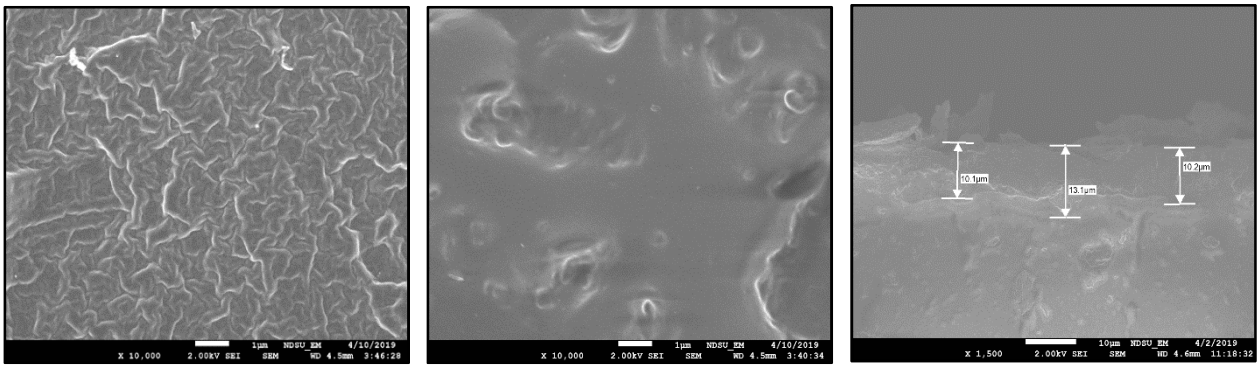

A) B) C)

Figure 4.6. SEM imaging on the (A) coated tube (B) non coated tubes (C) thickness of the coating.

4.4.3. Characterization of bioactivity of the protein coating

4.4.3.1. Colony Assay

Initially, the antimicrobial activity of the coating was analyzed by counting the number of colonies adhered to the surface after incubation with a planktonic bacterial culture. The number of colonies on the protein-coated, silicone sheets was 5 $\times 10^4$ CFU/ml whereas the uncoated samples showed 3 $\times$ 10^6 CFU/ml (n = 5) (Figure 4.7). The coated samples showed significantly lower number of colonies ($p<0.01$) when compared to the uncoated samples.

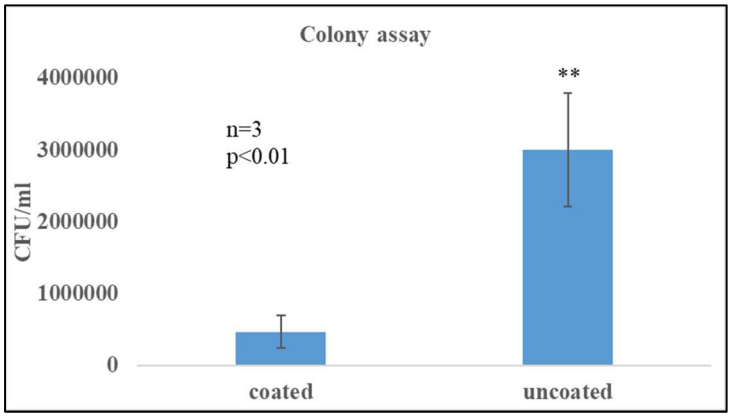

Figure 4.7. Colony assay to evaluate the antimicrobial properties of the coating.

4.4.3.2. ATP Assay

After establishing the antibacterial activity of the coating against planktonic bacteria, the ability of the coating to prevent a biofilm was also evaluated using an ATP assay. Luminesce (RLU) was calculated per unit area (mm^2) of the silicone sheets and was significantly lower ($p<0.01$, n=4) for S_4H_4 coated sheets compared to the non-coated samples (Figure 4.8).

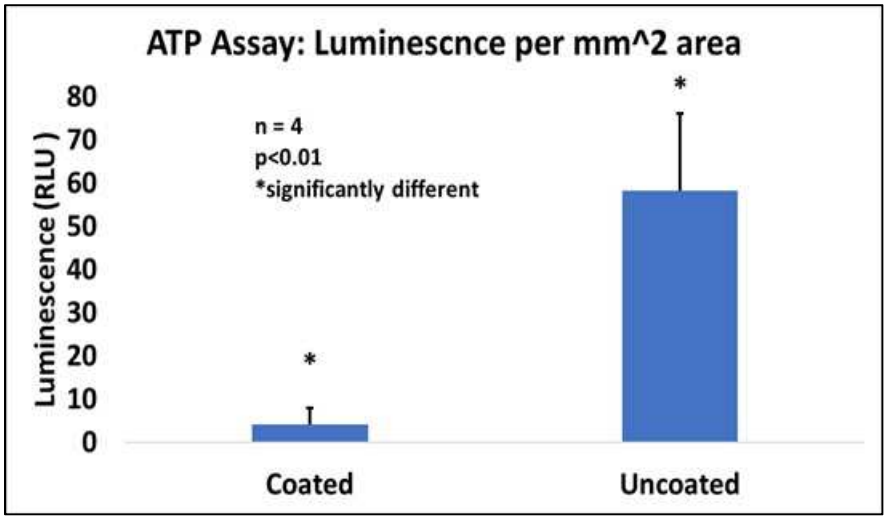

Figure 4.8. ATP assay of the coated sample showed significantly lesser luminescence compared to the noncoated sample confirming the biofilm prevention properties of the coating.

Simultaneous evaluation of antimicrobial anti-coagulant properties: After establishing that the coating had both antimicrobial and antithrombotic activity, it was evaluated to see if both activities could be achieved simultaneously. Initially, a biofilm was grown on both the protein-coated surface and an uncoated control. After rinsing the surface, an aPTT assay was performed to assess if a clot could still be formed. The optical density of the protein coated samples at wavelength of 600 nm ($n=3$, $p<0.001$) (Figure 4.9) was found to be less than the uncoated samples.

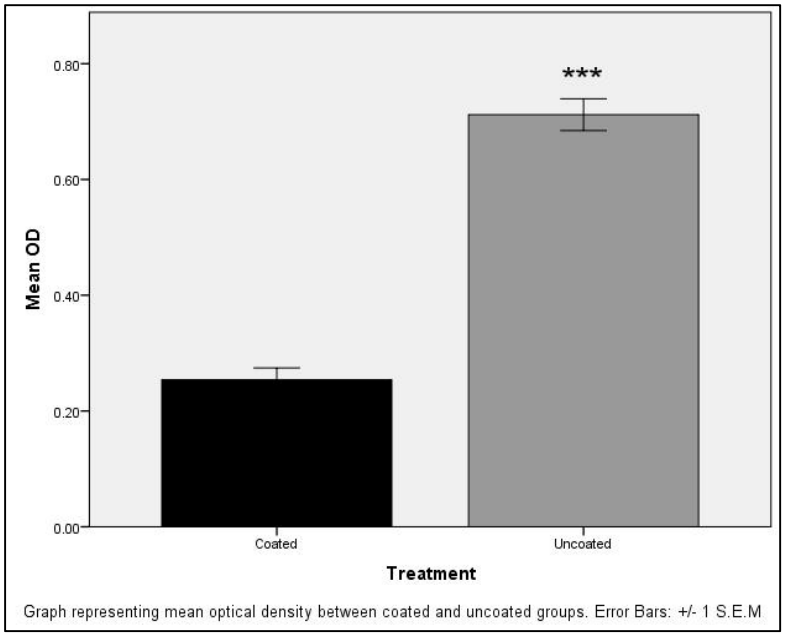

Figure 4.9. Simultaneous evaluation of antimicrobial and anti-coagulant properties of the coating where the coated sample showed significantly lower optical density compared to the non-coated sample.

4.5. Discussion

The common complications of long-term vascular access catheters are 1) infection, 2) thrombus formation, and 3) mechanical failure leading to poor blood flow, making these key design parameters for any catheter modification. Among these complications, the incidence of catheter infections has been cited to be as high as 29.6% and while approximately 70% of deep vein thrombotic events of upper extremity are due to intravenous catheters [9], [30]. Unfortunately, clinical treatment regimens often only address the single pathology, although it is clear that infection and thrombosis often occur almost simultaneously. Nevertheless, several strategies focused on modifying the biology/material interface through bulk material improvements, surface modifications, or pharmaceutical additions have been exploited with increasing importance to combat either thrombosis or biofilm formation. Specifically, heparin immobilization by covalent bonding or ionic interaction has demonstrated success as a coating for a variety of biomedical devices. Regrettably, unavailability of heparin's active site due to its involvement in covalent

bond or heparin disassociating from an ionic linkage [31] have prevented the widespread success of these strategies. Finally, mechanical compliance of the catheter, analogous to the third arm of Virchow's triad is fundamental to the longevity of vascular access catheters, and it cannot be compromised by the addition of any coating, regardless of its biological activity. To meet these design criteria, a recombinant fusion protein consisting of a spider silk amino acid motif and a heparin binding motif (S_4H_4) serves as a promising alternative, avoiding not only the drawbacks of heparin therapy but also providing the advantages of heparin while concurrently delivering a balance of strength and flexibility from the silk backbone. The fusion protein was successfully expressed in E. coli and validated by mass spectrometry. The heparin binding ability was determined by heparin affinity chromatography which confirms the affinity of the protein to heparin (Figure 4.2). The presence of plain silk protein in the eluted, unbound wash fraction (Figure 4.2) confirms that recombinant silk solution alone has limited affinity for immobilized heparin. Alternatively, when HBP was genetically linked to silk repeats, the resulting fusion protein was seen in the elution fraction, reflecting the dramatically increased ability of this recombinant protein to bind immobilized heparin on the column.

Silicone is the major choice of material for vascular access catheters [32]. However, the surface of silicone is not only inert but also hydrophobic [28], making it relatively unavailable for interaction with a coating material. Therefore, plasma oxygen treatment was employed to introduce reactive hydroxy groups onto the surface of the silicone [33], [34], as verified by increase in hydrophilicity of the silicone surface (data not shown). Plasma etching the surface of the silicone allowed the protein to bind to the surface, creating a coating. Contact angle measurements showed a substantial decrease in the contact angle after coating suggesting the silicone surface had become hydrophilic (Figure 4.3) [33]. This also indicated that both oxygen treatment and coating

deposition contributed to the surface wettability of the silicone surface. Subsequently, the chemical structure and thickness of the coating was evaluated. X-ray electron spectroscopy was able to confirm the presence of a protein coating by determining the chemical composition of the surface of the coated silicone sheet (Table 4.1). Nitrogen content increased from 1 to 6% after coating, which is probably due to the amine groups from the side chains of lysine and arginine in heparin binding region of the protein coating. In addition, the silicone elemental composition percentage decreased, further confirming that the surface is covered by the protein. Raman spectroscopy was employed to determine the fingerprint regions of specific amino acids particularly symmetrical compounds. Of particular importance among the Raman spectral shifts is the region at 1260 cm^{-1} (Figure 4.4), which shows the amide linkage and also the α-helix. The presence of this band shows that the secondary structure of the protein is not altered with the addition of HBM motifs in the spider silk backbone. Fingerprint regions of the protein were further confirmed by ATR spectroscopy (Figure 4.5) which showed C=O and aromatic C=C stretching of glutamine and tyrosine respectively. Next SEM imaging was performed to evaluate the thickness of the coating. A cross section of the coated and non-coated silicone sheets were evaluated by SEM and the thickness was found to be 10μm (Figure 4.6). Coating prior to the plasma activation resulted in a thickness of nano scale (data not shown); whereas, plasma activation increased the thickness.

The structural prerequisite of HBM is the presence of a basic residue separated by a consensus of hydrophobic residues [22], [35]. Segregation of discrete hydrophobic and cationic amino acid sectors in this consensus sequence is analogous to many identified antimicrobial peptides (AMPs) and thought to be fundamental to their bactericidal function allowing permeation of the bacterial membrane [21]. Most AMPs are broad spectrum and do not have a particular bacterial target, which minimizes the development of bacterial resistance to the coating. The

activity of the fusion protein as an antibacterial coating material was evaluated by counting the number of colonies after incubation with bacteria. From the figure 4.7, it is evident that in the presence of coating, the number of bacterial colonies was reduced significantly compared to the uncoated sheets. In addition to antimicrobial activity, ATP assay was performed to evaluate the bacterial cell viability (Figure 4.8). In this assay lower luminescence values corresponds to lower number of cells adhered to the surface. From the bar graph in figure 8, the coated sheets have significantly lower number of adhered cells compared to the uncoated samples. This further confirms that the coating not only shows antibacterial activity but can also prevent the formation of biofilm on the catheter surface.

In addition to the fusion protein's demonstrated antibacterial properties when bound to a surface, it also demonstrates anticoagulation properties. Heparin-binding peptides have proven efficacious in both soluble and immobilized forms being able to selectivity bind heparin from solutions [36]. For the fusion protein described here, the aPTT clotting assay confirmed the heparin capturing ability of the protein, since heparin from the sample is rinsed off before the assay. The uncoated samples were unable to capture and retain the heparin and hence showed the formation of clot.

However, these independent assays were not able to assess the ability of the coating to function as both and antimicrobial and anticoagulation. Thus, to evaluate simultaneous antibacterial and anticoagulation properties of the coating, an aPTT assay was conducted following incubation with bacteria, under the supposition that since the ATP assay previously established that the coating could prevent a biofilm, if the optical density of the clotting assay was lower it would indicate that the coating maintains its ability to function as an anticoagulation surface even after exposure to bacteria (Figure 4.9). Three possible mechanisms for this simultaneous property

are proposed; either the residues responsible for antimicrobial activity and anticoagulant properties were different or the amount of bacteria does not fully saturate the protein coating, or the bacteria disassociate from the coating, freeing up the necessary sites for heparin binding.

4.6. Conclusion

A genetically modified recombinant fusion protein consisting of a spider silk protein motif and a heparin-binding motif was cloned and expressed in bacteria. This fusion protein was successfully coated onto a silicone surface, which is a commonly used catheter material. Coating changed the hydrophobic silicone surface to a hydrophilic surface. The coating not only showed antimicrobial properties but also prevented the formation of biofilm. Finally, the coating proved to be both anti-coagulant and anti-infective simultaneously. This unique approach may prove effective to address and resolve many of the issues like infection, and thrombosis surrounding the use of blood-contacting medical devices.

4.8. Acknowledgements

This research was supported by NIH R21 and ND EPSCoR funding. We thank Jim Bahr for his assistance on XPS and Greg Stromann for his assistance with the plasma etching and Raman spectroscopy. Funding for the Core Synthesis and Analytical Services Facility used in this publication was made possible by NIH Grant P30 GM103332 (NIGMS). Manuscript contents are solely the responsibility of the authors and do not necessarily represent the official views of the NIH.

4.7. References

[1] H. M. Bos, R. A. de Boer, G. L. Burns, and S. F. Mohammad, “Evidence that bacteria prefer to adhere to thrombus,” *ASAIO J.*, vol. 42, no. 5, pp. M881-884, Oct. 1996.

[2] M. Levi, “New insights into pathways that determine the link between infection and thrombosis,” vol. 70, no. 3, p. 7, 2012.

[3] S. F. Mohammad, “Enhanced risk of infection with device-associated thrombi,” *ASAIO J.*, vol. 46, no. 6, pp. S63-68, Dec. 2000.

[4] E. T. M. Berends, A. Kuipers, M. M. Ravesloot, R. T. Urbanus, and S. H. M. Rooijakkers, “Bacteria under stress by complement and coagulation,” *FEMS Microbiol Rev*, vol. 38, no. 6, pp. 1146–1171, Nov. 2014.

[5] V. G. Gavalas, M. J. Berrocal, and L. G. Bachas, “Enhancing the blood compatibility of ion-selective electrodes,” *Anal Bioanal Chem*, vol. 384, no. 1, pp. 65–72, Jan. 2006.

[6] T. M. Ma, J. S. VanEpps, and M. J. Solomon, “Structure, Mechanics, and Instability of Fibrin Clot Infected with Staphylococcus epidermidis,” *Biophysical Journal*, vol. 113, no. 9, pp. 2100–2109, Nov. 2017.

[7] H. Shah, W. Bosch, K. M. Thompson, and W. C. Hellinger, “Intravascular Catheter-Related Bloodstream Infection,” *Neurohospitalist*, vol. 3, no. 3, pp. 144–151, Jul. 2013.

[8] M. Schroeder, B. D. Brooks, and A. E. Brooks, “The Complex Relationship between Virulence and Antibiotic Resistance,” *Genes*, vol. 8, no. 1, p. 39, Jan. 2017.

[9] G. A. Beathard, “Catheter Thrombosis,” *Seminars in Dialysis*, vol. 14, no. 6, pp. 441–445, Jan. 2004.

[10] N. Mackman, “Triggers, targets and treatments for thrombosis,” *Nature*, vol. 451, no. 7181, pp. 914–918, Feb. 2008.

[11] J. G. Kelton and T. E. Warkentin, “Heparin-induced thrombocytopenia: a historical perspective,” *Blood*, vol. 112, no. 7, pp. 2607–2616, Oct. 2008.

[12] O. Ranze, A. Rakow, P. Ranze, P. Eichler, A. Greinacher, and C. Fusch, “Low-dose danaparoid sodium catheter flushes in an intensive care infant suffering from heparin-induced thrombocytopenia,” *Pediatr Crit Care Med*, vol. 2, no. 2, pp. 175–177, Apr. 2001.

[13] J. A. Justo and P. B. Bookstaver, “Antibiotic lock therapy: review of technique and logistical challenges,” *Infect Drug Resist*, vol. 7, pp. 343–363, Dec. 2014.

[14] J. K. Broom, R. Krishnasamy, C. M. Hawley, E. G. Playford, and D. W. Johnson, “A randomised controlled trial of Heparin versus EthAnol Lock THerapY for the prevention of Catheter Associated infecTion in Haemodialysis patients – the HEALTHY-CATH trial,” *BMC Nephrology*, vol. 13, no. 1, p. 146, Nov. 2012.

[15] R. Biran and D. Pond, “Heparin coatings for improving blood compatibility of medical devices,” *Advanced Drug Delivery Reviews*, vol. 112, pp. 12–23, Mar. 2017.

[16] P. A. Hårdhammar *et al.*, “Reduction in thrombotic events with heparin-coated Palmaz-Schatz stents in normal porcine coronary arteries,” *Circulation*, vol. 93, no. 3, pp. 423–430, Feb. 1996.

[17] S. Kapoor and S. C. Kundu, “Silk protein-based hydrogels: Promising advanced materials for biomedical applications,” *Acta Biomater*, vol. 31, pp. 17–32, Feb. 2016.

[18] L.-D. Koh *et al.*, “Structures, mechanical properties and applications of silk fibroin materials,” *Progress in Polymer Science*, vol. 46, pp. 86–110, Jul. 2015.

[19] “Properties of Synthetic Spider Silk Fibers Based on Argiope aurantia MaSp2 - Biomacromolecules (ACS Publications).” [Online]. Available: https://pubs.acs.org/doi/abs/10.1021/bm701124p. [Accessed: 24-Jul-2018].

[20] L. Nilebäck *et al.*, "Self-Assembly of Recombinant Silk as a Strategy for Chemical-Free Formation of Bioactive Coatings: A Real-Time Study," *Biomacromolecules*, vol. 18, no. 3, pp. 846–854, Mar. 2017.

[21] E. Andersson, V. Rydengård, A. Sonesson, M. Mörgelin, L. Björck, and A. Schmidtchen, "Antimicrobial activities of heparin-binding peptides," *Eur. J. Biochem.*, vol. 271, no. 6, pp. 1219–1226, Mar. 2004.

[22] A. Verrecchio, M. W. Germann, B. P. Schick, B. Kung, T. Twardowski, and J. D. S. Antonio, "Design of Peptides with High Affinities for Heparin and Endothelial Cell Proteoglycans," *J. Biol. Chem.*, vol. 275, no. 11, pp. 7701–7707, Mar. 2000.

[23] M. Pasupuleti, A. Schmidtchen, and M. Malmsten, "Antimicrobial peptides: key components of the innate immune system," *Crit. Rev. Biotechnol.*, vol. 32, no. 2, pp. 143–171, Jun. 2012.

[24] R. Chang, K. Subramanian, M. Wang, and T. J. Webster, "Enhanced Antibacterial Properties of Self-Assembling Peptide Amphiphiles Functionalized with Heparin-Binding Cardin-Motifs," *ACS Appl. Mater. Interfaces*, vol. 9, no. 27, pp. 22350–22360, Jul. 2017.

[25] B. An *et al.*, "Reproducing Natural Spider Silks' Copolymer Behavior in Synthetic Silk Mimics," *Biomacromolecules*, vol. 13, no. 12, pp. 3938–3948, Dec. 2012.

[26] S. Najjam, R. V. Gibbs, M. Y. Gordon, and C. C. Rider, "Characterization of human recombinant interleukin 2 binding to heparin and heparan sulfate using an ELISA approach," *Cytokine*, vol. 9, no. 12, pp. 1013–1022, Dec. 1997.

[27] S. Larson, D. Carlson, B. Ai, and Y. Zhao, “The extraordinary optical transmission and sensing properties of Ag/Ti composite nanohole arrays,” *Physical Chemistry Chemical Physics*, vol. 21, no. 7, pp. 3771–3780, 2019.

[28] B. Liu *et al.*, “Superhydrophobic organosilicon-based coating system by a novel ultravoilet-curable method,” *Nanomaterials and Nanotechnology*, vol. 7, p. 1847980417702795, Jan. 2017.

[29] P. Musto, D. Larobina, S. Cotugno, P. Straffi, G. Di Florio, and G. Mensitieri, “Confocal Raman imaging, FTIR spectroscopy and kinetic modelling of the zinc oxide/stearic acid reaction in a vulcanizing rubber,” *Polymer*, vol. 54, no. 2, pp. 685–693, Jan. 2013.

[30] M. J. Oliver, S. M. Callery, K. E. Thorpe, S. J. Schwab, and D. N. Churchill, “Risk of bacteremia from temporary hemodialysis catheters by site of insertion and duration of use: a prospective study,” *Kidney Int.*, vol. 58, no. 6, pp. 2543–2545, Dec. 2000.

[31] T. M. Maul, M. P. Massicotte, and P. D. Wearden, “ECMO Biocompatibility: Surface Coatings, Anticoagulation, and Coagulation Monitoring,” *Extracorporeal Membrane Oxygenation - Advances in Therapy*, Sep. 2016.

[32] M. Wildgruber *et al.*, “Polyurethane versus silicone catheters for central venous port devices implanted at the forearm,” *European Journal of Cancer*, vol. 59, pp. 113–124, May 2016.

[33] Y. Zheng *et al.*, “Surface modification of a polyethylene film for anticoagulant and anti-microbial catheter,” *React Funct Polym*, vol. 100, pp. 142–150, Mar. 2016.

[34] S. Kaya, P. Rajan, H. Dasari, D. C. Ingram, W. Jadwisienczak, and F. Rahman, “A Systematic Study of Plasma Activation of Silicon Surfaces for Self Assembly,” *ACS Appl. Mater. Interfaces*, vol. 7, no. 45, pp. 25024–25031, Nov. 2015.

[35] M. Pushpanathan, P. Gunasekaran, and J. Rajendhran, “Antimicrobial Peptides: Versatile Biological Properties,” *International Journal of Peptides*, 2013. [Online]. Available: https://www.hindawi.com/journals/ijpep/2013/675391/. [Accessed: 30-Jul-2019].

[36] M. C. L. Martins, S. A. Curtin, S. C. Freitas, P. Salgueiro, B. D. Ratner, and M. A. Barbosa, “Molecularly designed surfaces for blood deheparinization using an immobilized heparin-binding peptide,” *J Biomed Mater Res A*, vol. 88, no. 1, pp. 162–173, Jan. 2009.

CHAPTER 7. CONCLUSION

Silk is a unique fibrous protein with remarkably high mechanical strength. The unique structure of silk, versatility in processing, biocompatibility, genetic variations of silks, thermal stability, surface chemistry for facile chemical modifications, and controllable degradation features make silks promising biomaterials for many clinical functions. Moreover, different approaches to functionalize silk allows for further improvement of silk's remarkable properties, generating new fusion proteins.

Use of spider silk as a drug carrier provides the advantage of encapsulating large amount of drug without leaching due to its elastic and mechanical properties. Local delivery of these particles also ensures that the particles can release required concentration of the drug at the disease site. Thus, we developed an infection responsive spider silk nanospheres which can release the drug only at the site of infection by chemical modification with a thrombin sensitive linker. This conjugate was tested in vitro for infection responsive release and in in vivo septic arthritis model which showed promising results that may represent a new and promising approach to design a new generation of multifunctional biomaterials bioengineered to prevent the onset of infections.

Spider silk consensus was also embedded with a heparin-binding peptide by genetic modification, expressed, purified and shown to bind heparin both at surfaces and in buffer solutions. Due to the structural similarity of the HBP with antimicrobial peptides, this fusion protein was also evaluated for antimicrobial functions which showed that not only it is antimicrobial but it prevents the formation of biofilm. Utility of this protein as a biomaterial material, exploiting both the recombinant protein-bound heparin and also the intrinsic antimicrobial potential based on its AMP-like structure, represents the next application for this newly engineered recombinant chimera. Further, this fusion protein was utilized as a catheter

coating. This fusion protein was successfully coated onto a silicone surface, which is a commonly used catheter material providing both anti-coagulant and anti-infective surface simultaneously.

With numerous potential modifications that have yet to be explored and applied to silk, a silk-based polymer is a very promising platform for safe biomaterials with tunable features and may soon be applied in cancer treatment, in regenerative medicine and as gene-delivery systems.